



UPPSALA  
UNIVERSITET

*Digital Comprehensive Summaries of Uppsala Dissertations  
from the Faculty of Pharmacy 307*

# Affibody-Based Molecular Imaging and Targeted Therapy of HER3- Expressing Cancer

SARA SOPHIE RINNE



ACTA  
UNIVERSITATIS  
UPSALIENSIS  
UPPSALA  
2022

ISSN 1651-6192  
ISBN 978-91-513-1418-1  
URN urn:nbn:se:uu:diva-467281

Dissertation presented at Uppsala University to be publicly examined in Rudbecksalen, Rudbecklaboratoriet, Dag Hammarskjölds Väg 20, Uppsala, Friday, 1 April 2022 at 10:00 for the degree of Doctor of Philosophy (Faculty of Pharmacy). The examination will be conducted in English. Faculty examiner: Prof. Dr. phil. Melpomeni Fani (University Hospital Basel, Switzerland).

### Abstract

Rinne, S. S. 2022. Affibody-Based Molecular Imaging and Targeted Therapy of HER3-Expressing Cancer. *Digital Comprehensive Summaries of Uppsala Dissertations from the Faculty of Pharmacy* 307. 92 pp. Uppsala: Acta Universitatis Upsaliensis. ISBN 978-91-513-1418-1.

The human epidermal growth factor receptor type 3 (HER3) is overexpressed in different types of cancer and is a known contributor to disease progression and resistance to cancer therapy. This thesis is based on five original articles, which aimed to improve the diagnostic and therapeutic potential of affibody-based agents for management of HER3-expressing cancers.

Papers I-III focused on the development and optimization of radiolabeled affibody molecules for radionuclide molecular imaging of HER3 expression. In particular, they investigated the influence of different radiometal/chelator complexes and hydrophilicity on the biodistribution and imaging properties of the HER3-targeting affibody molecule  $Z_{\text{HER3}}$ . Paper IV compared the optimized  $Z_{\text{HER3}}$ -based radiotracer with antibody and antibody-fragment based radiotracers for PET imaging of HER3 expression. In Paper V, a preclinical therapy study was conducted to investigate the efficacy of different monomeric and dimeric HER3-targeting affibody constructs for treatment of HER3-expressing cancer.

It was shown that by optimizing the radiometal/chelator complex and incorporation of a hydrophilic (HE)<sub>3</sub>-tag the imaging properties of  $Z_{\text{HER3}}$ -based radiotracers could be improved (Papers I-III). Generally, replacing a positively charged radiometal/chelator complex with a neutral or negatively charged complex improved the image contrast by reducing the normal organ uptake, especially in the liver. Further, it was demonstrated that the optimized affibody-based tracer [<sup>68</sup>Ga]Ga-(HE)<sub>3</sub>- $Z_{\text{HER3}}$ -NODAGA could provide higher contrast PET images of HER3 expression than the <sup>89</sup>Zr-labeled antibody seribantumab and a seribantumab-derived F(ab')<sub>2</sub> fragment (Paper IV). The therapy study showed that the arrangement of the molecular building blocks affected the therapeutic efficacy of  $Z_{\text{HER3}}$ -based affibody constructs. The monomeric and dimeric ABD-conjugated affibody constructs 3A and 3A3 showed the best therapeutic efficacy among the tested constructs and were able to delay tumor growth and prolong survival with the same efficacy as the therapeutic HER3-targeting antibody seribantumab (Paper V).

In conclusion, the results described in this thesis show that HER3-targeting affibody-based agents could be well-suited for molecular imaging of HER3 expression and HER3-targeted therapy in cancer. Careful optimization of the molecular design could improve the imaging properties and therapeutic efficacy of HER3-targeting affibody molecules. Most importantly, it was demonstrated that HER3-targeting affibody molecules could provide superior diagnostic images and similar therapeutic effect than more traditional approaches for management of HER3-expressing cancer.

*Keywords:* Molecular Imaging, PET, SPECT, Cancer, Affibody, HER3, Targeted Therapy

*Sara Sophie Rinne, Department of Medicinal Chemistry, Box 574, Uppsala University, SE-75123 Uppsala, Sweden.*

© Sara Sophie Rinne 2022

ISSN 1651-6192

ISBN 978-91-513-1418-1

URN urn:nbn:se:uu:diva-467281 (<http://urn.kb.se/resolve?urn=urn:nbn:se:uu:diva-467281>)

*“We are almost there, but nowhere near  
it. All that matters is that we are going.”  
-Lorelai Gilmore*



# List of Papers

This thesis is based on the following papers, which are referred to in the text by their Roman numerals.

- I **Rinne SS\***, Leitao CD\*, Mitran B, Bass TZ, Andersson KG, Tolmachev V, Ståhl S, Löfblom J, Orlova A. (2019) Optimization of HER3 Expression Imaging Using Affibody Molecules: Influence of Chelator for Labeling with Indium-111. *Sci Rep.* Jan 24;9(1):655.
- II Dahlsson Leitao C\*, **Rinne SS\***, Mitran B, Vorobyeva A, Andersson KG, Tolmachev V, Ståhl S, Löfblom J, Orlova A. (2019) Molecular Design of HER3-Targeting Affibody Molecules: Influence of Chelator and Presence of HEHEHE-Tag on Biodistribution of <sup>68</sup>Ga-Labeled Tracers. *Int J Mol Sci.* Mar 2;20(5).
- III **Rinne SS**, Dahlsson Leitao C, Saleh-Nihad Z, Mitran B, Tolmachev V, Ståhl S, Löfblom J, Orlova A. (2020) Benefit of Later-Time-Point PET Imaging of HER3 Expression Using Optimized Radiocobalt-Labeled Affibody Molecules. *Int J Mol Sci.* Mar 13;21(6):1972.
- IV **Rinne SS\***, Dahlsson Leitao C\*, Abouzayed A, Vorobyeva A, Tolmachev V, Ståhl S, Löfblom J, Orlova A. (2021) HER3 PET Imaging: <sup>68</sup>Ga-labeled Affibody Molecules Provide Superior HER3 Contrast to <sup>89</sup>Zr-labeled Antibody and Antibody-Fragment Based Tracers. *Cancers (Basel).* Sep 24;13(19):4791.
- V Dahlsson Leitao C\*, **Rinne SS\***, Altai M\*, Vorontsova O, Dunås F, Jonasson P, Tolmachev V, Löfblom J, Ståhl S, Orlova A. (2020) Evaluating the Therapeutic Efficacy of Mono- and Bivalent Affibody-Based Fusion Proteins Targeting HER3 in a Pancreatic Cancer Xenograft Model. *Pharmaceutics.* Jun 13;12(6):551.

Reprints were made with permission from the respective publishers.

\*Equal contribution

## Publications not included in this thesis:

- I Deyev SM, Xu T, Liu Y, Schulga A, Konovalova E, Garousi J, **Rinne SS**, Larkina M, Ding H, Gräslund T, Orlova A, Tolmachev V, Vorobyeva A. (2021) Influence of the Position and Composition of Radiometals and Radioiodine Labels on Imaging of Epcam Expression in Prostate Cancer Model Using the DARPin Ec1. *Cancers (Basel)*. 13(14):3589
- II **Rinne SS**, Orlova A, Tolmachev V. (2021) PET and SPECT Imaging of the EGFR Family (RTK Class I) in Oncology. Review. *Int J Mol Sci*. 22(7), 3663.
- III Oroujeni M\*, **Rinne SS\***, Vorobyeva A, Loftenius A, Feldwisch J, Jonasson P, Chernov V, Orlova A, Frejd FY, Tolmachev V. (2021) Preclinical Evaluation of <sup>99m</sup>Tc-ZHER2:41071, a Second-Generation Affibody-Based HER2-Visualizing Imaging Probe with a Low Renal Uptake. *Int J Mol Sci*. 22(5):2770.
- IV Oroujeni M, Xu T, Gagnon K, **Rinne SS**, Weis J, Garousi J, Andersson KG, Löfblom J, Orlova A, Tolmachev V. (2021) The Use of a Non-Conventional Long-Lived Gallium Radioisotope <sup>66</sup>Ga Improves Imaging Contrast of EGFR Expression in Malignant Tumours Using DFO-ZEGFR:2377 Affibody Molecule. *Pharmaceutics*.13(2):292.
- V **Rinne SS**, Abouzayed A, Gagnon K, Tolmachev V, Orlova A. (2021) <sup>66</sup>Ga-PET-imaging of GRPR-expression in prostate cancer: production and characterization of [<sup>66</sup>Ga]Ga-NOTA-PEG2-RM26. *Sci Rep*. 11(1):3631.
- VI Abouzayed A, **Rinne SS**, Sabahnoo H, Sörensen J, Chernov V, Tolmachev V, Orlova A. (2021) Preclinical Evaluation of <sup>99m</sup>Tc-Labeled GRPR Antagonists maSSS/SES-PEG2-RM26 for Imaging of Prostate Cancer. *Pharmaceutics*. 13(2):182.
- VII Baun C, Mitran B, **Rinne SS**, Dam JH, Olsen BB, Tolmachev V, Orlova A, Thisgaard H. (2020) Preclinical Evaluation of the Copper-64 Labeled GRPR-Antagonist RM26 in Comparison with the Cobalt-55 Labeled Counterpart for PET-Imaging of Prostate Cancer. *Molecules*. 25(24):5993.

- VIII Abouzayed A, Tano H, Nagy Á, **Rinne SS**, Wadea F, Kumar S, Westerlund K, Tolmachev V, Eriksson Karlström A, Orlova A. (2020) Preclinical Evaluation of the GRPR-Targeting Antagonist RM26 Conjugated to the Albumin-Binding Domain for GRPR-Targeting Therapy of Cancer. *Pharmaceutics*. 12(10):E977.
- IX Vorobyeva A, Oroujeni M, Lindbo S, Hober S, Xu T, Liu Y, **Rinne SS**, Garousi J. (2020) Investigation of a Pharmacological Approach for Reduction of Renal Uptake of Radiolabeled ADAPT Scaffold Protein. *Molecules*. 25(19):E4448.
- X Lundmark F, Abouzayed A, Mitran B, **Rinne SS**, Varasteh Z, Larhed M, Tolmachev V, Rosenström U, Orlova A. (2020) Heterodimeric Radiotracer Targeting PSMA and GRPR for Imaging of Prostate Cancer-Optimization of the Affinity towards PSMA by Linker Modification in Murine Model. *Pharmaceutics*. 12(7):614.
- XI Vorobyeva A, Konovalova E, Xu T, Schulga A, Altai M, Garousi J, **Rinne SS**, Orlova A, Tolmachev V, Deyev S. (2020) Feasibility of Imaging EpCAM Expression in Ovarian Cancer Using Radiolabeled DARPIn Ec1. *Int J Mol Sci*. 21(9):3310.
- XII **Rinne SS**, Xu T, Dahlsson Leitao C, Ståhl S, Löfblom J, Orlova A, Tolmachev V, Vorobyeva A. (2020) Influence of Residualizing Properties of the Radiolabel on Radionuclide Molecular Imaging of HER3 Using Affibody Molecules. *Int J Mol Sci*. 21(4):1312.
- XIII Altai M, Garousi J, **Rinne SS**, Schulga A, Deyev S, Vorobyeva A. (2020) On the prevention of kidney uptake of radiolabeled DARPins. *EJNMMI Res*. 10(1):7.
- XIV **Rinne SS\***, Dahlsson Leitao C\*, Gentry J, Mitran B, Abouzayed A, Tolmachev V, Ståhl S, Löfblom J, Orlova A. (2019) Increase in negative charge of <sup>68</sup>Ga/chelator complex reduces unspecific hepatic uptake but does not improve imaging properties of HER3-targeting affibody molecules. *Sci Rep*. 9(1):17710.
- XV Mitran B, Varasteh Z, Abouzayed A, **Rinne SS**, Puuvuori E, De Rosa M, Larhed M, Tolmachev V, Orlova A, Rosenström U. (2019) Bispecific GRPR-Antagonistic Anti-PSMA/GRPR Heterodimer for PET and SPECT Diagnostic Imaging of Prostate Cancer. *Cancers (Basel)*. 11(9):1371.

- XVI Ding H, Altai M, **Rinne SS**, Vorobyeva A, Tolmachev V, Gräslund T, Orlova A. (2019) Incorporation of a Hydrophilic Spacer Reduces Hepatic Uptake of HER2-Targeting Affibody-DM1 Drug Conjugates. *Cancers (Basel)*. 11(8):1168.
- XVII Abouzayed A, Yim CB, Mitran B, **Rinne SS**, Tolmachev V, Larhed M, Rosenström U, Orlova A. Synthesis and Preclinical Evaluation of Radio-Iodinated GRPR/PSMA Bispecific Heterodimers for the Theranostics Application in Prostate Cancer. *Pharmaceutics*. 11(7):358.
- XVIII Vorobyeva A, Schulga A, **Rinne SS**, Günther T, Orlova A, Deyev S, Tolmachev V. (2019) Indirect Radioiodination of DARPIn G3 Using N-succinimidyl-Para-Iodobenzoate Improves the Contrast of HER2 Molecular Imaging. *Int J Mol Sci*. 20(12):3047.
- XIX Mitran B, **Rinne SS**, Konijnenberg MW, Maina T, Nock BA, Altai M, Vorobyeva A, Larhed M, Tolmachev V, de Jong M, Rosenström U, Orlova A. (2019) Trastuzumab cotreatment improves survival of mice with PC-3 prostate cancer xenografts treated with the GRPR antagonist <sup>177</sup>Lu-DOTAGA-PEG2 -RM26. *Int J Cancer*. 145(11), 3347–335811.
- XX Rosestedt M\*, Andersson KG\*, **Rinne SS\***, Leitao CD, Mitran B, Vorobyeva A, Ståhl S, Löfblom J, Tolmachev V, Orlova A. (2019) Improved contrast of affibody-mediated imaging of HER3 expression in mouse xenograft model through co-injection of a trivalent affibody for in vivo blocking of hepatic uptake. *Sci Rep*. 9(1):6779.
- XXI Vorobyeva A, Schulga A, Konovalova E, Güler R, Mitran B, Garousi J, **Rinne SS**, Löfblom J, Orlova A, Deyev S, Tolmachev V. (2019) Comparison of tumor- targeting properties of directly and indirectly radioiodinated designed ankyrin repeat protein (DARPIn) G3 variants for molecular imaging of HER2. *Int J Oncol*. 54(4):1209-1220.
- XXII Altai M, Leitao CD, **Rinne SS**, Vorobyeva A, Atterby C, Ståhl S, Tolmachev V, Löfblom J, Orlova A. (2018) Influence of Molecular Design on the Targeting Properties of ABD-Fused Mono- and Bi-Valent Anti-HER3 Affibody Therapeutic Constructs. *Cells*. 7(10). pii: E164.

- XXIII Orlova A, Bass TZ, **Rinne SS**, Leitao CD, Rosestedt M, Atterby C, Gudmundsdotter L, Frejd FY, Löfblom J, Tolmachev V, Ståhl S. (2018) Evaluation of the Therapeutic Potential of a HER3-Binding Affibody Construct TAM-HER3 in Comparison with a Monoclonal Antibody, Seribantumab. *Mol Pharm.* 15(8):3394-3403.
- XXIV Mitran B, Güler R, Roche FP, Lindström E, Selvaraju RK, Fleetwood F, **Rinne SS**, Claesson-Welsh L, Tolmachev V, Ståhl S, Orlova A, Löfblom J. (2018) Radionuclide imaging of VEGFR2 in glioma vasculature using biparatopic affibody conjugate: proof-of-principle in a murine model. *Theranostics.* 8(16):4462-4476.
- XXV Rosestedt M, Andersson KG, Mitran B, **Rinne SS**, Tolmachev V, Löfblom J, Orlova A, Ståhl S. (2017) Evaluation of a radiocobalt-labelled affibody molecule for imaging of human epidermal growth factor receptor 3 expression. *Int J Oncol.* 51(6):1765-1774.

\* Equal contribution



# Contents

Introduction.....	15
Cancer .....	15
Precision Medicine and Targeted Therapy in Cancer.....	15
The Theranostic Concept.....	16
Human Epidermal Growth Factor Receptor Family and its Role in Cancer .....	16
HER Family .....	16
HER3: The Odd One Out .....	17
HER Family-Targeted Therapy in Cancer .....	18
HER3-Targeted Therapy .....	18
Radionuclide Molecular Imaging .....	20
Radionuclide Molecular Imaging in Oncology .....	21
Diagnostic Agents for Radionuclide Molecular Imaging in Oncology ....	22
General Considerations.....	22
Choice of the Targeting Molecule .....	23
Choice of the Radionuclide and Labeling Chemistry .....	26
Off-Target Interactions and Strategies for Modification .....	26
Radiometal Labeling .....	27
Radionuclide Molecular Imaging of HER3 expression: Challenges and Current Status.....	30
Affibody Molecules for Medical Applications in Cancer .....	32
HER3 Theranostics based on Affibody Molecules .....	33
Affibody Molecules for HER3-Targeted Therapy.....	33
Affibody Molecules for Imaging of HER3 Expression .....	33
Aims of this Thesis .....	35
Methodology.....	36
The Present Investigation.....	40
<b>Paper I:</b> Optimization of HER3 Expression Imaging using Affibody Molecules: Influence of Chelator for Labeling with Indium-111 .....	40
<b>Paper II:</b> Molecular Design of HER3-Targeting Affibody Molecules: Influence of Chelator and Presence of HEHEHE-Tag on Biodistribution of <sup>68</sup> Ga-Labeled Tracers .....	45
<b>Paper III:</b> Benefit of Later-Time-Point PET Imaging of HER3 Expression Using Optimized Radiocobalt-Labeled Affibody Molecules	51

<b>Paper IV:</b> HER3 PET-Imaging: $^{68}\text{Ga}$ -Labeled Affibody Molecules Provide Superior HER3 Contrast to $^{89}\text{Zr}$ -Labeled Antibody and Antibody-Fragment-Based Tracers .....	57
<b>Paper V:</b> Evaluating the Therapeutic Efficacy of Mono- and Bivalent Affibody-Based Fusion Proteins Targeting HER3 in a Pancreatic Cancer Xenograft Model .....	65
Concluding Remarks .....	71
Future Directions .....	73
References .....	83

# Abbreviations

ABD	albumin-binding domain
ADC	antibody-drug conjugate
CT	computed tomography
DFO	deferoxamine
DOTA	1,4,7,10-tetraazacyclododecane-1,4,7,10-tetraacetic acid
DOTAGA	1,4,7,10-tetraazacyclododecane,1-(glutaric acid)-4,7,10-tri-acetic acid
ECD	extracellular domain
EGFR	epidermal growth factor receptor
ESCC	esophageal squamous cell carcinoma
ESP	engineered scaffold protein
HER	human epidermal growth factor receptor
HNSCC	head and neck squamous cell carcinoma
HRG	heregulin
HSA	human serum albumin
IA	injected activity
mAb	monoclonal antibody
mErbB3	murine epidermal growth factor receptor type 3
mCRC	metastatic colorectal cancer
MRI	magnetic resonance imaging
MSA	murine serum albumin
NODAGA	1,4,7-triazacyclononane,1-glutaric acid-4,7-acetic acid
NOTA	1,4,7-triazacyclononane-1,4,7-triacetic acid
NSCLC	non-small cell lung cancer
PBS	phosphate buffered saline
PET	positron emission tomography
pi	post-injection
RTK	receptor tyrosine kinase
scFv	single-chain variable fragment
sdAb	single-domain antibody
SPECT	single photon emission computed tomography
SPR	surface plasmon resonance
SUV	standardized uptake value
TK	tyrosine kinase
TKI	tyrosine kinase inhibitor
VEGFR	vascular endothelial growth factor receptor



# Introduction

## Cancer

It is estimated that one in five people worldwide will develop cancer during their lifetime (3). The word cancer is a collective term for hundreds of diseases, which claim millions of lives each year. Cancer is characterized by abnormal, uncontrollable growth of cells due to genetic alterations, which can eventually lead to the formation of malignant tumors and spread from one site in the body to another (metastasis). In 2000, Hanahan and Weinberg proposed a set of six traits shared among cancer types, also known as the hallmarks of cancer (4). Today, the hallmarks of cancer comprise a widely recognized set of 10 underlying principles, including self-sufficiency in growth signals, insensitivity to anti-growth signals, escaping immune destruction, limitless replicative potential, tumor-promoting inflammation, tissue invasion and metastasis, inducing angiogenesis, genome instability and mutation, resistance to cell death, and deregulation of cellular energetics (5).

Chemotherapy, radiation therapy, and – when possible – surgery, or a combination of these approaches are common treatment regimens for cancer patients. Treating cancer patients is challenging, not only because healthy tissue should be spared, but also because there is no one-size-fits-all approach. Although different cancer types may share the traits mentioned above, they can vary appreciably in their molecular characteristics (6). It is therefore not guaranteed that patients, even patients with the same tumor origin, will respond in the same way to a given treatment. Identifying patients with different cancer subtypes and tailoring the treatment approach to patient subgroups with the same molecular disease profile is thus a central concept in modern cancer therapy.

## Precision Medicine and Targeted Therapy in Cancer

Precision medicine follows the philosophy of developing and giving treatment to patients which matches the molecular characteristics of their disease (7). Treating patients according to their molecular disease profile could result in

---

<sup>1</sup> Parts of this chapter are based on: Rinne SS et al. (2021) PET and SPECT Imaging of the EGFR Family (RTK Class I) in Oncology. *Int. J. Mol. Sci.* 22(7):3663 (1) and Rinne SS and Vorobyeva A. (2021) Radiometals—Chemistry and radiolabeling. In: *Reference Module in Biomedical Sciences*. Elsevier (2).

more effective treatment and, hopefully, better treatment outcomes. In cancer, this could include tailored treatment to patients based on the genetic profile of the cancer and expression of cancer cell specific markers (7).

The development of targeted therapy approaches is an integral part of precision medicine. Targeted therapy is based on the idea of the “magic bullet” introduced by Paul Ehrlich in the early 1900s: to develop drugs that find their intended site of action, while being harmless to healthy tissue (8). In cancer, this can be applied by using molecules that bind to molecular markers found in or on cancer cells – such as cell-surface receptors – to block their activity, deliver cytotoxic drugs, or attract immune cells to eradicate the cancer cells (9).

## The Theranostic Concept

The term “theranostics” is a blend of the words *therapy* and *diagnostics* that describes the liaison between a targeted treatment approach and a diagnostic companion. The diagnostic companion is used to detect and visualize the presence of the therapeutic target or another predictive biomarker and identify suitable candidates for a certain therapy, prior to the intervention. Later, the diagnostic companion could ideally also be used for monitoring of treatment response.

Theranostic approaches are particularly attractive for precision medicine and targeted therapy where diagnostic testing is essential for identifying patients who could respond to a certain therapy.

## Human Epidermal Growth Factor Receptor Family and its Role in Cancer

### HER Family

The human epidermal growth factor receptor family (also HER family or receptor tyrosine kinase (RTK) class I) is a family of four tyrosine kinase receptors (HER1–HER4, also known as ErbB1–ErbB4) involved in basic cellular processes such as cell proliferation and cell survival (10). Structurally, they consist of an extracellular domain (ECD) for ligand binding, a transmembrane domain, an intracellular tyrosine kinase (TK) domain and a tyrosine-rich C-terminal tail. With the exception of HER2, the receptors are activated by ligand binding, which initiates a conformation change of the ECD exposing a dimerization arm used for homo- or heterodimerization with another family member. The ECD of HER2 is in a constantly open conformation, allowing for dimerization without ligand binding. Dimerization eventually leads to activation of the TK and phosphorylation of tyrosine residues on the C-terminal

tail. The phosphorylated tyrosine residues subsequently initiate further downstream cellular signaling (10).

Aberrant expression and functional alterations of the HER family members have been linked to oncogenesis since the 1980s (11,12). Their overexpression is a driver for altered intracellular signaling, tumor growth and disease progression (13). Overexpression of HER1 (EGFR) is found to be involved in progression of, for example, head and neck, colon, and non-small cell lung cancer (14). HER2 is most widely known for its overexpression and role in breast cancer, but has been implicated in many other types of solid cancers, e.g., gastric, prostate, and ovarian cancer (15,16). The role of HER4 in cancer remains poorly understood; there are indications linking HER4 expression to both pro- and anti-tumor effects (17).

### HER3: The Odd One Out

HER3 was discovered in 1989 through its structural similarity to EGFR (18). The main reason HER3 stands out among its family members is its impaired TK domain. It was long speculated that the intracellular TK domain of HER3 was non-functional, creating doubts about the role of HER3 within the HER family signaling network and as an oncogenic marker (19). HER3 is activated by its natural ligand heregulin (HRG), but relies on the formation of heterodimers to initiate intracellular signaling due to the low functioning kinase activity (20). It is now suggested that some kind of TK activity exists, but it is estimated to be one thousandth of that of the other family members (20,21).

Overexpression of HER3 in cancer was documented shortly after its discovery (22). However, the flawed TK domain, in addition to only moderate upregulation and unclear association with disease progression, caused HER3 to initially attract little attention as an oncogenic marker (19,23). Although many underlying mechanisms and interactions remain unknown, HER3 is now recognized for its central role in maintenance of oncogenic signaling and contribution to cancer development and progression (19,24). Involvement of HER3 overexpression is well-documented in several cancers, such as breast, gastric, ovarian, and prostate cancer (25).

HER3's link to therapeutic resistance has further elevated the interest in the receptor as a potential therapeutic target (26). HER3 is a strong activator for the PI3K/Akt and MAPK signaling pathways and HER3 upregulation is a common mechanism to bypass signaling loss from targeted therapies and maintain (oncogenic) proliferative and survival signaling (26,27). For example, in breast cancer, HER3 activity is a cause for resistance to HER2-targeted therapy (e.g., using trastuzumab) and estrogen receptor therapy (28,29). Increased HER3 expression and signaling in castration-resistant prostate cancer is one of the suspected resistance mechanism to androgen receptor therapy (30). HER3 expression has also been linked to resistance to tyrosine kinase

inhibitors (TKIs) and various chemotherapeutics, such as paclitaxel, camptothecin, or doxorubicin (31,32).

Oncogenic mutations of HER3 are relatively rare, but do exist. Jaiswal et al. were the first to report HER3 mutations in colon and gastric cancer; by 2020, close to 20 oncogenic mutations had been characterized (33,34).

## HER Family-Targeted Therapy in Cancer

The well-documented involvement of the HER family in oncogenesis has prompted the development of cancer therapeutics targeting its family members. In general, HER-targeted therapies follow one of two main strategies: 1) the use of TKIs to directly target and inhibit the TK domain; or 2) blocking receptor activity by targeting the ECD (often using mAbs) (35,36). In addition to being used to block receptor activities, mAbs can be used as delivery vehicles for cytotoxic payloads (antibody-drug conjugates (ADCs)) (37).

Because of their early discovery, prominence, and extensively studied engagement in cancer, therapies targeting HER1 and HER2 are the most advanced, with several pharmaceuticals approved for clinical use (36,38). The monoclonal antibodies cetuximab and panitumumab inhibit HER1 intracellular signaling by blocking the ligand-binding region on the ECD and obstructing the conformational change required for dimerization (39,40). Trastuzumab and pertuzumab are antibodies approved for anti-HER2 therapy. While trastuzumab's main mechanism of action is inhibition of signal transduction, inducing antibody-dependent cell-mediated cytotoxicity and preventing HER2 shedding, pertuzumab's main mechanism of action is inhibition of HER2/HER3 dimerization (41).

## HER3-Targeted Therapy

The development of HER3-targeting therapeutics has been trailing the advances in anti-HER1 and anti-HER2 therapy due to the later discovery and slow recognition of HER3 as a relevant therapeutic target. On the one hand, the lessons learned from developing HER1- and HER2-targeting therapeutics may aid the development of HER3 therapeutic agents. On the other hand, due to the functional aberrations of HER3 compared with the other family members, not all developed therapy strategies may be transferable to anti-HER3 therapy.

The primary approach in HER3-targeted therapy is targeting of the ECD with antibodies to inhibit HER3-induced downstream activity. This can be achieved by inhibiting dimerization, blocking HRG binding, or triggering receptor internalization (27).

Thus far, no HER3-targeting therapeutic agent has been approved for clinical use. More than ten HER3-targeting agents have been studied in clinical

trials (Table 1). Seribantumab (MM-121), patritumab (U3-1287), and lumretuzumab (RO5479599, RG7116) are the most advanced, but the success of HER3 monotherapy has been limited, with the most positive response being stable disease (19,42). In addition to antibody-based HER3 monotherapy, bispecific antibodies, combination therapies, ADCs, and even HER3-targeting vaccines stimulating the production of HER3-specific T-cells and antibodies are being explored in preclinical and clinical studies (19,27).

**Table 1.** HER3-targeting therapeutic agents currently or previously investigated in clinical trials (information from [clinicaltrials.gov](http://clinicaltrials.gov)).

Name	Type of molecule	Highest clinical trial phase	Type of cancer treated in highest trial phase	Trial number
Patritumab (U3-1287)	HER3 mAb	III	Metastatic NSCLC	NCT02134015
Seribantumab (MM-121)	HER3 mAb	II	Breast cancer, metastatic pancreatic cancer	NCT03241810 NCT04790695
Lumretuzumab (RO5479599, RG7116)	HER3 mAb	Ib/II	Squamous NSCLC	NCT02204345
CDX-3379 (KTN3379)	HER3 mAb	II	HNSCC, melanoma	NCT03254927 NCT03580382
Elgentumab (LJM716)	HER3 mAb	I	HER2+ breast and gastric cancer, ESCC	NCT01602406 NCT01822613
GSK2849330	HER3 mAb	I	Various solid tumors	NCT01966445
AV-203	HER3 mAb	I	Various solid tumors	NCT01603979
ISU104	HER3 mAb	I	recurrent/metastatic HNSCC	NCT03552406
REGN1400	HER3 mAb	I	Metastatic solid cancer	NCT01727869
U3-1402	HER3-targeting ADC	II	Metastatic breast cancer, NSCLC	NCT04699630 NCT04619004
Zenocutuzumab (MCLA-128)	HER2/HER3 bispecific mAb	I/II	Various solid tumors	NCT02912949 NCT03321981
Duligotuzumab (MEHD7945A)	EGFR/HER3 bispecific mAb	II	mCRC, recurrent/metastatic HNSCC	NCT01652482 NCT01577173
Istiratumab (MM-141)	HER3/IGF1R bispecific mAb	II	Pancreatic cancer	NCT02399137
MM-111	HER2/HER3 bispecific mAb	I/II	Esophagus and stomach cancer, HER2+ breast cancer	NCT01774851 NCT01097460
SI-B001	EGFR/HER3 bispecific mAb	II/III	NSCLC, HNSCC	NCT05054439 NCT05020769
Sym013	EGFR/HER2/HER3 anti-body cocktail	I/II	Epithelial malignancies	NCT02906670

## Radionuclide Molecular Imaging

In contrast to traditional anatomical imaging, radionuclide molecular imaging can be used to detect and quantify the expression of molecular markers in living subjects. In basic principle, a radionuclide is incorporated to a molecule that is designed to target a specific molecular marker or biological process of interest. The ionizing radiation emitted by the radionuclide is then used to visualize the location of the radiotracer. In some cases, radionuclides functioning as analogs to biologically relevant elements can be used as radiotracers.

Two types of modalities are used for radionuclide imaging: positron emission tomography (PET) and single photon emission computed tomography (SPECT). SPECT imaging is based on the detection of  $\gamma$ -rays emitted from radionuclides by using rotating detector systems capturing projection images from every angle. PET imaging uses tracers based on positron ( $\beta^+$ ) emitting radionuclides. PET cameras use a stationary detector ring that registers the 511 keV photons released as a result of the annihilation interaction between a positron and an electron. The detection of the two resulting annihilation photons is also called coincidence detection (43).

**Table 2.** Overview of common and promising radionuclides for PET and SPECT imaging. From (44).

Modality	Radionuclide	% $\beta^+$ decay*	Half-life	Production
PET	$^{11}\text{C}$	99.8	20.4 min	Cyclotron
PET	$^{15}\text{O}$	99.9	2 min	Cyclotron
PET	$^{18}\text{F}$	97	110 min	Cyclotron
PET	$^{44}\text{Sc}$	94.3	3.9 h	Cyclotron, $^{44}\text{Ti}/^{44}\text{Sc}$ Generator
PET	$^{55}\text{Co}$	76	17.5 h	Cyclotron
PET	$^{64}\text{Cu}$	17.8**	12.7 h	Cyclotron
PET	$^{68}\text{Ga}$	89	68 min	$^{68}\text{Ge}/^{68}\text{Ga}$ generator
PET	$^{89}\text{Zr}$	22.3	78.4 h	Cyclotron
PET	$^{124}\text{I}$	22	4.18 d	Cyclotron

Modality	Radionuclide	Energy (%abundance) of relevant emitted photons	Half-life	Production
SPECT	$^{99\text{m}}\text{Tc}$	141 keV (87%)	6 h	$^{99}\text{Mo}/^{99\text{m}}\text{Tc}$ generator
SPECT	$^{111}\text{In}$	171 keV (93%), 247 keV (94%)	2.8 d	Cyclotron
SPECT	$^{123}\text{I}$	159 keV (83%)	13.2 h	Cyclotron

\* remaining decay by electron capture (EC), if not otherwise stated. \*\*  $^{64}\text{Cu}$  also decays by  $\beta^-$  (38.4%) and EC (43.8%).

Both modalities are used clinically and can be combined with computed tomography (CT) or magnetic resonance imaging (MRI) for additional anatomic information to simplify image interpretation. SPECT cameras are generally more widely accessible and cost-efficient than PET cameras (45).  $^{99m}\text{Tc}$ , the most commonly used SPECT radionuclide, can be obtained from an on-site  $^{99}\text{Mo}/^{99m}\text{Tc}$  generator. PET can provide higher sensitivity and better resolution and quantification than SPECT, which is why increasing focus has been placed on the development of PET tracers (43,45). Unfortunately, on-site cyclotron access is required for the production of many commonly used PET radionuclides such as  $^{11}\text{C}$ ,  $^{15}\text{O}$  and  $^{18}\text{F}$ .  $^{68}\text{Ga}$  can be produced on-site using the more affordable  $^{68}\text{Ge}/^{68}\text{Ga}$ -generator system. An overview of some common and promising SPECT and PET radionuclides is provided in Table 2.

## Radionuclide Molecular Imaging in Oncology

Currently, biopsy-based methods are the clinical standard for diagnosing cancer and detecting overexpression of potential molecular targets for therapy. However, the increased risk of false negative results due to heterogeneous expression of the molecular target in tumor tissue, and the invasive sampling procedure, limit the repeatability and detection of inter-tumor heterogeneity and metastases, which are essential for effective patient care.

Radionuclide molecular imaging provides a more comprehensive and repeatable method for whole-body molecular profiling than biopsies, and its capabilities go far beyond the detection of molecular markers for selecting the right therapeutic agent. Because it is easily repeatable, it could be used for monitoring of changes in target expression, assessment of treatment response, and post-treatment follow-up. Furthermore, it can be applied in dosing studies to optimize and tailor treatment plans and is less impacted by heterogeneous expression than biopsy sampling (46).

The most widely used PET tracer in clinical oncology is [ $^{18}\text{F}$ ]FDG (47). As a glucose analog, it can be used to detect abnormal glucose metabolism, one of the hallmarks of cancer (4,47). Its clinical applications include tumor detection, cancer staging, and surgery or radiotherapy planning (47). Though it is widely used, [ $^{18}\text{F}$ ]FDG has a major drawback in that it does not provide any information about the presence of potential molecular targets for therapy such as, for example, members of the HER family. With the increasing focus on precision medicine and development of targeted therapy, simple tumor detection is no longer sufficient. Increasing attention has thus been directed at the development of radiotracers against molecular markers relevant for targeted cancer therapy that can function as companion diagnostic agents.

# Diagnostic Agents for Radionuclide Molecular Imaging in Oncology

## General Considerations

In radionuclide molecular imaging, the diagnostic accuracy depends on the imaging contrast, meaning the ratio between the uptake of the radiotracer in the tumor and the uptake in non-targeted surrounding tissue and blood. The contrast needs to be particularly high in the primary tumor site and likely metastatic sites, which vary depending on the medical context. In the ideal case, the tracer would only accumulate in the tumor and metastases and would be rapidly eliminated from the rest of the body. Other desirable features of the radiotracer include quantifiable uptake and a direct correlation between uptake and expression of the molecular target. The tracer should also be cost-efficient and easily producible for routine clinical use (48).

Blood-borne activity is one of the major contributors to the background signal and high activity concentration in the blood could appreciably compromise the image contrast. The targeting molecule should therefore have efficient clearance from the blood. Blood concentration often depends on the size of the radiolabeled molecule and its interaction with blood proteins. Tracers that clear slowly from the blood pool may be suboptimal for same-day image acquisition and the time point for image acquisition might need to be delayed to several days after injection to ensure clearance of the tracer and sufficient image contrast (1,48,49).

The natural occurrence of the molecular target in healthy tissue, off-target interactions, and the pathway for tracer elimination might pose additional challenges for the imaging contrast (48). Natural expression and off-target interactions can be particularly problematic if they occur in regions of medical interest, e.g., sites with high likelihood for metastases. Due to the specific interaction between the tracer and molecular target, it can be difficult to limit the uptake in tissues with endogenous target expression without affecting the uptake in the tumor. However, non-specific (off-target) tracer accumulation and accumulation in excretory organs could be manipulated and potentially be reduced by optimizing the tracer design and adjusting the injected dose.

Each targeting system presents with its individual set of challenges and requirements for a potential radiotracer. To achieve optimal image quality, the design of the probe should therefore be tailored to the specific requirements of the targeting system. This means that a number of different variables that can directly and indirectly influence each other and the overall success of the potential imaging probe need to be considered during development. These considerations include:

- Choice of the targeting molecule
- Choice of the radionuclide
- Labeling chemistry
- Off-target interactions

The targeting molecule should bind the target specifically and with high affinity. The radionuclide should, of course, be chosen with the desired imaging modality (PET or SPECT) in mind, but its physical half-life must also match the biological half-life of the targeting molecule. Labeling chemistry must ensure stable attachment of the radionuclide to the targeting molecule without compromising its binding properties. Lastly, non-specific accumulation of the radiotracer needs to be minimal to ensure high image contrast, but may be affected by the choice of targeting molecule and labeling chemistry (1,48).

## Choice of the Targeting Molecule

A wide selection of potential targeting molecules with different characteristics and sizes are available, with novel molecules continuously being developed. The targeting molecule should provide target-specific binding with sufficient affinity (48). High affinity is particularly important for targets with low expression due to the lower chances for rebinding after dissociation of the tracer (50), but might be less crucial for fast internalizing, residualizing tracers. As a general rule, a decrease in size of the molecule increases the clearance rate from blood, tumor penetration, and enables imaging with sufficient contrast closer to the time of injection (1,49). Molecules below the so-called “kidney cut-off” (at around 60 kDa) are generally excreted via the kidneys, whereas larger molecules tend to be eliminated via the hepatobiliary pathway (51,52). However, increased lipophilicity has also been shown to shift the elimination pathway of small molecules from renal towards hepatobiliary (53).

An overview of some commonly used targeting molecules and their key properties is provided in Figure 1.

### *Monoclonal Antibodies*

Monoclonal antibodies (mAbs) have historically been a popular choice for imaging of RTKs, such as the HER family receptors (54,55). The availability and use of existing therapeutic antibodies is an easy approach for the development of a potential radiolabeled diagnostic companion. The advantage is that it could not only detect target expression, but would also be well-suited to provide information on the distribution, accumulation, and dosing of the therapeutic agent.

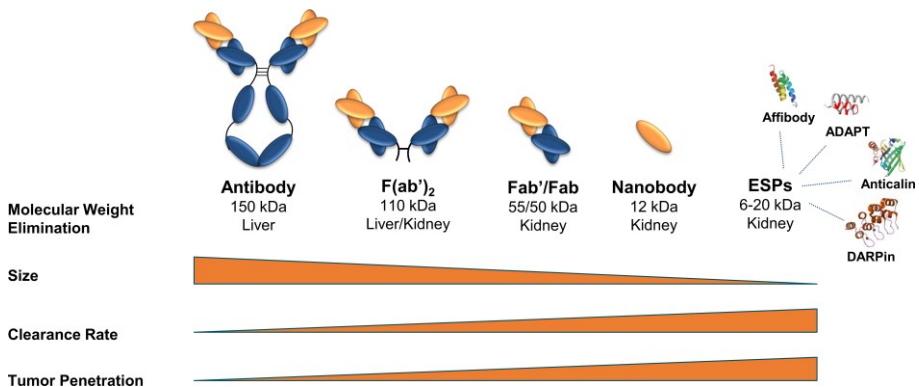


**Figure 1.** Overview of commonly used targeting molecules and their key properties: size, elimination pathway, clearance rate from blood and tumor penetration. Based on with modifications (54).

The drawbacks of using radiolabeled antibodies for PET and SPECT imaging are mainly related to their relatively large size (150 kDa) (54,56). Large molecules have limited extravasation, because the capillary permeability decreases with increasing molecular weight and effective radius of the molecule (57). Further, monoclonal antibodies can interact with neonatal FcRn receptors, which can rescue them from degradation and recycle them back into the blood stream (58). Both, the rather large size and the FcRn interaction contribute to the prolonged circulation of mAbs in blood and can increase the non-specific accumulation in non-targeted tissue. This often leads to significant background signal, especially shortly after injection, meaning that optimal image contrast with antibody-based tracers is usually achieved several days after injection (1,54,56).

Antibody-based tracers may also have increased non-specific accumulation in tumor tissue caused by hypervascularization with abnormal vasculature (enhanced permeability and retention (EPR) effect) (59). The hepatobiliary elimination of intact antibodies (52) can be another disadvantage as it complicates the detection of potential hepatic metastases, which are common in many cancer types.

The use of smaller-sized targeting molecules is one potential alternative to bypass some of the drawbacks associated with antibody-based imaging agents. There has been a noticeable trend of their use as PET and SPECT imaging agents against HER family members (1).

### *Antibody Fragments*

Antibody fragments (F(ab')<sub>2</sub>, Fab, single-chain variable fragment (scFv), or single-domain antibody (sdAb)) are engineered to retain only the basic antigen targeting function of full-length antibodies. Available antibody-derived fragments can vary in size and binding properties (monovalent, bivalent). Because of their smaller size compared with mAbs and the absence of the Fc region

(and thus FcRn interaction), they usually have faster pharmacokinetics and better tissue penetration than the full-length parent molecule (60).

Among the different types of antibody fragments, F(ab')<sub>2</sub> fragments (~110 kDa) are the largest. They could provide sufficient image contrast as early as 24 h post-injection (pi), but commonly imaging contrast further improves at later time points (1). Their effective molecular radius is only slightly smaller than that of antibodies and their extravasation is therefore still limited (57). Fragments consisting of the variable domains of the light and heavy chains linked by a polypeptide linker, so-called scFv, have a size of 25–27 kDa and commonly reach peak tumor uptake within hours after injection (1). ScFv dimers ((scFv)<sub>2</sub>) or other derivatives have also been explored for imaging (1,60).

In recent years, sdAbs (also called nanobodies or VHH, ~15 kDa in size) have become popular targeting vectors. They consist of the variable domain of heavy chain-only antibodies, which can be found in camelids, and their small size and amenability are suitable properties for potential diagnostic (and therapeutic) agents (54,61).

#### *Engineered Scaffold Proteins*

Engineered scaffold proteins (ESPs) are a class of targeting molecules consisting of a robust protein framework that can be engineered to bind different targets with high specificity and affinity. High thermodynamic and chemical stability, low immunogenicity, and small size (typically less than 20 kDa) are common advantages of ESPs compared with antibodies and make them a promising class of targeting molecules for molecular imaging (62,63). Indeed, ESPs have shown desirable features and great potential as imaging probes for PET and SPECT in preclinical and clinical studies (1,62). Affibody molecules have been one of the most studied types of ESPs for PET and SPECT imaging (54,64). Other ESPs that have shown promise in recent years include albumin-binding domain-derived affinity proteins (ADAPT)s and designed ankyrin repeat proteins (DARPin)s (1,65).

#### *Peptides*

Radiolabeled peptides are rapidly cleared from blood and normal tissue due to their small size, can penetrate deeply into tissue, and provide high image contrast shortly after injection (66,67). They are usually radiolabeled versions of natural peptides or derivatives thereof. Radiolabeled peptides have mainly been used for imaging of peptide-binding receptors such as the somatostatin receptor (SSTR), gastrin-releasing peptide receptor (GRPR), or the neurotensin receptor (NTR1) (67). A few peptide-based tracers have been evaluated for imaging of HER family members, but success has been limited thus far (1).

## Choice of the Radionuclide and Labeling Chemistry

The radionuclide should be chosen based on the desired application of the radiotracer (PET or SPECT). The radionuclide's half-life should match the biological half-life and pharmacokinetics of the targeting molecule (68). This means that tracers based on larger molecules with slow pharmacokinetics, which would reach peak accumulation in the target tissue after days (e.g., antibodies), are restricted to the use of longer-lived radionuclides, for example  $^{89}\text{Zr}$  ( $t_{1/2} = 3.3$  d) for PET or  $^{111}\text{In}$  ( $t_{1/2} = 2.8$  d) for SPECT. Smaller molecules, such as peptides or ESPs, can be labeled with shorter-lived radionuclides. Popular choices for labeling of smaller molecules with fast kinetics include  $^{18}\text{F}$  ( $t_{1/2} = 110$  min) or  $^{68}\text{Ga}$  ( $t_{1/2} = 68$  min).

Non-metallic radionuclides (e.g.,  $^{11}\text{C}$ ,  $^{15}\text{O}$ ,  $^{18}\text{F}$ ,  $^{123/124}\text{I}$ ) are incorporated into a molecule through formation of a covalent bond. Labeling with radiometals (e.g.,  $^{68}\text{Ga}$ ,  $^{89}\text{Zr}$ ,  $^{111}\text{In}$ ) is achieved via chelation (2). Regardless of the labeling approach, the labeling chemistry must ensure a stable attachment of the radionuclide to the targeting molecule without damaging the protein. Extreme pH shifts and high temperatures during radiolabeling can compromise the folding of the protein and impair its binding to the intended molecular target (69,70). In vivo, dissociation of the radionuclide from the targeting molecules leads to non-specific accumulation of the radionuclide in non-targeted tissue and increases the background signal. In addition, the positioning of the radiolabel could affect the binding properties and biodistribution of the radiotracer (71,72).

When choosing a radiolabeling approach, one might also want to consider the residualizing properties of the radiolabel in combination with the internalization behavior of the targeting molecule in cells. Once internalized, the radiotracer is degraded in the lysosomes. The resulting radio-catabolites can thereafter either be trapped inside the cell (residualizing labels) or diffuse through the cell membrane and leak into the extracellular space (non-residualizing labels). Most radiometal labels are residualizing, whereas most radio-halogen labels are non-residualizing.

## Off-Target Interactions and Strategies for Modification

As mentioned above, the goal of tracer development is to achieve high accumulation of the tracer at the intended site while keeping the uptake in the rest of the body to a minimum. However, the tracer might interact with blood proteins or healthy tissues in a target receptor-independent manner. These interactions can be referred to as off-target or non-specific interactions and can interfere with tracer clearance and thereby reduce the image contrast. Off-target interactions can, for example, be linked to electrostatic interactions or sur-

face exposure of hydrophilic or lipophilic patches. They can generally be difficult to predict during the design and in vitro evaluation and are often first observed when a tracer is studied in vivo.

To enhance the imaging contrast one has to either increase the uptake of activity in the target or reduce the signal from the background (or both). Modifications to the targeting molecule (e.g., by incorporation of hydrophilic/lipophilic linkers, or exchange of certain amino acids) or the radiolabeling approach could be potential tools to lower off-target interactions.

Alteration of the radiometal/chelator complex provides a convenient approach to influence off-target interactions for radiometal-labeled tracers. It has been shown that different combinations of the radiometal and chelator can form complexes with different charge and geometry, and affect the biodistribution of radiolabeled ESPs and peptides (73–75). Introduction and exchange of amino acids (e.g., histidine-based purification tags) have been shown to alter the uptake and retention of the radiolabeled molecules in normal tissues and target (76,77). For instance, presence of a hydrophilic and negatively charged histidine-glutamate-histidine-glutamate-histidine-glutamate-tag ((HE)<sub>3</sub>-tag) in place of a hexahistidine-tag (H<sub>6</sub>-tag) lowered the hepatic uptake of anti-HER2 affibody molecules (76). These approaches have mainly shown success with smaller molecules, such as ESPs and peptide-based tracers. In case of bulkier molecules, e.g., antibodies, this strategy might not have any substantial effect, because the modifications might be too minor in relation to the size of the molecules.

In general, any modification of the targeting molecule to reduce off-target interactions should be carefully considered, critically evaluated, not pursued beyond reason, and – most importantly – not be made at the cost of functionality of the radiotracer and convenience of its production.

## Radiometal Labeling

Radiometals comprise a large group of radionuclides relevant for PET and SPECT imaging and theranostic applications. Particularly, the existence of radiometals with prolonged half-life suitable for PET imaging (e.g., <sup>55</sup>Co, <sup>64</sup>Cu, <sup>89</sup>Zr) makes them appealing for radiotracer development. Radiometal labeling is generally a straightforward approach. Instead of incorporation through the formation of a covalent bond, radiometals are attached to targeting molecules through chelation (2,78). This section is intended to give a short overview on radiometal chelation and different types of chelators, and describe some aspects of matching radiometals and chelators for the design of radiotracers.

### *Chelation*

The attachment of a radiometal to a targeting vector requires the presence of a chelating moiety. A chelator (or chelating agent) is a structure containing

multiple functional electron-donating groups which create a coordinating complex with a central metal ion through the formation of dative bonds (2). Denticity refers to the number of donor groups (often amino or carboxylic groups) with which a chelator coordinates the central metal atom. A chelating framework containing multiple donor groups generally provides more stable metal/chelator complexes than monodentate ligands because more energy is required to break multiple bonds than single bonds (chelate effect) (79). Bi-functional chelators are used for the radiolabeling of targeting molecules. They have two functional groups: one for conjugation of the chelating component to the targeting molecule, which is usually done before labeling, and another for the chelation of the radiometal.

Upon administration of the radiotracer to the patient, the radiometal/chelator complex is challenged by a shift in equilibrium favoring dissociation, due to large dilution in the blood pool, and the presence of natural chelators in blood, like transferrin, that compete for chelation of the radiometal. High stability of the formed radiometal/chelator complex is therefore crucial to prevent dissociation of the radiometal from the chelator in vivo.

#### *Acyclic and Macrocyclic Chelators*

There are two main classes of chelators. Acyclic chelators are open-chained ligands that enclose the metal during chelation (2,78). They can chelate metals with quantitative yields in 15 min at room temperature. The use of acyclic chelators is appealing because the labeling reaction is gentle and efficient, but metal complexes formed with acyclic chelators are generally less kinetically inert than metal complexes formed with macrocyclic chelators. Macrocyclic chelators have a more rigid, pre-organized structure with a pre-defined cavity to accommodate the radiometal (2,78). They undergo less reorganization during chelation, which results in less entropic loss and increased stability, which is referred to as the macrocyclic effect (80). However, higher activation energy, often achieved by elevated temperatures, and longer reaction times are required to achieve quantitative yields. Figure 2 shows a selection of common acyclic and macrocyclic chelators.

#### *Matching Chelator and Radiometal*

The stability of the radiometal/chelator complex depends on the strength of the bond between the electron-donating group(s) and the metal. Every metal is unique in valency and ionic radius and has individual preferences for chelation (2). The chelating pocket should fit the ionic radius of the metal and the chelator should be able to adapt the favored coordination geometry of the metal without putting too much stress on the chelator's structure (2,81). The denticity of the chelator should match the desired coordination number of the metal to saturate its coordination sphere (2,81). Metal ions usually prefer hard Lewis bases as donor ligands, for example oxygen from the carboxylic arms of the chelator. An unfavorable coordination geometry could make the metal

an easy target for transchelation. Given all these factors, matching the radio-metal with the appropriate chelator is a delicate, but critical, balancing act in the design of radiometal-labeled targeting agents.

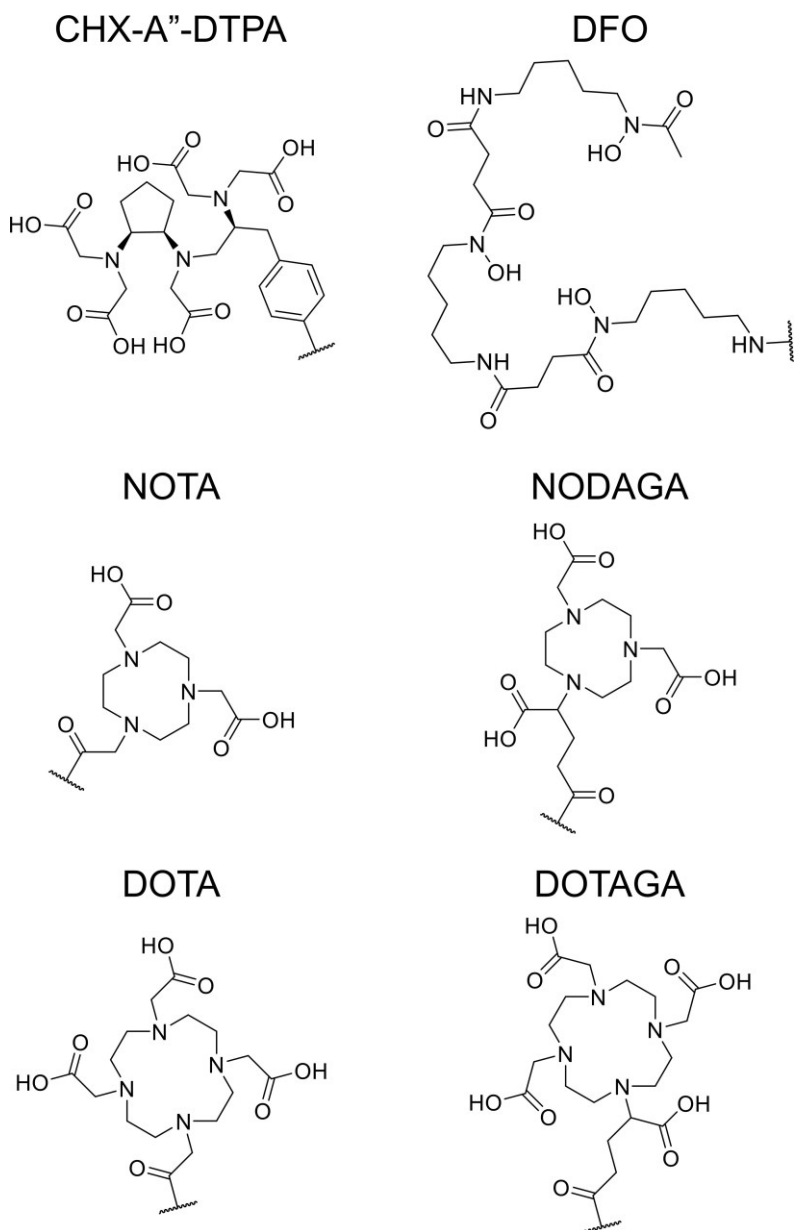


**Figure 2.** Examples of commonly used acyclic (CHX-A''-DTPA, DFO) and macrocyclic (NOTA, NODAGA, DOTA, DOTAGA) chelators for radiometal labeling.

## Radionuclide Molecular Imaging of HER3 expression: Challenges and Current Status

The ongoing development of HER3-targeting therapies necessitates simultaneous development of reliable diagnostic approaches for the detection of HER3 expression. Repeatable, whole-body assessment of HER3 expression is essential, as inter-tumor heterogeneity is common and expression can be up-regulated in response to therapy and sometimes changes rapidly. Radionuclide molecular imaging is well-suited to accommodate these needs.

The development of HER3-targeting imaging probes for PET and SPECT is a demanding task. Two key challenges make it particularly difficult to achieve images of HER3 expression with sufficient contrast. The overexpression of HER3 receptors in cancer cells is relatively low. The upper limit of expression in cancer cells is approximately 50,000 receptors/cell (82). For comparison, the number of HER2 receptors in patients considered HER2-positive is  $\sim 2.3 \pm 10^6$  receptors/cell (83). In addition, HER3 is naturally expressed in the body, notably in the liver and organs of the gastrointestinal tract (proteinatlas.org). The natural expression causes accumulation of the tracer in these organs, which increases the background signal in these areas, and could potentially limit tracer delivery to the tumor. Increasing hepatic contrast is of particular interest when evaluating HER3-imaging agents, because the occurrence of hepatic metastases is common for many cancers. Due to these challenges, developing HER3-imaging agents with high affinity and minimal off-target interactions is crucial. Recent detailed summaries of HER3-targeting imaging agents in preclinical and clinical studies can be found in references (1,84).

The strategy of applying antibody-based tracers has been suitable for imaging of EGFR and HER2 expression, but has not yet proven to be overly successful for HER3 imaging (1). Three HER3-targeting radiolabeled antibodies have been tested in clinical trials: [ $^{64}\text{Cu}$ ]Cu-patritumab, [ $^{89}\text{Zr}$ ]Zr-GSK2849330, and [ $^{89}\text{Zr}$ ]Zr-lumretuzumab (85–87). All are based on mAbs that were initially developed for HER3-targeted therapy. Studies with [ $^{64}\text{Cu}$ ]Cu-patritumab were discontinued due to low tracer uptake (87). Both  $^{89}\text{Zr}$ -labeled antibodies were able to visualize HER3 expression providing the highest imaging contrast within 4–7 days after injection (85,86). However, neither of these tracers could provide reliable detection or quantification of HER3-expressing lesions and at best showed a tentative correlation between uptake and expression (85,86). All tracers had high uptake in the liver, which did not allow for the visualization of hepatic metastases with positive contrast.

### *Tracers in the Preclinical Stage*

While the clinical studies are antibody-dominated, preclinical development is marked by a more diverse selection of tracers. Most are based on alternative

targeting molecules that are smaller in size and have a higher degree of flexibility and possibility for fine-tuning of their imaging properties (1). Table 3 summarizes the preclinically evaluated HER3-imaging agents.

**Table 3.** HER3 imaging agents in the preclinical stage.

Tracer (time point)	Molecule	Modality	Tumor-to-Blood ratio	Tumor-to-Liver ratio	Xenograft model	Ref
[ <sup>89</sup> Zr]Zr-Mab#58 (4 d pi)	Monoclonal antibody	PET	1.1	1.3	RH7777	(88)
[ <sup>89</sup> Zr]Zr-mAb3481* (6 d pi)	Murine antibody	PET	53.7 ± 31.7	n/a	BT474	(89)
[ <sup>89</sup> Zr]Zr-MSB0010853 (96 h pi)	Nanobody	PET	33.1 ± 7.9	< 1	H441	(90)
[ <sup>68</sup> Ga]Ga-NOTA-HER3P1 (1 h pi)	Peptide	PET	2.78	0.71	22RV1	(91)
[ <sup>99m</sup> Tc]Tc-(HE) <sub>3</sub> -ZHER3:08699 (8 h pi)	Affibody	SPECT	9.1	< 1	LS174T	(92)
[ <sup>68</sup> Ga]Ga-(HE) <sub>3</sub> -ZHER3:08698-NOTA (3 h pi)	Affibody	PET	25 ± 6	0.6	BT474	(93)
[ <sup>18</sup> F]AlF-NOTA-ZHER3:08698 (1 h pi)	Affibody	PET	24.61 ± 14.45	0.77	MCF-7	(94)
[ <sup>89</sup> Zr]Zr-DFO-ZHER3:08698 (3 h pi)	Affibody	PET	4.75	1.18	MCF-7	(95)
[ <sup>57</sup> Co]Co-ZHER3:08698-NOTA (24 h pi)	Affibody	SPECT/ PET**	8.2	1.3	LS174T	(96)
[ <sup>111</sup> In]In-(HE) <sub>3</sub> -ZHER3:08698-NOTA (24 h pi)	Affibody	SPECT	15.5 ± 0.7	0.75	BT474	(97)
[ <sup>125</sup> I]I-PIB-(HE) <sub>3</sub> -ZHER3:08698-DOTAGA (4 h)	Affibody	SPECT/ PET***	2	2.4	BxPC-3	(98)
[ <sup>64</sup> Cu]Cu-anti-HER3-F(ab') <sub>2</sub>	F(ab') <sub>2</sub> fragment	PET	n/a	n/a	MDA-MB-468	(99)

\* murine origin, no humanized version yet available \*\* <sup>55</sup>Co could be used for PET imaging instead of <sup>57</sup>Co, \*\*\* <sup>124</sup>I could be used for PET-imaging instead of <sup>125</sup>I.

It should be mentioned that the murine antibody [<sup>89</sup>Zr]Zr-mab3481 has shown promising results in preclinical studies, with high tumor uptake and tumor-to-blood ratios. However, at this point, no humanized version of this antibody is available (89).

Warnders et al. proposed a biparatopic nanobody construct for imaging of HER3 expression (90). The construct, called [<sup>89</sup>Zr]Zr-MSB0010853, consists of an albumin-binding nanobody framed by two HER3-targeting nanobodies. Four days after injection, [<sup>89</sup>Zr]Zr-MSB0010853 provided higher tumor-to-blood ratios than a bispecific trastuzumab-Fab-HRG conjugate, [<sup>89</sup>Zr]Zr-GSK2849330, or [<sup>89</sup>Zr]Zr-lumretuzumab (100–102). A <sup>64</sup>Cu-labeled F(ab')<sub>2</sub>

fragment and a  $^{68}\text{Ga}$ -labeled HER3-targeting peptide ( $^{68}\text{Ga}$ ]-Ga-NOTA-HER3P1) could visualize therapy-induced changes in HER3 expression in mice (99,103). Unfortunately, no biodistribution data are available for the  $\text{F(ab}')_2$  fragment. The biodistribution of  $^{68}\text{Ga}$ ]-Ga-NOTA-HER3P1 was characterized by rapid washout and uptake in xenografts was  $< 1\%$  injected activity (IA)/g one hour after injection (91).

Affibody molecules for PET and SPECT imaging of HER3 expression have been developed and have shown good image contrast as early as 1 h pi. They were also able to distinguish between HER3 expression levels in different xenografts models (104). Moreover, they bound the HER3 receptor with high affinity and provided excellent tumor-to-blood ratios, thanks to their fast clearance from blood (93,97).

## Affibody Molecules for Medical Applications in Cancer

Affibody molecules are a sub-class of ESPs that were first reported in 1997 (105). They are 58-amino acid, three-helical, high-affinity scaffold proteins engineered from the B-domain of the immunoglobulin-binding domain of staphylococcal protein A (106). Their size (7–8 kDa) is approximately 20-times smaller than the size of a full-length mAb and half the size of the smallest antibody fragments, nanobodies (106). Affibody molecules can be generated against a large variety of targets through randomization of 13 amino acids on helices one and two (107). EGFR, HER2, IGFR-1, PD-L1, CD28, and CAIX are some examples for cancer-related targets against which affibody molecules have been selected (49,107).

The robust yet versatile scaffold framework allows for, for example, multimerization to modulate valency and specificity, or functionalization, such as albumin-binding for extended blood circulation (106,107). The scaffold itself is cysteine-free, but addition of a unique C-terminal cysteine allows for site-specific conjugation of chelators for radiolabeling, or cytotoxic payloads (106,107). Because of their small size, affibody molecules have high tissue penetration and are rapidly cleared from the body via the kidneys (107).

Their amenability and small size make affibody molecules excellent probes for molecular imaging and targeted therapy (64,106). Modification of the local charge and hydrophilicity have been shown to affect the biodistribution and targeting properties of anti-HER2 affibody molecules (73,77). The HER2-targeting  $^{68}\text{Ga}$ -labeled affibody molecule  $^{68}\text{Ga}$ -ABY025 has successfully been applied in clinical trials for imaging of HER2-positive cancer lesions, achieving high image contrast within hours after injection (108,109). Affibody molecules labeled with therapeutic radionuclides or conjugated to cytotoxins have shown therapeutic effects in mice (110,111).

## HER3 Theranostics based on Affibody Molecules

Much of the early groundwork in the development of HER3-targeting affibody molecules for therapy and diagnostics of HER3-expressing malignancies has been described in detail in the doctoral theses of M. Malm (112), T. Bass (113), and M. Rosestedt (93).

Selection of the first generation of HER3-targeting affibody molecules was reported by Kronqvist et al. in 2011 (114). Second-generation affibody molecules against HER3, with improved affinity in the low picomolar range, were later reported by Malm et al. (115). Both generations of affibody molecules were engineered to be cross-reactive to murine ErbB3, thus allowing for a more accurate representation of the targeting system in preclinical models.

### Affibody Molecules for HER3-Targeted Therapy

The first generation of HER3-targeting affibody molecules demonstrated the ability to block the binding of HRG, and inhibit HRG-induced receptor phosphorylation and cell growth in vitro (116). The cytostatic effect encouraged further investigations of anti-HER3 affibody molecules for HER3-targeted cancer therapy. In subsequent studies, affibody molecules were conjugated to an ABD to prolong their circulatory half-life (117,118). A preclinical therapy study by our group, involving the second generation of a bivalent affibody conjugate called TAM-HER3 (two anti-HER3 affibody molecules linked by an ABD), showed similar therapeutic efficacy to the HER3-targeting antibody seribantumab (MM-121) (118,119). Recently, results by Schardt et al. indicated that the therapeutic effect of HER3-targeting affibody constructs depends on their valency (120). These findings strongly indicate that affibody-based therapy might be a viable approach for treatment of HER3-expressing cancer and warrant further investigation.

### Affibody Molecules for Imaging of HER3 Expression

In 2014, the first study using the  $^{99m}\text{Tc}$ -labeled HER3-targeting affibody molecule HEHEHE- $Z_{\text{HER3}:08699}$  demonstrated the general feasibility of an affibody-based approach for imaging of HER3 expression in a preclinical model (92). [ $^{99m}\text{Tc}$ ]Tc- $Z_{\text{HER3}:08699}$  successfully imaged HER3 expression in two different HER3-expressing xenografts. Due to better blood clearance, the  $Z_{\text{HER3}:08698}$  (hereafter  $Z_{\text{HER3}}$ ) scaffold replaced the  $Z_{\text{HER3}:08699}$  scaffold in later studies (97). Up to this point, efforts by our group and others have been focused on the development of  $Z_{\text{HER3}}$ -based imaging agents labeled with various radionuclides for PET and SPECT (radiocobalt (96),  $^{18}\text{F}$  (using [ $^{18}\text{F}$ ]AIF chemistry, (94)),  $^{68}\text{Ga}$  (104),  $^{89}\text{Zr}$  (95),  $^{111}\text{In}$  (97),  $^{125}\text{I}$  (98)). The different variants were able to visualize HER3-expressing xenografts in mice as early as

1 h pi (94), and to distinguish between high and low expression in the targeted tissue (104).

The available data present strong indications for the suitability of radio-labeled affibody molecules as imaging agents for HER3 expression and for being a promising alternative to antibody-based tracers. However, the general challenges associated with imaging of HER3 expression remain. While the fast clearance of affibody molecules seems to be beneficial for imaging contrast, the activity uptake in organs with natural HER3 expression, especially the liver, and potential off-target interactions need to be investigated and addressed prior to further translational action.

# Aims of this Thesis

The overall aim of this thesis was to investigate the influence of different molecular modifications to improve the diagnostic and therapeutic potential of affibody-based agents in HER3-expressing cancers.

The individual papers included in this thesis aimed to:

- Investigate how the radiolabeling approach (choice of radiolabel, structure and charge of the radiometal/chelator complex) influenced the PET and SPECT imaging contrast of HER3-targeting affibody molecules (**Papers I–III**).
- Investigate how the modification of hydrophilicity influenced the imaging contrast of anti-HER3 affibody molecules (**Paper II**).
- Select the most favorable affibody conjugates for SPECT and PET imaging of HER3 expression (**Papers I–III**).
- Investigate the use of radiocobalt, a PET-isotope with intermediate half-life, for later time point affibody-based PET-imaging of HER3 expression (**Paper III**).
- Investigate the influence of valency and molecular design of affibody-ABD conjugates on the therapeutic efficacy in HER3-expressing cancer (**Paper V**).
- Compare optimized diagnostic and therapeutic agents with known HER3-targeting agents for HER3 theranostics (**Papers IV and V**).

# Methodology

## Affibody Production

Affibody molecules were produced at KTH Royal Institute of Technology in Stockholm, Sweden. A detailed description of the production can be found in the references (105,114).

## Radiolabeling

All conjugates were radiolabeled in metal-free conditions. Standard reaction conditions for labeling of the Z<sub>HER3</sub> affibody constructs are summarized in Table 4. If needed, standard labeling conditions were optimized to improve radiochemical yield and provide stable attachment of the radionuclide.

**Table 4.** Standard labeling conditions for the affibody molecule Z<sub>HER3</sub> with different radiometals.

Radionuclide	Buffer	Temperature	Incubation Time	Paper
<sup>68</sup> Ga	1 M ascorbic acid, pH 3.6	85 °C	15 min	II, III, IV,V
<sup>57</sup> Co*	0.2 M sodium acetate, pH 5.5	60 °C	45 min	III
<sup>111</sup> In	0.2 M ammonium acetate, pH 5.5	85 °C	40 min	I

\*used as a surrogate for <sup>55</sup>Co

In Paper IV, <sup>89</sup>Zr-labeling of the monoclonal antibody seribantumab (MM-121) and seribantumab-F(ab)<sub>2</sub> fragment via a DFO chelator was performed using a modified version of the protocol described in reference (121). Seribantumab-F(ab)<sub>2</sub> was also labeled with <sup>68</sup>Ga in 7.6 M sodium acetate buffer, pH 4, at room temperature.

In vitro stability of the radiolabeled conjugates was tested by incubating samples of the radiolabeled proteins in excess amounts of PBS, EDTA, or human serum.

## In Vitro Studies

### Cell lines

HER3-expressing cell lines BxPC-3 (pancreatic cancer, approx.  $17 \times 10^3$  receptors/cell) and DU145 (prostate cancer, approx.  $9.9 \times 10^3$  receptors/cell)

were used for the in vitro assays characterizing the radiolabeled and therapeutic conjugates (122).

#### *In Vitro Binding Specificity Assay*

The binding specificity assay is a qualitative assay that was used to validate the specific binding of the radiolabeled conjugate to its intended target (in this case HER3). The assay is performed by comparing the uptake of the radiolabeled conjugate in one set of cells with the uptake in a second set of cells, where the target receptors have been blocked (and are thus no longer available for binding).

#### *Uptake and Internalization Assay*

An uptake and internalization assay was performed to investigate the internalization profile of radiolabeled proteins after binding to the cells.

During the assay, cells are continuously incubated with the radiotracer at 37 °C. At pre-determined time points, the membrane-bound and internalized activities are collected. The “acid wash method” developed by Wällberg and Orlova (123) was used to separate the internalized activity from the membrane-bound activity. With this method, the membrane-bound activity could be collected after incubation of the cells with 0.2 M glycine buffer (with 0.15 M NaCl, 4 M Urea, pH 2) for 5 min on ice. The activity remaining thereafter is considered internalized and can be collected by scraping cell lysates after incubation with 1 M NaOH for 30 min at 37 °C.

#### *Affinity Measurements*

The binding affinity to the intended molecular target is an important characteristic of a potential radiotracer as it describes the strength of the binding between the two. The LigandTracer technology allows measurement of the binding of radiolabeled molecules to living cells in real time and determination of the kinetic properties of the ligand-target interaction.

#### *Phospho-ELISA and in Vitro Proliferation Assay*

These assays were used in Paper V to evaluate the therapeutic potential of therapeutic anti-HER3 affibody conjugates in vitro prior to the in vivo therapy experiment.

Blocking the HER3 receptor and preventing receptor phosphorylation is one mechanism of action for HER3-targeted therapy. A commercially available Phospho-ELISA kit was used to investigate the ability of the anti-HER3 affibody conjugates to inhibit the phosphorylation in the presence of the HER3-stimulating ligand HRG.

The in vitro proliferation assay was used to study the effect of the therapeutic anti-HER3 affibody conjugates on cell growth. For this assay, BxPC-3 cells were incubated with the therapeutic conjugates at 37 °C for 5 days. At

the end of the incubation period, cell viability was measured and compared with a control group.

## In Vivo Studies

### *Mouse Model*

All in vivo experiments were conducted in immune-deficient Balb/c nu/nu mice. Mice were inoculated with BxPC-3 pancreatic cancer cells and allowed to develop visible xenografts prior to the experiments. Ethical permission for the animal studies was obtained from the Ethics Committee for Animal Research in Uppsala.

### *Biodistribution and in Vivo Specificity*

Biodistribution and in vivo specificity experiments were conducted to study the biodistribution and targeting properties of the developed molecules in a more complex living system. An overview of the injected protein doses and activities used in the biodistribution studies is shown in Table 5.

**Table 5.** Intravenously injected amounts of protein and activity for biodistribution studies

Molecule	Radiolabel	Protein dose/mouse (µg)	Injected activity/mouse (MBq)	Paper(s)
Z <sub>HER3</sub>	<sup>111</sup> In	2	0.03	I
	<sup>68</sup> Ga	2	0.3 - 0.7	II, III, IV
	<sup>57</sup> Co	2	0.03	III
Seribantumab	<sup>89</sup> Zr	35	0.05 - 0.08	IV
Seribantumab-F(ab') <sub>2</sub>	<sup>68</sup> Ga	27	0.25	IV
	<sup>89</sup> Zr	27	0.04 - 0.05	IV

For the in vivo specificity studies performed in Papers I–III, animals were co-injected with excess amounts of HER3-targeting affibody (70 µg) to block HER3 receptors. In Paper IV, in vivo specificity of [<sup>89</sup>Zr]Zr-seribantumab and [<sup>68</sup>Ga]Ga/[<sup>89</sup>Zr]Zr-seribantumab-F(ab')<sub>2</sub> was studied using mice bearing HER3-negative RAMOS xenografts.

### *Preclinical Imaging*

Preclinical imaging was performed using nanoPET/CT and nanoSPECT/CT to visualize the activity distribution and confirm the results from the biodistribution studies. Mice were intravenously injected with the maximum possible activity, while adhering to the protein doses indicated in Table 5.

### *Therapy Study*

In the work described in Paper V, an in vivo therapy study was performed in BxPC-3 xenograft-bearing mice to investigate the therapeutic efficacy of our

developed affibody conjugates. Mice were treated with intraperitoneal injection of conjugate solution or PBS (control). Tumor size was measured, and mouse status and well-being were assessed two times per week. Mice were euthanized when they reached one of the pre-determined humane endpoints or at the practical endpoint of 93 days after treatment start.

# The Present Investigation

## **Paper I: Optimization of HER3 Expression Imaging using Affibody Molecules: Influence of Chelator for Labeling with Indium-111**

### **Background**

Previous studies by our group and others have demonstrated that radiolabeled anti-HER3 affibody molecules are promising probes for radionuclide molecular imaging of HER3 expression (92,97,104). As for all HER3-imaging probes, the moderate endogenous expression and low HER3 expression in cancer cells limit the imaging contrast and sensitivity for detection of hepatic metastases, which are common in many HER3-expressing cancers. It appears that non-specific uptake mechanisms contribute to tracer accumulation in the liver, in addition to the HER3-mediated uptake (53,96,124). Reduction of this non-specific hepatic uptake would be desirable to improve HER3 image quality.

The polarity and local charge of the targeting molecule can influence the non-specific accumulation in the liver (53,124). One strategy to modify the local distribution of charge in affibody-based radiotracers is modification of the radiolabeling approach, particularly through the (macrocylic) chelator. The charge of the radiometal/chelator complex can vary depending on the metal and charged groups available on the chelator and thereby influence the biodistribution and imaging properties of the imaging agent (73,78). Modifying the macrocylic chelator has been shown to have noticeable influence on the biodistribution and imaging contrast of HER2-targeting affibody molecules (73,126). An increase of (local) negative charge of the targeting molecules was found to reduce non-specific hepatic uptake and improve blood clearance.

### **Aim**

The aim of Paper I was to investigate how the choice of macrocylic chelator influenced the biodistribution and SPECT imaging properties of <sup>111</sup>In-labeled HER3-targeting affibody molecules.

We hypothesized that we could lower the non-specific hepatic uptake and improve the imaging contrast of HER3-targeting affibody molecules by mod-

ification and increase of the negative charge of the radionuclide/chelator complex. For this purpose, we created a panel of four affibody variants based on Z<sub>08698</sub> (Z<sub>HER3</sub>) that differed in the macrocyclic chelator conjugated to the C-terminus. For simplicity, the variants are hereafter referred to as Z<sub>HER3</sub>-X with X = NOTA, NODAGA, DOTA, DOTAGA.

## Results

All variants were stably labeled with indium-111. HER3-mediated binding was confirmed in HER3-expressing BxPC-3 and DU145 cells. Binding affinities of the labeled conjugates were in the range 0.008–0.16 nM, measured in real time with LigandTracer. The internalized fraction of cell-bound affibody molecules was below 36% for all conjugates after 24 hours of continuous incubation (Figure 3).

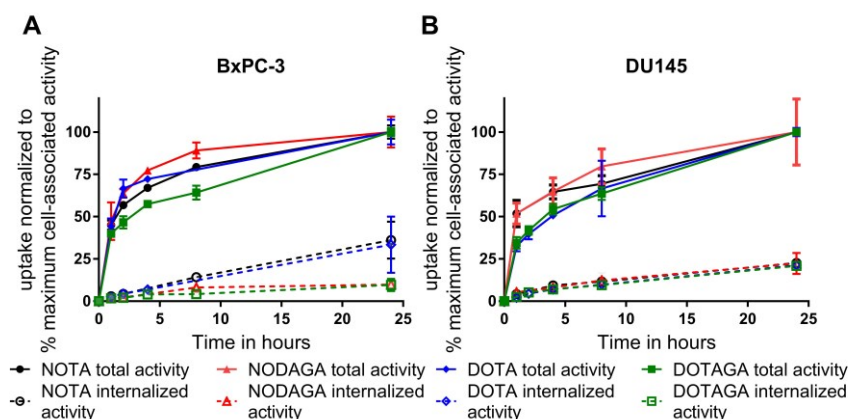


**Figure 3.** Uptake and internalization of [<sup>111</sup>In]In-Z<sub>HER3</sub>-X in (A) BxPC-3 and (B) DU145 cells. Cells were continuously incubated with 0.1 nM of the radiolabeled conjugates.

The biodistribution showed accumulation of [<sup>111</sup>In]In-Z<sub>HER3</sub>-X in HER3-expressing xenografts and in organs with endogenous mErbB3 (murine analog of HER3) expression (Figure 4A, B). As expected, the conjugates were cleared via the renal pathway. Activity uptake in the xenografts was between 3–4%IA/g for all conjugates, with high retention from 4 h to 24 h pi and no significant differences between the conjugates. However, the activity uptake in normal organs and tissue differed between the conjugates. Activity concentration of [<sup>111</sup>In]In-Z<sub>HER3</sub>-NOTA in blood was significantly higher than for any other conjugate at both selected time points. Importantly, the hepatic uptake of [<sup>111</sup>In]In-Z<sub>HER3</sub>-DOTA and [<sup>111</sup>In]In-Z<sub>HER3</sub>-DOTAGA was significantly lower than that of [<sup>111</sup>In]In-Z<sub>HER3</sub>-NOTA, at both time points (Figure 5).

Because the activity uptake in healthy organs and tissues decreased with time without significant change in tumor uptake, the tumor-to-non-tumor ratios generally increased with time (Figure 4C, D). Twenty-four hours pi,

$[^{111}\text{In}]\text{In-Z}_{\text{HER3}}\text{-DOTAGA}$  had significantly higher tumor-to-liver, -spleen and -muscle ratios, and an almost 2-fold higher tumor-to-blood ratio than  $[^{111}\text{In}]\text{In-Z}_{\text{HER3}}\text{-NOTA}$ . NanoSPECT/CT imaging clearly visualized the xenografts and confirmed the results from the ex vivo study (Figure 6).

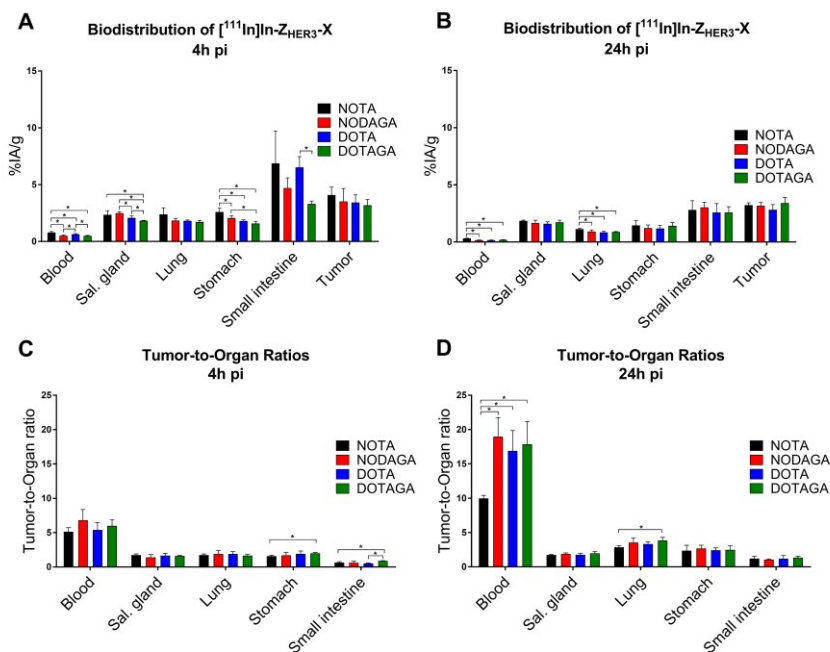


**Figure 4.** (A, B) Biodistribution of  $[^{111}\text{In}]\text{In-Z}_{\text{HER3}}\text{-X}$  in Balb/c nu/nu mice bearing HER3-expressing BxPC-3 xenografts 4 h and 24 h pi, presented as %IA/g. (C, D) Tumor-to-organ ratios 4 h and 24 h pi. Mice were injected with 2  $\mu\text{g}$  (30 kBq)  $[^{111}\text{In}]\text{In-Z}_{\text{HER3}}\text{-X}$  in the tail vein. \*indicates statistical significance between the conjugates ( $p < 0.05$ ).

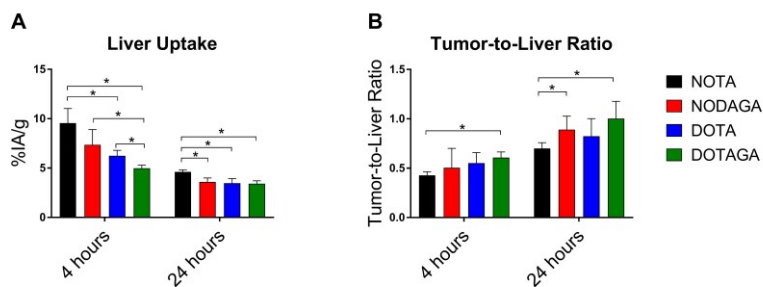


**Figure 5.** (A) Liver uptakes and (B) tumor-to-liver ratios of  $[^{111}\text{In}]\text{In-Z}_{\text{HER3}}\text{-X}$  at 4 h and 24 h pi. \*indicates statistically significant ( $p < 0.05$ ) differences between the conjugates.

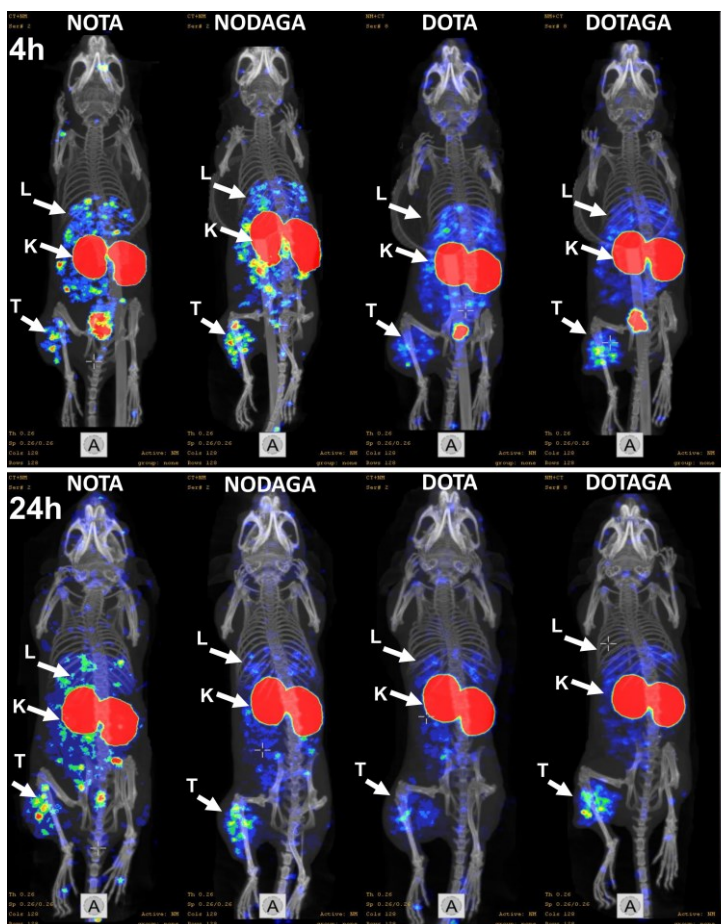


**Figure 6.** NanoSPECT/CT imaging of  $[^{111}\text{In}]\text{In-Z}_{\text{HER3-X}}$  in Balb/c nu/nu mice bearing BxPC-3 xenografts 4 h and 24 h pi. Mice were injected with  $2\ \mu\text{g}$  ( $\sim 1.5\ \text{MBq}$ ) of  $[^{111}\text{In}]\text{In-Z}_{\text{HER3-X}}$ . Tracer uptake in tumors (T) could be visualized clearly. High activity uptake was seen in kidneys (K) and mErbB3-expressing organs, especially the liver (L).

## Discussion

In this study, we aimed to investigate the influence of the  $[^{111}\text{In}]\text{In}/\text{chelator}$  complex on the biodistribution of the HER3-targeting affibody molecule  $Z_{\text{HER3}}$ . We hypothesized that an increased negative charge of the radio-metal/chelator complex might decrease the uptake of  $[^{111}\text{In}]\text{In-Z}_{\text{HER3}}$  in the liver and would thereby improve the image contrast, particularly in the liver.

No major differences were observed between the conjugates in vitro. In vivo, the general biodistribution pattern of  $[^{111}\text{In}]\text{In-Z}_{\text{HER3-X}}$  (blood clearance, elimination via renal pathway) was coherent with previous reports on HER3-targeting affibody molecules (97). The choice of chelator did not greatly impact the tumor-targeting properties of  $[^{111}\text{In}]\text{In-Z}_{\text{HER3}}$ , but had significant impact on the uptake in normal organs and the imaging properties of  $[^{111}\text{In}]\text{In-}$

$Z_{\text{HER3-X}}$ . In particular, we observed that the activity uptake in the liver decreased with increasing negative charge of the indium-111/chelator complex. The  $[^{111}\text{In}]\text{In-}Z_{\text{HER3-NOTA}}$  conjugate with a single positive charge of the radiometal/chelator complex had significantly higher hepatic uptake than any other conjugate at both investigated time points. The variant with the most negatively charged complex,  $[^{111}\text{In}]\text{In-}Z_{\text{HER3-DOTAGA}}$ , had the lowest uptake in liver, which was half of the liver uptake of  $[^{111}\text{In}]\text{In-}Z_{\text{HER3-NOTA}}$  at 4 h pi. We speculated that the local negative charge of the  $[^{111}\text{In}]\text{In-DOTAGA}$  complex resulted in reduced off-target interaction and thus led to the decrease in hepatic uptake (53,124). Similar influence of the negative charge of the  $[^{111}\text{In}]\text{In-DOTAGA}$  complex was observed when it was compared with a neutrally charged  $[^{111}\text{In}]\text{In-DOTA}$  complex conjugated to a HER2-targeting affibody molecule (126). The charge also appeared to have an influence on blood clearance, as the  $Z_{\text{HER3}}$  variant with the positively charged  $[^{111}\text{In}]\text{In-NOTA}$  complex cleared slower from blood than the other variants, presumably due to stronger interactions with blood proteins.

The results from the biodistribution translated into the SPECT images and  $[^{111}\text{In}]\text{In-}Z_{\text{HER3-DOTAGA}}$  provided the most favorable imaging contrast overall at both time points.

## Conclusion

In conclusion, the imaging properties of anti-HER3 affibody molecules are influenced by the composition and charge of the radiometal/chelator complex. The increased negative charge of the  $[^{111}\text{In}]\text{In-DOTAGA}$  complex improved the imaging contrast in the liver by reducing non-specific hepatic uptake. We therefore concluded that  $[^{111}\text{In}]\text{In-}Z_{\text{HER3-DOTAGA}}$  was the most favorable variant for in vivo SPECT imaging of HER3 expression.

## **Paper II: Molecular Design of HER3-Targeting Affibody Molecules: Influence of Chelator and Presence of HEHEHE-Tag on Biodistribution of <sup>68</sup>Ga-Labeled Tracers**

### **Background**

Paper I showed that the SPECT imaging contrast of anti-HER3 affibody molecules was influenced by the composition of the radiometal/chelator complex and that an increased negative charge of the complex could significantly decrease non-specific hepatic uptake (127). Because the detection of liver metastasis is relevant for many types of HER3-expressing cancers, we wanted to further investigate factors that could improve the hepatic contrast of our HER3-targeting affibody molecules.

Besides the influence of the charge of the radiometal/chelator complex, there are also indications that the presence of hydrophilic patches could lower hepatic uptake of targeting molecules (53). A histidine-glutamate tag ((HE)<sub>3</sub>-tag) is negatively charged and hydrophilic and can be used as a potential purification tag. For example, it has been reported that the placement of a (HE)<sub>3</sub>-tag at the N-terminus of anti-HER2 affibody molecules lowers hepatic uptake by up to a factor of 10 (76,128). Similar observations that a general increase in hydrophilicity through exchange of one or several amino acids or modification of linkers decreases hepatic uptake have been reported for targeting agents other than affibody molecules (129,130).

SPECT cameras are generally more widely available than PET cameras, but PET imaging is often preferred due to its higher sensitivity (45). Gallium-68 is a clinically used PET isotope with a half-life of 68 minutes. An initial study demonstrated the feasibility of [<sup>68</sup>Ga]Ga-(HE)<sub>3</sub>-Z<sub>HER3</sub>-NOTA to image HER3 expression and distinguish between high and low expressing xenografts in rodents (104). The results we had seen with indium-111 hinted that choosing an optimal gallium-68/chelator complex could potentially improve imaging properties of <sup>68</sup>Ga-labeled Z<sub>HER3</sub>. Gallium-68 and indium-111 are both trivalent metals and therefore form complexes of similar charge with the commonly used macrocyclic chelators NOTA, NODAGA, DOTA and DOTAGA. However, due to their difference in ionic radius, they form metal/chelator complexes with different geometries (131).

DOTA could be considered the most frequently used chelator for gallium-labeling (2). Although the DOTA macrocycle, as an octadentate ligand, can more than sufficiently saturate the coordination sphere of Ga(III) ions, its chelating pocket is rather large for a relatively small ion such as gallium. Because of its relatively small size, gallium prefers triaza-chelators with smaller chelating pockets, like NOTA or its derivative NODAGA, which provide an almost perfect fit for the gallium ion (131,132).

## Aim

The overall aim of Paper II was to improve affibody-based  $^{68}\text{Ga}$ -PET imaging of HER3 expression and gain further knowledge on how different variables influence the properties of affibody-based imaging probes. We therefore investigated i) the influence of a negatively charged, hydrophilic, N-terminal  $(\text{HE})_3$ -tag, and ii) the influence of charge of different C-terminal  $^{68}\text{Ga}$ /chelator complexes with NOTA and the NOTA-derivative NODAGA on the imaging properties of  $Z_{\text{HER3}}$ .

## Results

Four different gallium-68-labeled variants of the anti-HER3 affibody molecule  $Z_{\text{HER3}}$  were included in this study: two  $(\text{HE})_3$ -tag-containing variants ( $(\text{HE})_3$ - $Z_{\text{HER3}}$ ) and two non-tagged variants ( $Z_{\text{HER3}}$ ) conjugated to either a NOTA or a NODAGA chelator at the C-terminus.  $[^{68}\text{Ga}]\text{Ga}-(\text{HE})_3$ - $Z_{\text{HER3}}$ -NOTA had been extensively characterized in vitro and in vivo in a previous study (104), and was therefore not included in the in vitro experiments and the in vivo specificity study.

All conjugates were labeled with  $^{68}\text{Ga}$  with sufficient radiochemical yield and the final products had high radiochemical purity ( $> 98\%$ ). Binding in vitro was HER3-mediated and the internalization of all variants was equally slow in vitro (Figure 7).

Biodistribution and in vivo specificity were studied in BxPC-3 xenograft-bearing mice 3 h pi. Injection of excess amounts of unlabeled  $Z_{\text{HER3}}$  affibody resulted in significant decrease in activity uptake in xenografts and HER3-expressing organs (liver, stomach, and small intestines), confirming in vivo binding specificity of the affibody conjugates (Figure 8). The general activity uptake pattern correlated with those in previous studies of  $[^{68}\text{Ga}]\text{Ga}-(\text{HE})_3$ - $Z_{\text{HER3}}$ -NOTA (104). However, presence or absence of the  $(\text{HE})_3$ -tag and the choice of chelator influenced the biodistribution of the  $Z_{\text{HER3}}$  conjugates (Tables 6 and 7).

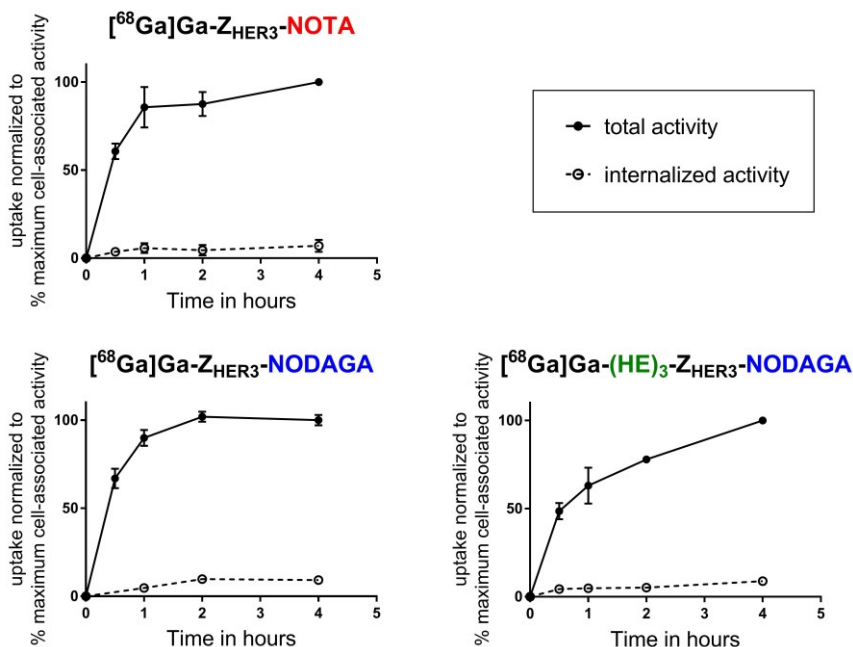


**Figure 7.** Uptake and internalization of  $[^{68}\text{Ga}]\text{Ga-Z}_{\text{HER}3}\text{-NOTA}$ ,  $[^{68}\text{Ga}]\text{Ga-Z}_{\text{HER}3}\text{-NODAGA}$ , and  $[^{68}\text{Ga}]\text{Ga-(HE)}_3\text{-Z}_{\text{HER}3}\text{-NODAGA}$  in BxPC-3 cells. Internalization of  $[^{68}\text{Ga}]\text{Ga-(HE)}_3\text{-Z}_{\text{HER}3}\text{-NOTA}$  has been studied before (104).

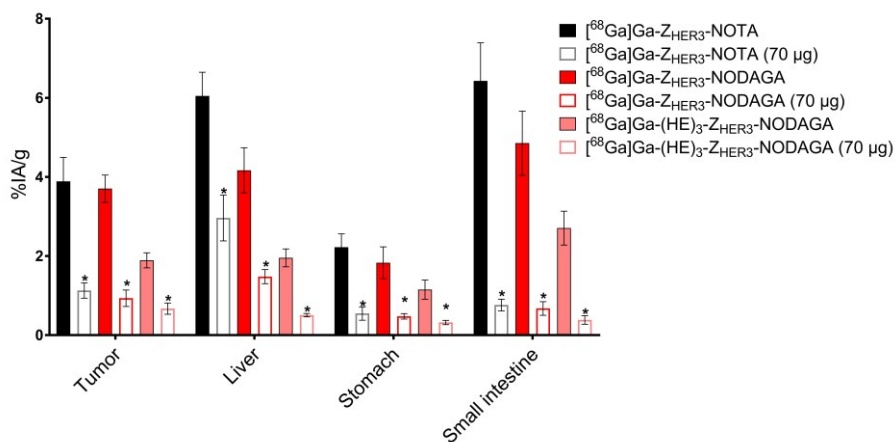


**Figure 8.** In vivo specificity of  $[^{68}\text{Ga}]\text{Ga-Z}_{\text{HER}3}\text{-NOTA}$ ,  $[^{68}\text{Ga}]\text{Ga-Z}_{\text{HER}3}\text{-NODAGA}$ , and  $[^{68}\text{Ga}]\text{Ga-(HE)}_3\text{-Z}_{\text{HER}3}\text{-NODAGA}$ . Mice were injected with 2  $\mu\text{g}$  of radiolabeled affibody. For the specificity test, the protein dose was adjusted to 70  $\mu\text{g}$  using an unlabeled anti-HER3 affibody molecule. \* indicates statistically significant difference ( $p < 0.05$ ) in uptake between mice injected with 2  $\mu\text{g}$  and 70  $\mu\text{g}$ . The specificity of  $[^{68}\text{Ga}]\text{Ga-(HE)}_3\text{-Z}_{\text{HER}3}\text{-NOTA}$  has been shown previously (104).

Presence of the (HE)<sub>3</sub>-tag reduced the overall activity uptake in normal organs and tissues, including tumor and liver. Hepatic uptake of [<sup>68</sup>Ga]Ga-(HE)<sub>3</sub>-Z<sub>HER3</sub>-X (X=NOTA,NODAGA) was down to almost a third of that of the non-tagged variants, but tumor uptake was only reduced by about half. This resulted in a higher tumor-to-liver contrast for the (HE)<sub>3</sub>-containing variants, despite the lower tumor uptake.

The choice of chelator influenced hepatic uptake, but had no significant effect on tumor uptake. The non-tagged NODAGA-conjugated Z<sub>HER3</sub> with a neutral charge of the <sup>68</sup>Ga/chelator complex had significantly lower hepatic uptake than its NOTA-conjugated counterpart with a positively charged complex. The effect of the chelator on normal organ uptake was less pronounced for the (HE)<sub>3</sub>-tagged conjugates. In fact, the only significant difference in tumor-to-non-tumor ratios between [<sup>68</sup>Ga]Ga-(HE)<sub>3</sub>-Z<sub>HER3</sub>-NOTA and [<sup>68</sup>Ga]Ga-(HE)<sub>3</sub>-Z<sub>HER3</sub>-NODAGA was in the tumor-to-blood ratio, which was almost two-fold higher for [<sup>68</sup>Ga]Ga-(HE)<sub>3</sub>-Z<sub>HER3</sub>-NODAGA.

NanoPET/CT imaging performed with [<sup>68</sup>Ga]Ga-(HE)<sub>3</sub>-Z<sub>HER3</sub>-X and [<sup>68</sup>Ga]Ga-Z<sub>HER3</sub>-X could clearly visualize the HER3-expressing BxPC-3 xenografts (Figure 9).

**Table 6.** Biodistribution results of [<sup>68</sup>Ga]Ga-Z<sub>HER3</sub>-NOTA, [<sup>68</sup>Ga]Ga-(HE)<sub>3</sub>-Z<sub>HER3</sub>-NOTA, [<sup>68</sup>Ga]Ga-Z<sub>HER3</sub>-NODAGA and [<sup>68</sup>Ga]Ga-(HE)<sub>3</sub>-Z<sub>HER3</sub>-NODAGA in Balb/c nu/nu mice with BxPC-3 xenografts 3 h pi presented as % injected activity per gram tissue (average ± SD).

Organ	[ <sup>68</sup> Ga]Ga-Z <sub>HER3</sub> -NOTA	[ <sup>68</sup> Ga]Ga-(HE) <sub>3</sub> -Z <sub>HER3</sub> -NOTA	[ <sup>68</sup> Ga]Ga-Z <sub>HER3</sub> -NODAGA	[ <sup>68</sup> Ga]Ga-(HE) <sub>3</sub> -Z <sub>HER3</sub> -NODAGA
Blood	0.28 ± 0.04 <sup>d</sup>	0.22 ± 0.08	0.31 ± 0.06 <sup>f</sup>	0.126 ± 0.004 <sup>d,f</sup>
Salivary glands	2.2 ± 0.3 <sup>a,d</sup>	0.9 ± 0.3 <sup>a,c</sup>	1.8 ± 0.3 <sup>c,f</sup>	1.0 ± 0.1 <sup>d,f</sup>
Lung	1.7 ± 0.1 <sup>a,d</sup>	0.9 ± 0.3 <sup>a,c</sup>	1.6 ± 0.2 <sup>c,f</sup>	0.94 ± 0.06 <sup>d,f</sup>
Liver	6.0 ± 0.6 <sup>a,d,e</sup>	2.2 ± 0.7 <sup>a,c</sup>	4.5 ± 0.6 <sup>c,e,f</sup>	2.0 ± 0.2 <sup>d,f</sup>
Spleen	0.67 ± 0.06 <sup>d,e</sup>	0.3 ± 0.1	0.45 ± 0.6 <sup>e</sup>	0.3 ± 0.01 <sup>d</sup>
Stomach	2.2 ± 0.3 <sup>a,d</sup>	0.9 ± 0.4 <sup>a,c</sup>	1.8 ± 0.4 <sup>c,f</sup>	1.2 ± 0.2 <sup>d,f</sup>
Small intestine	6 ± 2 <sup>a,d</sup>	2.0 ± 0.1 <sup>a,c</sup>	5.1 ± 0.8 <sup>c,f</sup>	2.7 ± 0.4 <sup>d,f</sup>
Kidney	214 ± 22 <sup>a,d</sup>	138 ± 28 <sup>a,b,c</sup>	237 ± 24 <sup>c,f</sup>	324 ± 11 <sup>b,d,f</sup>
Tumor	3.9 ± 0.6 <sup>a,d</sup>	1.9 ± 0.7 <sup>a,c</sup>	3.3 ± 0.5 <sup>c,f</sup>	1.9 ± 0.2 <sup>d,f</sup>
Muscle	0.19 ± 0.04	0.12 ± 0.08	0.18 ± 0.04	0.11 ± 0.04
Bone	0.42 ± 0.08	0.32 ± 0.09	0.42 ± 0.1	0.4 ± 0.2

Statistical significance (p < 0.05) between <sup>a</sup> [<sup>68</sup>Ga]Ga-(HE)<sub>3</sub>-Z<sub>HER3</sub>-NOTA and [<sup>68</sup>Ga]Ga-Z<sub>HER3</sub>-NOTA, <sup>b</sup> [<sup>68</sup>Ga]Ga-(HE)<sub>3</sub>-Z<sub>HER3</sub>-NOTA and [<sup>68</sup>Ga]Ga-(HE)<sub>3</sub>-Z<sub>HER3</sub>-NODAGA, <sup>c</sup> [<sup>68</sup>Ga]Ga-(HE)<sub>3</sub>-Z<sub>HER3</sub>-NOTA and [<sup>68</sup>Ga]Ga-Z<sub>HER3</sub>-NODAGA, <sup>d</sup> [<sup>68</sup>Ga]Ga-Z<sub>HER3</sub>-NOTA and [<sup>68</sup>Ga]Ga-(HE)<sub>3</sub>-Z<sub>HER3</sub>-NODAGA, <sup>e</sup> [<sup>68</sup>Ga]Ga-Z<sub>HER3</sub>-NOTA and [<sup>68</sup>Ga]Ga-Z<sub>HER3</sub>-NODAGA, <sup>f</sup> [<sup>68</sup>Ga]Ga-(HE)<sub>3</sub>-Z<sub>HER3</sub>-NODAGA and [<sup>68</sup>Ga]Ga-Z<sub>HER3</sub>-NODAGA

**Table 7.** Tumor-to-organ ratios for [ $^{68}\text{Ga}$ ]Ga-Z<sub>HER3</sub>-NOTA, [ $^{68}\text{Ga}$ ]Ga-(HE)<sub>3</sub>-Z<sub>HER3</sub>-NOTA, [ $^{68}\text{Ga}$ ]Ga-Z<sub>HER3</sub>-NODAGA, and [ $^{68}\text{Ga}$ ]Ga-(HE)<sub>3</sub>-Z<sub>HER3</sub>-NODAGA in Balb/c nu/nu mice with BxPC-3 xenografts 3 h pi (average  $\pm$  SD).

Organ	[ $^{68}\text{Ga}$ ]Ga-Z <sub>HER3</sub> -NOTA	[ $^{68}\text{Ga}$ ]Ga-(HE) <sub>3</sub> -Z <sub>HER3</sub> -NOTA	[ $^{68}\text{Ga}$ ]Ga-Z <sub>HER3</sub> -NODAGA	[ $^{68}\text{Ga}$ ]Ga-(HE) <sub>3</sub> -Z <sub>HER3</sub> -NODAGA
Blood	14 $\pm$ 2 <sup>a,e</sup>	8.5 $\pm$ 0.6 <sup>a,b,c</sup>	11 $\pm$ 1 <sup>c,e,f</sup>	15 $\pm$ 2 <sup>b,f</sup>
Salivary glands	1.8 $\pm$ 0.2	2.0 $\pm$ 0.1	1.9 $\pm$ 0.2	1.8 $\pm$ 0.4
Lung	2.3 $\pm$ 0.4	2.0 $\pm$ 0.2	2.0 $\pm$ 0.2	2.0 $\pm$ 0.1
Liver	0.64 $\pm$ 0.07 <sup>d</sup>	0.83 $\pm$ 0.10	0.8 $\pm$ 0.2	1.0 $\pm$ 0.2 <sup>d</sup>
Spleen	5.8 $\pm$ 0.6	5.5 $\pm$ 0.8	7.5 $\pm$ 0.9	8 $\pm$ 1
Stomach	1.8 $\pm$ 0.5	2.2 $\pm$ 0.2	1.8 $\pm$ 0.5	1.7 $\pm$ 0.3
Small intestine	0.8 $\pm$ 0.4	0.75 $\pm$ 0.08	0.7 $\pm$ 0.1	0.7 $\pm$ 0.1
Muscle	20 $\pm$ 2	16 $\pm$ 3	20 $\pm$ 4	14 $\pm$ 1
Bone	9 $\pm$ 1	6.0 $\pm$ 0.7	9 $\pm$ 3	7 $\pm$ 5

Statistical significance ( $p < 0.05$ ) between <sup>a</sup> [ $^{68}\text{Ga}$ ]Ga-(HE)<sub>3</sub>-Z<sub>HER3</sub>-NOTA and [ $^{68}\text{Ga}$ ]Ga-Z<sub>HER3</sub>-NOTA, <sup>b</sup> [ $^{68}\text{Ga}$ ]Ga-(HE)<sub>3</sub>-Z<sub>HER3</sub>-NOTA and [ $^{68}\text{Ga}$ ]Ga-(HE)<sub>3</sub>-Z<sub>HER3</sub>-NODAGA, <sup>c</sup> [ $^{68}\text{Ga}$ ]Ga-(HE)<sub>3</sub>-Z<sub>HER3</sub>-NOTA and [ $^{68}\text{Ga}$ ]Ga-Z<sub>HER3</sub>-NODAGA, <sup>d</sup> [ $^{68}\text{Ga}$ ]Ga-Z<sub>HER3</sub>-NOTA and [ $^{68}\text{Ga}$ ]Ga-(HE)<sub>3</sub>-Z<sub>HER3</sub>-NODAGA, <sup>e</sup> [ $^{68}\text{Ga}$ ]Ga-Z<sub>HER3</sub>-NOTA and [ $^{68}\text{Ga}$ ]Ga-Z<sub>HER3</sub>-NODAGA, <sup>f</sup> [ $^{68}\text{Ga}$ ]Ga-(HE)<sub>3</sub>-Z<sub>HER3</sub>-NODAGA and [ $^{68}\text{Ga}$ ]Ga-Z<sub>HER3</sub>-NODAGA

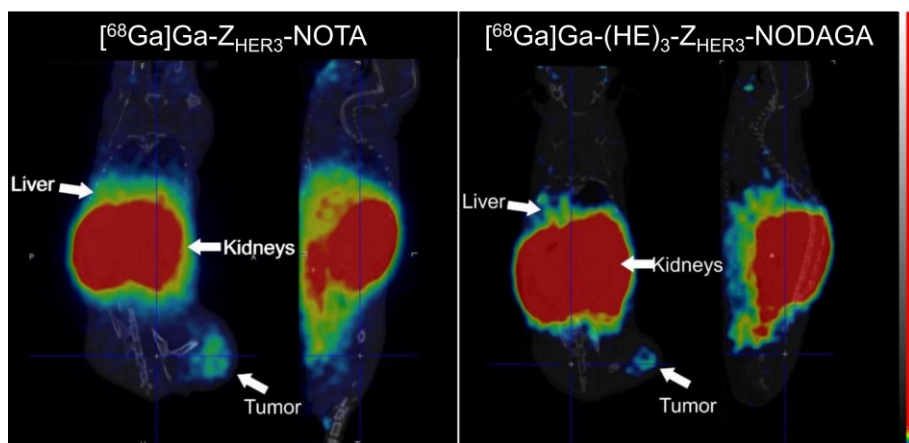


**Figure 9.** NanoPET/CT images of [ $^{68}\text{Ga}$ ]Ga-Z<sub>HER3</sub>-NOTA and [ $^{68}\text{Ga}$ ]Ga-(HE)<sub>3</sub>-Z<sub>HER3</sub>-NODAGA in mice with HER3-expressing BxPC-3 xenografts 3 h pi.

## Discussion

The in vivo behavior of affibody molecules and other targeting agents is influenced by many variables. Small modifications in the molecular design and the radiolabeling approaches could have a profound effect on both the target and off-target interactions and therefore on the imaging contrast.

Neither the presence of a (HE)<sub>3</sub>-tag nor the choice of the chelator had a negative impact on the stability of the radiolabel or on the in vitro and in vivo binding specificity of Z<sub>HER3</sub> towards HER3. The biodistribution of all tracers correlated with the general biodistribution pattern for HER3-targeting affibody molecules, including renal clearance and elevated uptake in organs

with mErbB3 expression (104). However, modification of local hydrophilicity and charge via an N-terminal (HE)<sub>3</sub>-tag and the macrocyclic chelator on the C-terminus influenced the clearance and tumor and normal organ uptake of [<sup>68</sup>Ga]Ga-Z<sub>HER3</sub>.

N-terminal placement of a negatively charged, hydrophilic (HE)<sub>3</sub>-tag reduced the uptake of the Z<sub>HER3</sub> conjugates in normal tissue and tumors, presumably because of increased clearance. However, the presence of the (HE)<sub>3</sub>-tag tended to affect the uptake in healthy organs, particularly liver, more than the uptake in xenografts. We concluded that the presence of the (HE)<sub>3</sub>-tag was favorable for in vivo imaging of HER3 expression, despite causing lower uptake in xenografts.

The results from this study further supported the conclusion from Paper I that a reduction of the positive charge of the radiometal/chelator complex could lower the hepatic uptake of Z<sub>HER3</sub> (127). The [<sup>68</sup>Ga]Ga-Z<sub>HER3</sub>-NODAGA conjugate with a neutrally charged chelator complex had 25% lower hepatic uptake compared with [<sup>68</sup>Ga]Ga-Z<sub>HER3</sub>-NOTA, with a positively charged complex. The presence of the (HE)<sub>3</sub>-tag appeared to mask the effect of the chelator complex charge on hepatic uptake. Nonetheless, combination of an (HE)<sub>3</sub>-tag and a NODAGA chelator significantly increased the tumor-to-liver ratio over the tumor-to-liver ratio seen with the non-tagged NOTA-conjugate.

Overall, [<sup>68</sup>Ga]Ga-(HE)<sub>3</sub>-Z<sub>HER3</sub>-NODAGA provided significantly higher tumor-to-blood ratios than [<sup>68</sup>Ga]Ga-(HE)<sub>3</sub>-Z<sub>HER3</sub>-NOTA and [<sup>68</sup>Ga]Ga-Z<sub>HER3</sub>-NODAGA and a significantly higher tumor-to-liver ratio than [<sup>68</sup>Ga]Ga-Z<sub>HER3</sub>-NOTA. We therefore considered it the most favorable variant of Z<sub>HER3</sub> for <sup>68</sup>Ga-PET imaging of HER3 expression.

## Conclusions

In this paper, we demonstrated that an increase of local hydrophilicity by addition of an N-terminal (HE)<sub>3</sub>-tag improved the clearance and reduced non-specific uptake of <sup>68</sup>Ga-labeled anti-HER3 affibody molecules in healthy organs. Confirming the results of Paper I, we found that a decrease in positive charge of the <sup>68</sup>Ga/chelator complex improved hepatic contrast. In summary, the combination of an N-terminal (HE)<sub>3</sub>-tag and a [<sup>68</sup>Ga]Ga-NODAGA complex at C-terminus provided the best contrast for <sup>68</sup>Ga-affibody PET imaging of HER3 expression.

## Paper III: Benefit of Later-Time-Point PET Imaging of HER3 Expression Using Optimized Radiocobalt-Labeled Affibody Molecules

### Background

The two major conclusions from Papers I and II were that an increase in negative charge of the radiometal/chelator complex could decrease the non-specific uptake in the liver and that increased hydrophilicity due to the presence of a (HE)<sub>3</sub>-tag facilitated clearance and reduced hepatic uptake of Z<sub>HER3</sub>. This led to improved tumor-to-background ratios and enhanced HER3 image contrast. An additional observation from Paper I was that later time point imaging improved the tumor-to-background ratios because of continuous clearance of activity from normal organs. This suggests that the use of longer-lived radionuclides for next-day imaging might improve imaging contrast.

PET imaging can provide higher sensitivity than SPECT imaging and is therefore generally preferred (43,45). <sup>68</sup>Ga ( $t_{1/2}({}^{68}\text{Ga}) = 68\text{min}$ ) and <sup>18</sup>F ( $t_{1/2}({}^{18}\text{F}) = 110\text{min}$ ) are commonly used radionuclides for PET imaging and are easily accessible, but do not allow for next-day PET imaging due to their relatively short half-lives. On the opposite, <sup>89</sup>Zr has a half-life of 3.3 days and is often used for imaging with antibody-based tracers. <sup>89</sup>Zr has also been used for radiolabeling of affibody molecules (95,133). The HER3-targeting affibody molecule [<sup>89</sup>Zr]Zr-DFO-Z<sub>HER3:08698</sub> was able to detect changes in HER3 expression in response to treatment with an HSP90 inhibitor in rodents (95). However, a drawback of this affibody conjugate was the 50% decrease of tumor-associated activity from 3 h to 24 h, which prevented any increase of tumor-to-non-tumor contrast with time. Another possible disadvantage of the <sup>89</sup>Zr-label is that its half-life might be too long, making it a less-than-ideal match for the fast kinetics of affibody molecules.

Cobalt-55, with a half-life of 17.5 h, could be a compromise between short-lived radionuclides like <sup>68</sup>Ga and <sup>18</sup>F and long-lived ones like <sup>89</sup>Zr. An initial study with the radiocobalt-labeled anti-HER3 affibody molecule (HE)<sub>3</sub>-Z<sub>HER3</sub>-NOTA showed promising results: for the first time, a tumor-to-liver ratio > 1 was achieved using an HER3-targeting affibody-based imaging agent (125). The radiocobalt label is slightly different from indium and gallium labels. Cobalt and gallium have considerably smaller ionic radii than indium, which may influence their preference of type of macrocyclic chelator. Furthermore, cobalt engages in the radiolabeling in a divalent state (134), whereas gallium and indium are trivalent. Thus, they form chelator complexes of different charges. The lower charge of the cobalt-chelator complex could potentially benefit hepatic contrast.

## Aim

Paper III had two aims. The first was to select the chelator providing the best imaging contrast of radiocobalt-labeled  $(\text{HE})_3\text{-Z}_{\text{HER}3}$ . The  $(\text{HE})_3$ -tagged variant of  $\text{Z}_{\text{HER}3}$  was chosen based on the results from Paper II. We compared three new radiocobalt-labeled variants of  $(\text{HE})_3\text{-Z}_{\text{HER}3}$  (hereafter referred to as  $(\text{HE})_3\text{-Z}_{\text{HER}3}\text{-X}$  with  $\text{X} = \text{NODAGA}$ ,  $\text{DOTA}$ , or  $\text{DOTAGA}$ ) with the previously reported  $[^{57}\text{Co}]\text{Co-}(\text{HE})_3\text{-Z}_{\text{HER}3}\text{-NOTA}$ , in vitro and in vivo.

The second aim of this study was to investigate potential benefits of delayed PET imaging with the longer-lived radiocobalt-label compared with early time point imaging with a short-lived  $^{68}\text{Ga}$ -label. For this purpose, we included a side-by-side in vivo comparison of the selected radiocobalt-labeled conjugate with  $[^{68}\text{Ga}]\text{Ga-}(\text{HE})_3\text{-Z}_{\text{HER}3}\text{-NODAGA}$  (hereafter referred to as  $[^{68}\text{Ga}]\text{Ga-Z}_{\text{HER}3}$ ), which was selected as the best  $^{68}\text{Ga}$ -labeled variant in Paper II.

## Results

For reasons of availability and convenience, all experiments were performed with cobalt-57 ( $t_{1/2} = 271$  d) as a surrogate for cobalt-55. The feasibility of this approach was previously demonstrated using cobalt-55/57-labeled bombesin analogs (135).

All conjugates were stably labeled with radiocobalt with almost quantitative yields. The in vitro studies demonstrated specific binding and  $K_D$ -values in the range of 90–200 pM. In both cell lines, all conjugates showed similar activity uptakes and internalization patterns, but the internalized fraction did not exceed 5% of the total cell-associated activity (Figure 10).

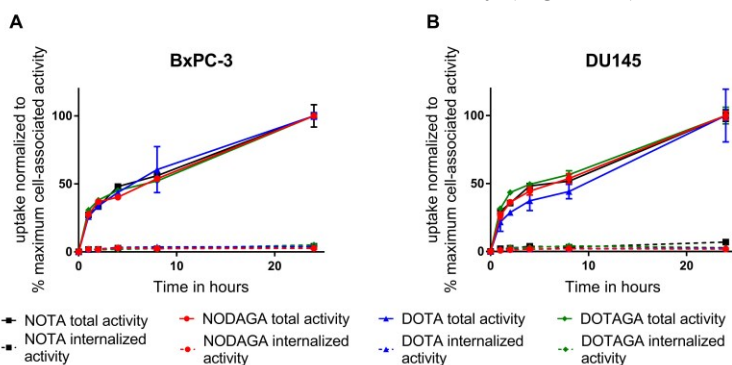


**Figure 10.** Uptake and internalization of  $[^{57}\text{Co}]\text{Co-}(\text{HE})_3\text{-Z}_{\text{HER}3}\text{-X}$  in (A) BxPC-3 and (B) DU145 cells. Cells were continuously incubated with 0.1 nM of the radiolabeled conjugates for up to 24 hours.

The in vivo specificity test showed significant decrease in uptake of  $[^{57}\text{Co}]\text{Co-}(\text{HE})_3\text{-Z}_{\text{HER}3}\text{-NODAGA}$  and  $[^{57}\text{Co}]\text{Co-}(\text{HE})_3\text{-Z}_{\text{HER}3}\text{-DOTA}$  in tumors and mErbB3-expressing organs upon co-injection of excess amounts of unlabeled HER3-targeting affibody. Activity uptake of  $[^{57}\text{Co}]\text{Co-}(\text{HE})_3\text{-Z}_{\text{HER}3}\text{-DOTAGA}$  significantly decreased in mErbB3-expressing liver and small intestine,

but did not significantly decrease in the HER3-expressing tumors (Figure 11). In vivo binding specificity of [ $^{57}\text{Co}$ ]Co-(HE) $_3$ -Z $_{\text{HER}3}$ -NOTA has been demonstrated previously (125).

The biodistribution of all conjugates except [ $^{57}\text{Co}$ ]Co-(HE) $_3$ -Z $_{\text{HER}3}$ -DOTAGA was comparable with previously reported results for [ $^{57}\text{Co}$ ]Co-(HE) $_3$ -Z $_{\text{HER}3}$ -NOTA (Figure 12). The activity uptake of [ $^{57}\text{Co}$ ]Co-(HE) $_3$ -Z $_{\text{HER}3}$ -DOTAGA was much lower than that of the other conjugates and activity uptake in the HER3-expressing xenografts did not exceed 1%IA/g.

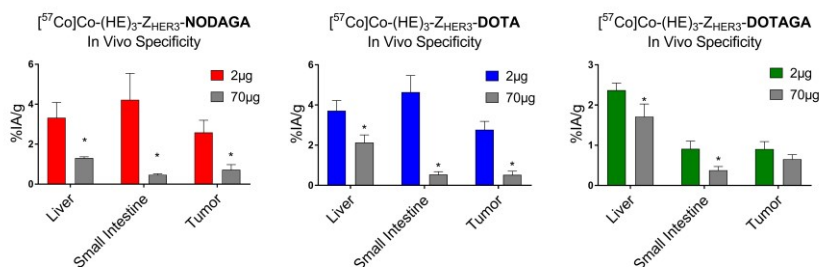


**Figure 11.** In vivo specificity of [ $^{57}\text{Co}$ ]Co-(HE) $_3$ -Z $_{\text{HER}3}$ -X 3 h pi. Mice were injected with either 2  $\mu\text{g}$  of radiolabeled affibody molecule or co-injected with excess amounts of non-labeled HER3-binding affibody molecule. \*statistically significant difference ( $p < 0.05$ ) in uptake between groups. The specificity of [ $^{57}\text{Co}$ ]Co-(HE) $_3$ -Z $_{\text{HER}3}$ -NOTA has been shown previously (96).

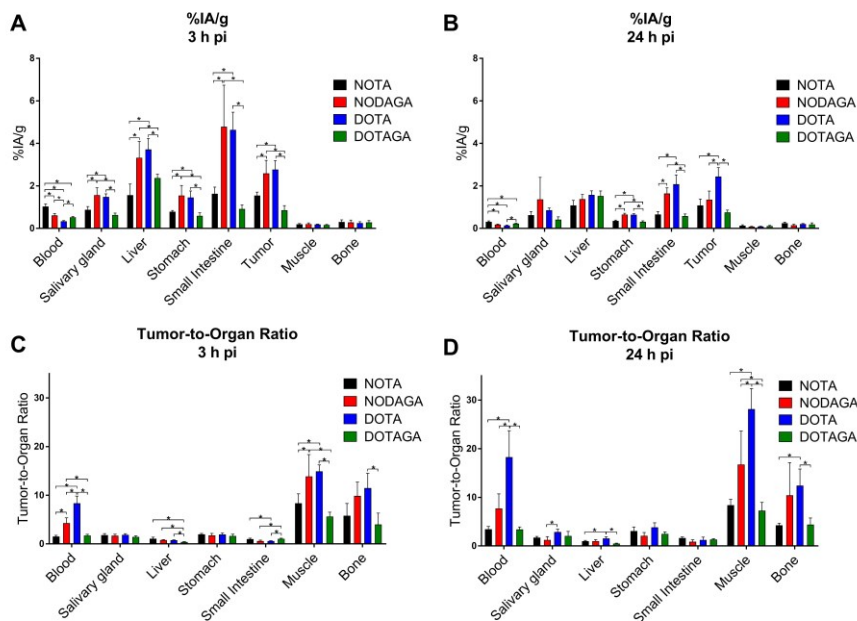


**Figure 12.** (A, B) Biodistribution of [ $^{57}\text{Co}$ ]Co-(HE) $_3$ -Z $_{\text{HER}3}$ -X in BxPC-3 xenograft-bearing mice 3 h and 24 h pi, and (C, D) tumor-to-organ ratios 3 h and 24 h pi.

$[^{57}\text{Co}]\text{Co}-(\text{HE})_3\text{-Z}_{\text{HER}3}\text{-NODAGA}$  and  $[^{57}\text{Co}]\text{Co}-(\text{HE})_3\text{-Z}_{\text{HER}3}\text{-DOTA}$  had the highest activity uptake in tumors and normal organs, except for blood. The DOTA conjugate had the fastest clearance from blood among all conjugates. The activity uptake in normal organs cleared from 3 h to 24 h pi.  $[^{57}\text{Co}]\text{Co}-(\text{HE})_3\text{-Z}_{\text{HER}3}\text{-NOTA}$  and  $[^{57}\text{Co}]\text{Co}-(\text{HE})_3\text{-Z}_{\text{HER}3}\text{-DOTA}$  were retained well in tumors. An almost 50% release of tumor-associated activity was observed for  $[^{57}\text{Co}]\text{Co}-(\text{HE})_3\text{-Z}_{\text{HER}3}\text{-NODAGA}$  after 24 h. Among all conjugates and time points,  $[^{57}\text{Co}]\text{Co}-(\text{HE})_3\text{-Z}_{\text{HER}3}\text{-DOTA}$  24 h pi provided the highest tumor-to-blood ( $18 \pm 5$ ) and tumor-to-liver ( $1.6 \pm 0.3$ ) ratios.

The biodistribution of  $[^{68}\text{Ga}]\text{Ga-Z}_{\text{HER}3}$  3 h pi was included in this study and compared with  $[^{57}\text{Co}]\text{Co}-(\text{HE})_3\text{-Z}_{\text{HER}3}\text{-DOTA}$  (Table 8). Biodistribution of  $[^{68}\text{Ga}]\text{Ga-Z}_{\text{HER}3}$  was in agreement with what had been seen in previous studies (136). While no difference in tumor-associated activity was observed between  $[^{68}\text{Ga}]\text{Ga-Z}_{\text{HER}3}$  3 h pi and  $[^{57}\text{Co}]\text{Co}-(\text{HE})_3\text{-Z}_{\text{HER}3}\text{-DOTA}$  24 h pi,  $[^{57}\text{Co}]\text{Co}-(\text{HE})_3\text{-Z}_{\text{HER}3}\text{-DOTA}$  24 h pi had significantly lower activity concentration in blood, liver, and stomach (Table 8). The tumor-to-liver and tumor-to-lung ratios of  $[^{57}\text{Co}]\text{Co}-(\text{HE})_3\text{-Z}_{\text{HER}3}\text{-DOTA}$  24 h pi were significantly higher than those for  $[^{68}\text{Ga}]\text{Ga-Z}_{\text{HER}3}$  (3 h pi).

**Table 8.** Comparison of uptake and tumor-to-organ ratios between  $[^{68}\text{Ga}]\text{Ga-Z}_{\text{HER}3}$  3 h pi and  $[^{57}\text{Co}]\text{Co}-(\text{HE})_3\text{-Z}_{\text{HER}3}\text{-DOTA}$  3 h and 24 h pi.

Organ	%IA/g			Tumor-to-Organ Ratio		
	$[^{68}\text{Ga}]\text{Ga-Z}_{\text{HER}3}$	$[^{57}\text{Co}]\text{Co}-(\text{HE})_3\text{-Z}_{\text{HER}3}\text{-DOTA}$		$[^{68}\text{Ga}]\text{Ga-Z}_{\text{HER}3}$	$[^{57}\text{Co}]\text{Co}-(\text{HE})_3\text{-Z}_{\text{HER}3}\text{-DOTA}$	
	3 h	3 h	24 h	3 h	3 h	24 h
Blood	$0.18 \pm 0.01^{ab}$	$0.33 \pm 0.04^*$	$0.14 \pm 0.02$	$12 \pm 2^a$	$8 \pm 1^*$	$18 \pm 5$
Salivary Glands	$0.7 \pm 0.1^a$	$1.5 \pm 0.1^*$	$0.9 \pm 0.1$	$3.1 \pm 0.6^a$	$1.9 \pm 0.2^*$	$2.9 \pm 0.6$
Lung	$0.81 \pm 0.08^a$	$1.7 \pm 0.2^*$	$0.6 \pm 0.2$	$2.8 \pm 0.3^{a,b}$	$1.6 \pm 0.4^*$	$4.1 \pm 0.9$
Liver	$2.2 \pm 0.1^{a,b}$	$3.7 \pm 0.5^*$	$1.6 \pm 0.2$	$1.0 \pm 0.1^{a,b}$	$0.74 \pm 0.08^*$	$1.6 \pm 0.3$
Spleen	$0.29 \pm 0.04^{a,b}$	$0.43 \pm 0.05$	$0.42 \pm 0.08$	$8 \pm 2$	$6 \pm 1$	$6 \pm 1$
Stomach	$0.8 \pm 0.02^{a,b}$	$1.5 \pm 0.3^*$	$0.65 \pm 0.05$	$2.8 \pm 0.6$	$2 \pm 0.2^*$	$3.8 \pm 0.9$
Small Intestine	$1.7 \pm 0.04^a$	$4.6 \pm 0.8^*$	$2.1 \pm 0.04$	$1.3 \pm 0.2^a$	$0.60 \pm 0.05$	$1.3 \pm 0.6$
Kidney	$271 \pm 36$	$253 \pm 54$	$223 \pm 23$	$0.008 \pm 0.001$	$0.011 \pm 0.002$	$0.011 \pm 0.003$
Tumor	$2.3 \pm 0.2$	$2.8 \pm 0.4$	$2.4 \pm 0.4$	-	-	-
Muscle	$0.10 \pm 0.04^a$	$0.19 \pm 0.01^*$	$0.09 \pm 0.02$	$26 \pm 12$	$15 \pm 1^*$	$28 \pm 4$
Bone	$0.3 \pm 0.2$	$0.25 \pm 0.06$	$0.20 \pm 0.03$	$8 \pm 5$	$11 \pm 2$	$12 \pm 3$

Statistically significant differences ( $p < 0.05$ ) is indicated by <sup>a</sup> for  $[^{68}\text{Ga}]\text{Ga-Z}_{\text{HER}3}$  3 h pi vs.  $[^{57}\text{Co}]\text{Co}-(\text{HE})_3\text{-Z}_{\text{HER}3}\text{-DOTA}$  3 h pi, <sup>b</sup> for  $[^{68}\text{Ga}]\text{Ga-Z}_{\text{HER}3}$  3 h pi vs.  $[^{57}\text{Co}]\text{Co}-(\text{HE})_3\text{-Z}_{\text{HER}3}\text{-DOTA}$  24 h pi or \* for  $[^{57}\text{Co}]\text{Co}-(\text{HE})_3\text{-Z}_{\text{HER}3}\text{-DOTA}$  3 h vs. 24 h pi.

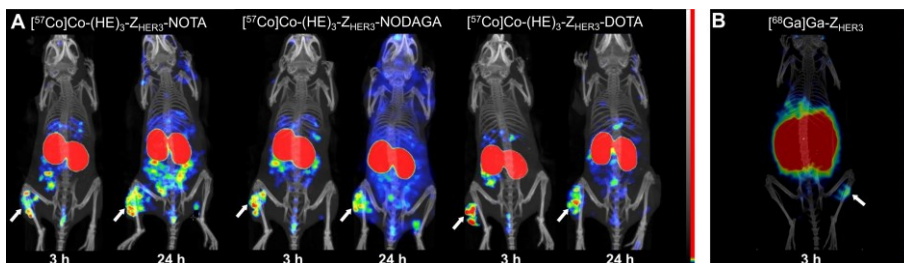


**Figure 13.** (A) NanoSPECT/CT images  $[^{57}\text{Co}]\text{Co}-(\text{HE})_3\text{-Z}_{\text{HER}3}\text{-X}$  3 and 24 h pi.  $[^{57}\text{Co}]\text{Co}-(\text{HE})_3\text{-Z}_{\text{HER}3}\text{-DOTAGA}$  was excluded due to the unfavorable biodistribution. (B) NanoPET/CT images of  $[^{68}\text{Ga}]\text{Ga-Z}_{\text{HER}3}$  3 h pi. BxPC-3 xenografts are indicated with white arrows.

NanoSPECT/CT (Figure 13A) and nanoPET/CT imaging (Figure 13B) were performed and confirmed the results of the biodistribution.

## Discussion

The composition of the radiocobalt/chelator complex had no significant influence on the *in vitro* binding of  $(\text{HE})_3\text{-Z}_{\text{HER}3}$ . The binding specificity was preserved after labeling and, as expected,  $K_D$  values were in the low picomolar range and comparable to values reported for  $^{111}\text{In}$ -labeled  $\text{Z}_{\text{HER}3}$  (137). However, the internalized fraction of  $[^{57}\text{Co}]\text{Co}-(\text{HE})_3\text{-Z}_{\text{HER}3}\text{-X}$  was noticeably lower than for the  $^{111}\text{In}$ - and  $^{68}\text{Ga}$ -labeled  $\text{Z}_{\text{HER}3}$  conjugates evaluated in Papers I and II (136,137). A similar observation was made for the radiocobalt-labeled anti-EGFR affibody molecule  $\text{Z}_{\text{EGFR:2377}}$  (138). We speculated that, because cobalt competes with biologically essential metal ions, the low internalized activity might be linked to cobalt efflux mechanisms, which are directly related to intracellular concentrations of cobalt ions (139).

*In vivo*,  $[^{57}\text{Co}]\text{Co}-(\text{HE})_3\text{-Z}_{\text{HER}3}\text{-DOTAGA}$ , with a double negative charge of the radiocobalt/chelator complex, was considered unfavorable because of non-blockable tumor uptake and noticeably lower activity uptake in all organs and in the tumor due to rapid clearance. This indicates that there are limitations to the beneficial effect of a local negative charge. A similar observation was made when  $(\text{HE})_3\text{-Z}_{\text{HER}3}\text{-DOTAGA}$  was labeled with gallium-68 (140). In contrast, DOTAGA-conjugated  $\text{Z}_{\text{HER}3}$  provided the best imaging contrast when labeled with indium-111 (137). This demonstrates the importance of careful characterization of new radio-conjugates.

Rapid tumor washout was observed for  $[^{57}\text{Co}]\text{Co}-(\text{HE})_3\text{-Z}_{\text{HER}3}\text{-NODAGA}$ . Because the aim was to select a conjugate for later time point imaging, we also considered  $[^{57}\text{Co}]\text{Co}-(\text{HE})_3\text{-Z}_{\text{HER}3}\text{-NODAGA}$  as unfavorable. Twenty-four hours pi,  $[^{57}\text{Co}]\text{Co}-(\text{HE})_3\text{-Z}_{\text{HER}3}\text{-DOTA}$  provided the best imaging contrast with a tumor-to-liver ratio of 1.6.  $[^{57}\text{Co}]\text{Co}-(\text{HE})_3\text{-Z}_{\text{HER}3}\text{-DOTA}$  was therefore selected as the most suitable conjugate for later time point PET imaging of HER3 expression with radiocobalt.

Comparison of [ $^{57}\text{Co}$ ]Co-(HE) $_3$ -Z $_{\text{HER}3}$ -DOTA (24 h pi) with [ $^{68}\text{Ga}$ ]Ga-Z $_{\text{HER}3}$  (3 h pi) showed significantly lower hepatic activity uptake for the radiocobalt-labeled conjugate, resulting in higher imaging contrast for [ $^{57}\text{Co}$ ]Co-(HE) $_3$ -Z $_{\text{HER}3}$ -DOTA.

## Conclusions

In this study, we evaluated the potential of radiocobalt-labeled HER3-targeting affibody molecules for later time point PET imaging. As was seen in Paper I, a cobalt/chelator complex with a single negative charge improved the bio-distribution and imaging properties of Z $_{\text{HER}3}$ . However, we also found that a further increase in negative charge resulted in rapid washout and diminished targeting properties.

(HE) $_3$ -Z $_{\text{HER}3}$ -DOTA was selected as the most favorable for imaging of HER3 expression with radiocobalt 24 h pi, because it provided the highest tumor-to-liver and tumor-to-blood ratios. Moreover, in comparison with [ $^{68}\text{Ga}$ ]Ga-Z $_{\text{HER}3}$ , [ $^{57}\text{Co}$ ]Co-(HE) $_3$ -Z $_{\text{HER}3}$ -DOTA demonstrated the potential benefit of the radiocobalt label for later time point PET imaging of HER3 expression. Although radiocobalt is not yet clinically available, this study indicated that its use should be considered a promising alternative to conventional PET isotopes like gallium-68 in the future.

## **Paper IV: HER3 PET-Imaging: $^{68}\text{Ga}$ -Labeled Affibody Molecules Provide Superior HER3 Contrast to $^{89}\text{Zr}$ -Labeled Antibody and Antibody-Fragment-Based Tracers**

### **Background**

Currently, radiolabeled antibodies are still the only HER3-targeting imaging probes that have been evaluated for imaging of HER3 expression in clinical trials. Arguments for the use of radiolabeled versions of existing therapeutic antibodies as imaging agents for HER3 are that they are available and, in addition to target detection, could be used for dosing studies for antibody-based HER3 therapy and imaging of receptor occupancy. However, this would require that they image the target receptor reliably, quantifiably, and with high sensitivity. The data available from clinical trials with radiolabeled HER3-targeting mAbs for imaging have thus far not provided extremely convincing results. The tracers have shown uptake in HER3-expressing tumors in patients, but high uptake in non-targeted tissue limits their sensitivity and the possibility for quantification (85–87).

The general disadvantages associated with radiolabeled antibodies (slow clearance, non-specific accumulation, and hepatobiliary clearance), together with the relatively low levels of HER3 overexpression on cancer cells and the natural expression of HER3 in healthy tissue, create a major obstacle for successful antibody-based imaging of HER3 expression. This raises the question of whether tracers based on other types of targeting molecules designed for imaging (particularly ones smaller in size) might be better suited for imaging of HER3 expression.

Papers I–III were dedicated to the development and optimization of HER3-targeting affibody molecules for imaging of HER3 expression. There, we showed that the radiolabeling approach and molecular design of HER3-targeting affibody molecules can profoundly improve the HER3 image contrast in preclinical models by reducing the uptake in non-targeted tissue (122,127,136).

There is an observable trend towards smaller-sized tracers for imaging of HER family members (1). While published literature may indicate that this also applies to HER3, comparison of different formats of HER3-targeting imaging agents from literature is difficult because of the use of different models and dosing. Up to this point, no head-to-head comparison of HER3-targeting imaging agents based on different targeting molecules has been reported.

## Aim

The aim of Paper IV was to compare the imaging properties of the affibody molecule [ $^{68}\text{Ga}$ ]Ga-(HE)<sub>3</sub>-Z<sub>HER3</sub>-NODAGA (hereafter [ $^{68}\text{Ga}$ ]Ga-Z<sub>HER3</sub>) developed and characterized in Papers II and III with those of an antibody and a newly produced antibody fragment-based tracer for PET imaging of HER3 expression.

For this purpose, we produced a  $^{89}\text{Zr}$ -labeled version of the HER3-targeting therapeutic antibody seribantumab (MM-121) and a seribantumab-derived F(ab')<sub>2</sub> fragment (called seribantumab-F(ab')<sub>2</sub>) labeled with  $^{68}\text{Ga}$  and  $^{89}\text{Zr}$ , which were compared head-to-head with [ $^{68}\text{Ga}$ ]Ga-Z<sub>HER3</sub> in the same preclinical model, at their respective favorable imaging time points.

## Results

The newly generated seribantumab-F(ab')<sub>2</sub> fragment and the full-length antibody seribantumab were successfully conjugated to DFO for labeling with  $^{89}\text{Zr}$  or  $^{68}\text{Ga}$ . Labeling of the new conjugates with  $^{68}\text{Ga}$  and  $^{89}\text{Zr}$  resulted in radiochemical purity > 97%. During the in vitro stability test, the  $^{89}\text{Zr}$ -labeled conjugates showed sufficient stability when incubated in PBS, but we observed close to 25% release of  $^{89}\text{Zr}$  after 24 hours of incubation in human serum. Over 80% release of  $^{68}\text{Ga}$  from [ $^{68}\text{Ga}$ ]Ga-seribantumab-F(ab')<sub>2</sub> was observed within 3 h of incubation in human serum.

Seribantumab and seribantumab-F(ab')<sub>2</sub> bound to both HER3 and mErbB3 with low nanomolar affinity. Binding specificity towards HER3 in vitro and in vivo was retained after labeling (Figure 14). We further demonstrated cross-blockability of the included conjugates in vitro (Figure 14A, C). The conjugates internalized slowly with < 35% and < 18% cell-associated activity internalized for the  $^{89}\text{Zr}$ -labeled tracers after 24 h and [ $^{68}\text{Ga}$ ]Ga-seribantumab-F(ab')<sub>2</sub> after 4 h, respectively.

Biodistribution was performed 3 h, 24 h and 48 h pi for [ $^{89}\text{Zr}$ ]Zr-seribantumab-F(ab')<sub>2</sub>, 48 h and 96 h pi for [ $^{89}\text{Zr}$ ]Zr-seribantumab, and 3 h pi for [ $^{68}\text{Ga}$ ]Ga-seribantumab-F(ab')<sub>2</sub> and [ $^{68}\text{Ga}$ ]Ga-Z<sub>HER3</sub> (Figure 15).

Overall, the blood clearance was fastest for [ $^{68}\text{Ga}$ ]Ga-Z<sub>HER3</sub>. The activity concentration of [ $^{68}\text{Ga}$ ]Ga-Z<sub>HER3</sub> in blood 3 h pi was more than 100-fold, 69-fold and 10-fold lower compared with [ $^{68}\text{Ga}$ ]Ga-seribantumab-F(ab')<sub>2</sub>, [ $^{89}\text{Zr}$ ]Zr-seribantumab-F(ab')<sub>2</sub> 3 h pi, and [ $^{89}\text{Zr}$ ]Zr-seribantumab 48 h pi, respectively. There was no significant difference in blood concentration between [ $^{89}\text{Zr}$ ]Zr-seribantumab-F(ab')<sub>2</sub> 48 h pi and [ $^{68}\text{Ga}$ ]Ga-Z<sub>HER3</sub> 3 h pi.

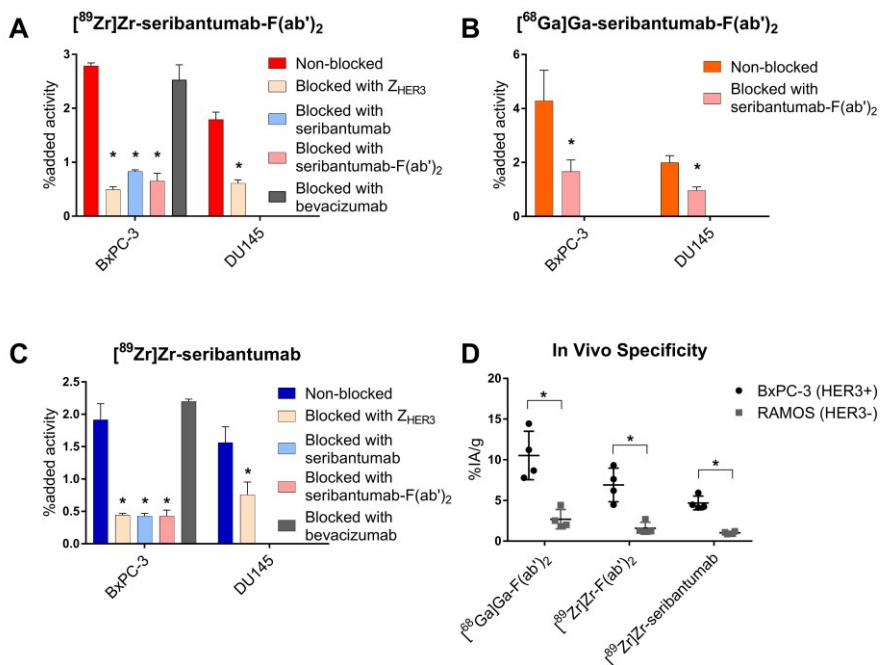


**Figure 14.** In vitro (A–C) and in vivo (D) specificity of  $[^{68}\text{Ga}]\text{Ga}/[^{89}\text{Zr}]\text{Zr-seribantumab-F(ab')}_2$  and  $[^{89}\text{Zr}]\text{Zr-seribantumab}$ . In vitro specificity was studied in HER3-expressing BxPC-3 and DU145 cells. In blocked groups, the cells were pre-incubated with excess amounts of unlabeled protein. Bevacizumab binds to VEGFR and was included as a negative control. In vivo specificity was studied 3 h pi for  $[^{68}\text{Ga}]\text{Ga}/[^{89}\text{Zr}]\text{Zr-seribantumab-F(ab')}_2$  and 96 h pi for  $[^{89}\text{Zr}]\text{Zr-seribantumab}$  comparing the uptake in HER3-positive BxPC-3 and HER3-negative RAMOS xenografts. \* indicates a statistically significant ( $p < 0.05$ ) difference compared with non-blocked group (A–C) and between uptake in BxPC-3 and DU145 xenografts (D).

The  $\text{F(ab')}_2$  fragment-based tracers at 3 h pi had the highest uptake in tumors overall ( $11 \pm 3$  and  $7 \pm 2\%$ IA/g). However, the tumor uptake of  $[^{89}\text{Zr}]\text{Zr-seribantumab-F(ab')}_2$  was halved from 3 h to 48 h pi. Tumor uptake of  $[^{89}\text{Zr}]\text{Zr-seribantumab}$  was 4.7–5.6%IA/g, without any significant difference between the time points. There was no significant difference in tumor uptake between  $[^{89}\text{Zr}]\text{Zr-seribantumab-F(ab')}_2$  and  $[^{89}\text{Zr}]\text{Zr-seribantumab}$  at later time points.  $[^{68}\text{Ga}]\text{Ga-Z}_{\text{HER3}}$  showed significantly lower uptake in tumors than  $[^{89}\text{Zr}]\text{Zr-seribantumab-F(ab')}_2$  and  $[^{68}\text{Ga}]\text{Ga-seribantumab-F(ab')}_2$ .

Aside from kidneys, the uptake of  $[^{68}\text{Ga}]\text{Ga-Z}_{\text{HER3}}$  was generally lower compared with the uptake of  $[^{68}\text{Ga}]\text{Ga-seribantumab-F(ab')}_2$ ,  $[^{89}\text{Zr}]\text{Zr-seribantumab-F(ab')}_2$ , and  $[^{89}\text{Zr}]\text{Zr-seribantumab}$ .

For both seribantumab- $\text{F(ab')}_2$ -based tracers, the uptake 3 h pi was the highest in blood, liver, lungs, small intestine, and spleen. The uptake of  $[^{68}\text{Ga}]\text{Ga-seribantumab-F(ab')}_2$  was higher than the uptake of  $[^{89}\text{Zr}]\text{Zr}$ -

seribantumab-F(ab')<sub>2</sub> in all normal organs. For [<sup>89</sup>Zr]Zr-seribantumab-F(ab')<sub>2</sub>, the uptake in most normal organs decreased from 3 h to 48 h pi. Most notably, the concentration in blood decreased from 14 ± 2%IA/g (3 h pi) to 0.23 ± 0.04%IA/g (48 h pi).

The highest uptake of [<sup>89</sup>Zr]Zr-seribantumab was observed in liver, where it remained constant from 48 h to 96 h pi. The uptake of [<sup>89</sup>Zr]Zr-seribantumab in most other normal organs decreased with time. The concentration of [<sup>89</sup>Zr]Zr-seribantumab in blood fell to a third from 48 h to 96 h pi (2.1 ± 0.2%IA/g to 0.7 ± 0.1%IA/g). Both <sup>89</sup>Zr-labeled tracers showed elevated uptake in bone.

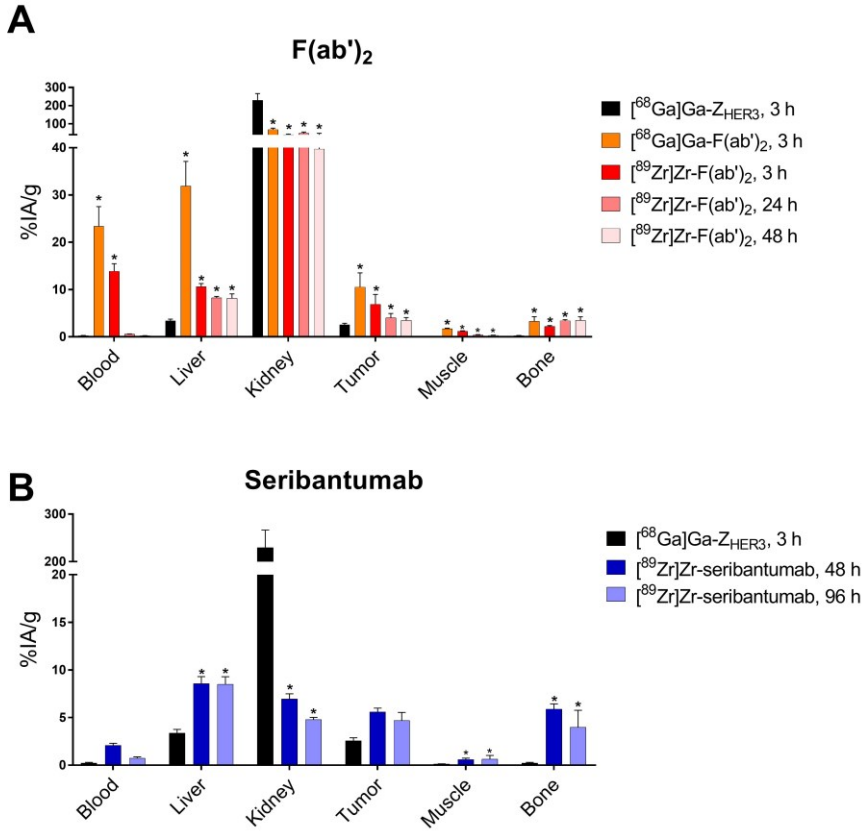


**Figure 15.** Biodistribution of (A) [<sup>68</sup>Ga]Ga-seribantumab-F(ab')<sub>2</sub>, [<sup>89</sup>Zr]Zr-seribantumab-F(ab')<sub>2</sub> and (B) [<sup>89</sup>Zr]Zr-seribantumab in comparison with [<sup>68</sup>Ga]Ga-Z<sub>HER3</sub>, presented as %IA/g. Mice were injected with equimolar tracer amounts. Data are presented as average of n = 4–6 mice per group, with SD. Statistical significance compared with [<sup>68</sup>Ga]Ga-Z<sub>HER3</sub> is indicated by \*.

Generally, the highest tumor-to-organ ratios were observed for [<sup>68</sup>Ga]Ga-Z<sub>HER3</sub>. The tumor-to-blood ratio for [<sup>68</sup>Ga]Ga-Z<sub>HER3</sub> (11 ± 2, 3 h pi) was sig-

nificantly higher than the tumor-to-blood ratios of the other conjugates, besides [<sup>89</sup>Zr]Zr-seribantumab-F(ab')<sub>2</sub> 24 h and 48 h pi (Table 9). Aside from the tumor-to-small intestine ratio, no significant increase in tumor-to-organ ratio was observed for [<sup>89</sup>Zr]Zr-seribantumab from 48 h to 96 h pi. The only significant increases in tumor-to-organ ratios for [<sup>89</sup>Zr]Zr-seribantumab-F(ab')<sub>2</sub> were observed in blood and lungs from 3 h to 48 h pi. The tumor-to-blood ratio of [<sup>89</sup>Zr]Zr-seribantumab-(Fab')<sub>2</sub> 48 h was significantly higher than the that of [<sup>89</sup>Zr]Zr-seribantumab at both time points.

**Table 9.** Tumor-to-organ ratios for [<sup>68</sup>Ga]Ga-seribantumab-F(ab')<sub>2</sub>, [<sup>89</sup>Zr]Zr-seribantumab-F(ab')<sub>2</sub> and [<sup>89</sup>Zr]Zr-seribantumab in comparison with [<sup>68</sup>Ga]Ga-Z<sub>HER3</sub>. Data are presented as average of n = 4–6 mice per group, with SD.

Organ	[ <sup>68</sup> Ga]Ga-F(ab') <sub>2</sub>	[ <sup>89</sup> Zr]Zr-F(ab') <sub>2</sub>			[ <sup>89</sup> Zr]Zr-seribantumab		[ <sup>68</sup> Ga]Ga-Z <sub>HER3</sub>
	3 h pi	3 h pi	24 h pi	48 h pi	48 h pi	96 h pi	3 h pi
Blood	0.45 ± 0.09 <sup>c,d,f,*</sup>	0.5 ± 0.1 <sup>c,d,f,*</sup>	7 ± 2 <sup>a,b,d</sup>	15 ± 4 <sup>a,b,c,e,f</sup>	2.7 ± 0.4 <sup>d,*</sup>	6 ± 2 <sup>a,b,d,*</sup>	11 ± 2 <sup>a,b,e,f</sup>
Salivary glands	2.6 ± 0.6 <sup>e,f</sup>	2.6 ± 0.5 <sup>e,f</sup>	2.1 ± 0.3	2.4 ± 0.7	1.6 ± 0.2 <sup>a,b</sup>	1.5 ± 0.3 <sup>a,b</sup>	2.0 ± 0.3
Lungs	0.8 ± 0.2 <sup>c,e,d,f,*</sup>	0.9 ± 0.2 <sup>c,d,e,f,*</sup>	2.3 ± 0.3	2.7 ± 0.6	2.2 ± 0.4	2.7 ± 0.6	2.4 ± 0.3
Liver	0.33 ± 0.05 <sup>b,e,*</sup>	0.6 ± 0.2	0.5 ± 0.1 <sup>*</sup>	0.4 ± 0.1 <sup>*</sup>	0.66 ± 0.08	0.6 ± 0.1	0.74 ± 0.05 <sup>a,c,d</sup>
Stomach	3 ± 1	2.6 ± 0.6	2.6 ± 0.2	3 ± 1	2.7 ± 0.06	3.6 ± 0.7 <sup>*</sup>	1.9 ± 0.2 <sup>f</sup>
Small intestine	0.8 ± 0.1 <sup>c,f</sup>	1.0 ± 0.2 <sup>f</sup>	1.1 ± 0.2 <sup>a,f</sup>	1.5 ± 0.5 <sup>*</sup>	0.9 ± 0.2 <sup>f</sup>	2.0 ± 0.5 <sup>a,b,c,e,*</sup>	0.7 ± 0.2 <sup>d</sup>
Muscle	6 ± 2 <sup>*</sup>	6 ± 1 <sup>*</sup>	10 ± 2 <sup>*</sup>	11 ± 2 <sup>*</sup>	10 ± 4 <sup>*</sup>	8 ± 2 <sup>*</sup>	21 ± 6 <sup>a,b,c,d,e,f</sup>
Bone	3.2 ± 0.5 <sup>*</sup>	3.1 ± 0.7 <sup>*</sup>	1.2 ± 0.3 <sup>*</sup>	1.1 ± 0.5 <sup>*</sup>	0.95 ± 0.09 <sup>*</sup>	2 ± 2 <sup>*</sup>	11 ± 2 <sup>a,b,c,d,e,f</sup>

Significant difference ( $p < 0.05$ ) between groups is indicated by <sup>a</sup> vs. [<sup>68</sup>Ga]Ga-F(ab')<sub>2</sub> <sup>b</sup> vs. [<sup>89</sup>Zr]Zr-F(ab')<sub>2</sub> 3 h pi, <sup>c</sup> vs. [<sup>89</sup>Zr]Zr-F(ab')<sub>2</sub> 24 h pi, <sup>d</sup> vs. [<sup>89</sup>Zr]Zr-F(ab')<sub>2</sub> 48 h pi, <sup>e</sup> vs. [<sup>89</sup>Zr]Zr-seribantumab 48 h pi, <sup>f</sup> vs. [<sup>89</sup>Zr]Zr-seribantumab 96 h pi, <sup>\*</sup> vs. [<sup>68</sup>Ga]Ga-Z<sub>HER3</sub>.

Autoradiography of BxPC-3 xenografts showed an even distribution of activity for all tracers. Areas of accumulation matched with the localization of tumor cells visualized by eosin and hematoxylin staining.

All tracers tested were able to visualize HER3 expression in xenografts on nanoPET/CT (Figure 16). No images were acquired with [<sup>68</sup>Ga]Ga-seribantumab-F(ab')<sub>2</sub> because this tracer was considered unsuitable based on the biodistribution results.

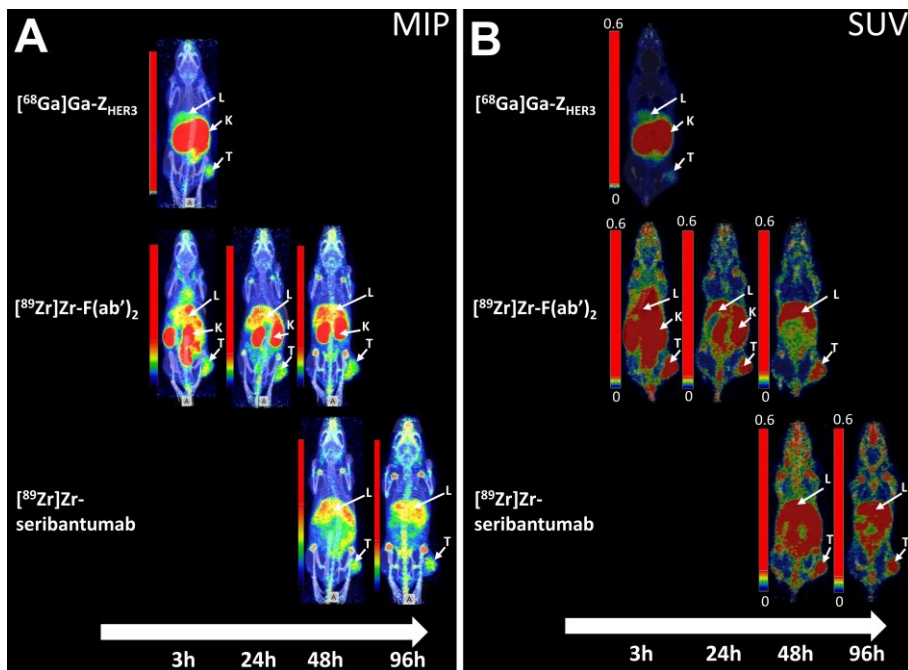


**Figure 16.** nanoPET/CT imaging with  $[^{89}\text{Zr}]\text{Zr-seribantumab}$  (48 h and 96 h pi),  $[^{89}\text{Zr}]\text{Zr-seribantumab-F(ab')}_2$  (3 h, 24 h, 48 h pi) and  $[^{68}\text{Ga}]\text{Ga-Z}_{\text{HER3}}$  in BxPC-3 xenograft-bearing balb/c nu/nu mice. (A) MIP images. (B) SUV images. Arrows indicate tumors (T), liver (L), and kidneys (K).

## Discussion

The need for non-invasive methods for detection of HER3 expression and stratification of patients for HER3-targeted therapy calls for HER3-targeting imaging probes that can repeatedly and reliably visualize HER3 expression in malignant tissue. Thus far, radiolabeled therapeutic antibodies investigated as HER3-imaging agents in clinical studies have failed to provide sufficient sensitivity and reliable detection of HER3-expressing cancer lesions. In this study, we produced a  $^{89}\text{Zr}$ -labeled HER3-targeting antibody ( $[^{89}\text{Zr}]\text{Zr-seribantumab}$ ), a seribantumab-derived  $^{68}\text{Ga}$ - and  $^{89}\text{Zr}$ -labeled  $\text{F(ab')}_2$  fragment ( $[^{68}\text{Ga}]\text{Ga}/[^{89}\text{Zr}]\text{Zr-seribantumab-F(ab')}_2$ ) and compared their imaging properties with the  $[^{68}\text{Ga}]\text{Ga-Z}_{\text{HER3}}$  affibody developed and characterized in Papers II and III.

We confirmed binding specificity of the newly produced tracers in vitro and in vivo. Seribantumab and seribantumab- $\text{F(ab')}_2$  also showed cross-reactivity to mErbB3. This provided the best possible pre-conditions for a fair comparison of the antibody-derived tracers with  $\text{Z}_{\text{HER3}}$ , which is known to bind to mErbB3 (92).

The biodistribution of  $[^{89}\text{Zr}]\text{Zr-seribantumab}$  was comparable to those of other anti-HER3 antibodies (88,89,100,101). The high uptake of  $[^{89}\text{Zr}]\text{Zr-seribantumab}$  in liver can be attributed to the hepatobiliary pathway being the

main elimination pathway for antibodies. The imaging contrast improved with time, primarily due to the clearance of [ $^{89}\text{Zr}$ ]Zr-seribantumab from blood. We consider 96 h pi to be a more suitable time point than 48 h pi for imaging with [ $^{89}\text{Zr}$ ]Zr-seribantumab. This is in agreement with other studies with  $^{89}\text{Zr}$ -labeled HER3 antibodies, which have reported optimal imaging time points between 4 and 7 days (85,86).

We decided to label seribantumab-F(ab')<sub>2</sub> with  $^{68}\text{Ga}$  in addition to  $^{89}\text{Zr}$  because of the anticipated faster clearance of the F(ab')<sub>2</sub> fragment and earlier time point imaging being reported with F(ab')<sub>2</sub>-based tracers. One clinical study has previously reported the use of a  $^{68}\text{Ga}$ -labeled F(ab')<sub>2</sub> fragment for imaging of HER2 expression and DFO has been reported as a possible chelator for  $^{68}\text{Ga}$  (141–143). In our case, use of the [ $^{68}\text{Ga}$ ]Ga-DFO label proved to be unsuitable for imaging of HER3 expression with seribantumab-F(ab')<sub>2</sub>. In most organs, the biodistribution of [ $^{68}\text{Ga}$ ]Ga-seribantumab-F(ab')<sub>2</sub> revealed significantly higher uptake compared with its  $^{89}\text{Zr}$ -labeled counterpart. The high accumulation of [ $^{68}\text{Ga}$ ]Ga-seribantumab-F(ab')<sub>2</sub> in spleen and liver as well as in blood further indicated instability of the  $^{68}\text{Ga}$  label, which was coherent with the dramatic release of  $^{68}\text{Ga}$  in the in vitro stability test. This, taken together with the increasing tumor-to-blood contrast with time that could be observed for [ $^{89}\text{Zr}$ ]Zr-seribantumab-F(ab')<sub>2</sub>, indicated that imaging of HER3 expression with [ $^{68}\text{Ga}$ ]Ga-seribantumab-F(ab')<sub>2</sub> 3 h pi would be unsuitable. Therefore, no PET images were acquired using [ $^{68}\text{Ga}$ ]Ga-seribantumab-F(ab')<sub>2</sub> and it will be excluded from further discussion.

Even though the tumor uptake of [ $^{89}\text{Zr}$ ]Zr-seribantumab-F(ab')<sub>2</sub> decreased with time, tumor-to-organ ratios remained stable for all organs except blood due to the clearance of the tracer from tissues with time. The clearance of [ $^{89}\text{Zr}$ ]Zr-seribantumab-F(ab')<sub>2</sub> from blood and the 30-fold increase in tumor-to-blood ratio resulted in a clearly superior PET image at 48 h pi compared with the images at 3 h and 24 h pi.

The biodistribution data for [ $^{68}\text{Ga}$ ]Ga-Z<sub>HER3</sub> matched the data from previous studies (122,136). In comparison with the uptake of [ $^{89}\text{Zr}$ ]Zr-seribantumab and [ $^{89}\text{Zr}$ ]Zr-seribantumab-F(ab')<sub>2</sub>, the uptake of [ $^{68}\text{Ga}$ ]Ga-Z<sub>HER3</sub> 3 h pi was lower in most of the organs, except the kidneys. The kidneys are known to be the primary excretory organ for affibody molecules (106,144). The lower uptake in the tumor and the normal organs is most likely due to the affibody molecules' smaller size and faster clearance compared with antibodies and antibody fragments.

Because of the faster clearance and lower uptake in normal tissue, most tumor-to-non-tumor ratios for [ $^{68}\text{Ga}$ ]Ga-Z<sub>HER3</sub> were equal to or significantly higher than the ratios for the  $^{89}\text{Zr}$ -labeled conjugates. For the same reason, [ $^{68}\text{Ga}$ ]Ga-Z<sub>HER3</sub> provided a visibly superior PET image contrast at 3 h pi compared with [ $^{89}\text{Zr}$ ]Zr-seribantumab and [ $^{89}\text{Zr}$ ]Zr-seribantumab-F(ab')<sub>2</sub> at their respective favorable time points.

Both  $^{89}\text{Zr}$ -labeled tracers showed elevated activity uptake in the bones, indicating the release of  $^{89}\text{Zr}$  from the DFO chelator in vivo. Free  $^{89}\text{Zr}$  tends to migrate to the bones (145), which was clearly visible in the PET images. Unfortunately, the release of  $^{89}\text{Zr}$  from the chelator complex is a known occurrence and well-documented in the literature. It has been speculated that the instability of the complex is due to the unsaturated coordination sphere of the Zr(IV) ion by DFO (142,146).

There might be additional advantages of using [ $^{68}\text{Ga}$ ]Ga-Z<sub>HER3</sub> instead of  $^{89}\text{Zr}$ -labeled antibodies and antibody fragments. The faster clearance of the affibody-conjugate reduces the radiation burden (85,147) and could also enable repeated imaging within a shorter time. The possibility to acquire images already 3 h after injection would also be more suitable for detection and following of rapid changes in expression.

## Conclusions

The results demonstrated a profound impact of the targeting molecule on the quality of HER3 PET imaging. Among the tested tracers, the  $^{68}\text{Ga}$ -labeled affibody molecule Z<sub>HER3</sub>, which we developed and investigated in Papers II and III, provided better image contrast than the antibody and F(ab')<sub>2</sub>-based tracers, already at 3 h pi, due to fast clearance from blood and low uptake in normal tissue. The results suggest that smaller-sized tracers might be more suitable for HER3 PET imaging than tracers based on therapeutic HER3 antibody molecules or F(ab')<sub>2</sub>-based tracers and that they should be further investigated in translational studies.

# Paper V: Evaluating the Therapeutic Efficacy of Mono- and Bivalent Affibody-Based Fusion Proteins Targeting HER3 in a Pancreatic Cancer Xenograft Model

## Background

The overexpression of HER3 in numerous types of solid cancers and its link to acquired therapy resistance have promoted the development of HER3-targeted therapy. Seribantumab, lumretuzumab, and patritumab are the therapeutic HER3-targeting antibodies that have advanced furthest in clinical trials (19). Thus far, no EMA- or FDA-approved HER3-targeted cancer treatment is available. However, a change of direction towards combination therapies, bispecific antibodies, and antibody-drug conjugates has raised new hope for successful HER3-targeted therapy (19).

Affibody molecules have attractive features for the development of novel therapeutic agents. Their smaller size can increase tissue penetration and their amenability in terms of valency, specificity, and addition of functional groups or conjugation of cytotoxic payloads allows for customized design and modification depending on the desired application (106). It has previously been shown that HER3-targeting affibody molecules have a cytostatic effect on HER3-expressing cancer cells (116).

The HER3-targeting affibody construct TAM-HER3 ( $Z_{\text{HER3:08698}}\text{-ABD-}Z_{\text{HER3:08698}}$ ), consisting of two HER3-binding affibody molecules linked by an albumin-binding domain (ABD), has previously been shown to have therapeutic efficacy similar to that of the anti-HER3 antibody seribantumab in a preclinical model (119). An ABD was conjugated with the aim to extend the half-life of the affibody construct in blood and thus slow renal excretion and increase the bioavailability of the affibody construct. In a previous study, we compared five HER3-binding ABD-conjugated affibody monomers and dimers, because we speculated that the position of the different building blocks could influence the biodistribution targeting properties of the constructs (148). We observed that C-terminal conjugation of the ABD (affibody conjugates 3A, 33A) and location of the ABD in the middle position (3A3 conjugate) provided promising biodistribution profiles for molecular targeted therapy with prolonged circulation in blood, and high accumulation in HER3-expressing tumors.

## Aim

Based on our previous findings regarding the influence of the molecular design of our HER3-targeting ABD-affibody conjugates on the biodistribution and targeting properties, we hypothesized that the molecular design could also significantly influence their therapeutic efficacy. The aim of Paper V was therefore to examine the therapeutic efficacies of the most promising HER3-

targeting affibody constructs (3A, 33A, 3A3) and compare it with that of the therapeutic HER3-targeting antibody seribantumab.

## Results

The affinities of the affibody constructs to human HER3, mErbB3, and human and mouse serum albumin were measured using surface plasmon resonance (SPR). Data are shown in Table 10. We tested the ability of the affibody constructs and seribantumab to inhibit the proliferation of HER3-expressing BxPC-3 cells and HRG-induced HER3 phosphorylation *in vitro*. Cell viability decreased in a dose-dependent manner when cells were incubated with the conjugates for five consecutive days, both in presence and absence of HRG (Figure 17A, B). No appreciable difference in potency was observed between treatment groups in either condition. All constructs were able to inhibit HRG-induced phosphorylation of HER3 (Figure 17C). The affibody conjugates showed similar potencies, which were considerably higher than the potency of seribantumab.

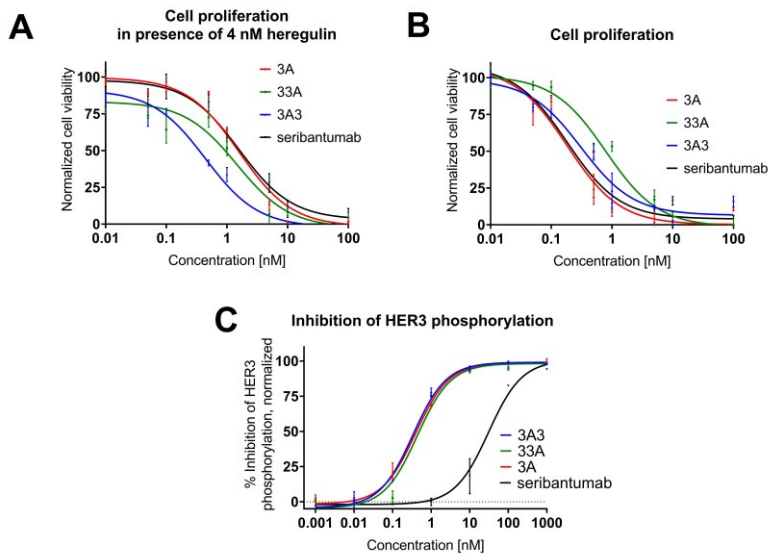


**Figure 17.** *In vitro* cell proliferation assay in the presence (A) and absence (B) of heregulin. BxPC-3 cells were incubated with the affibody conjugates or seribantumab for five consecutive days. (C) Inhibition of heregulin-induced HER3 phosphorylation was determined using a Phospho-ELISA assay.

BxPC-3 xenograft-bearing balb/c nu/nu mice received therapeutic injections intraperitoneally three times per week for up to 90 days. Significantly delayed tumor growth was observed in all treatment groups (Figure 18B). Average tumor volume in 3A-, 3A3- and seribantumab-treated groups was significantly smaller than that in the control group 15 days after treatment start. In the 33A-treated group, significantly smaller tumor size than in the control group was

observed on day 30 after treatment start. On day 58, tumors in the 3A- and seribantumab-treated groups were significantly smaller than in the 33A-treated group.

**Table 10.** Affinities of the affibody conjugates 3A, 33A, and 3A3 to HER3, mErbB3, human serum albumin (HSA), and mouse serum albumin (MSA) measured using SPR. Data presented as mean  $\pm$  SD.

Conjugate	K <sub>D</sub> , HER3 (nM)	K <sub>D</sub> , mErbB3 (nM)	K <sub>D</sub> , HSA (nM)	K <sub>D</sub> , MSA (nM)
3A	0.51 $\pm$ 0.08	1.01 $\pm$ 0.15	0.014 $\pm$ 0.002	0.16 $\pm$ 0.001
33A	1.04 $\pm$ 0.3	2.47 $\pm$ 0.25	0.006 $\pm$ 0.002	0.35 $\pm$ 0.002
3A3	1.73 $\pm$ 0.77	7.93 $\pm$ 0.95	0.011 $\pm$ 0.003	0.54 $\pm$ 0.008

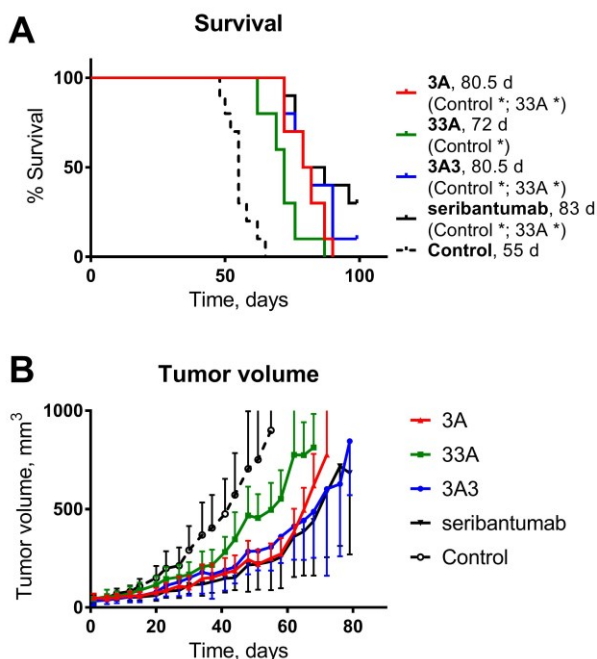


**Figure 18.** (A) Survival curve of BxPC-3 xenografted mice ( $n = 9-10$ ) treated with affibody conjugates 3A, 33A, 3A3, the HER3-targeting antibody seribantumab, and the control group. Median survival for each treatment group is noted in the legend, significant differences compared with other treatment groups are indicated in brackets. (B) Tumor growth. Treatment started on Day 0 (7 d after tumor cell inoculation). Treatment was administered by intraperitoneal injection 3 times per week for 90 days. Remaining animals were euthanized on day 93. Curves were interrupted when more than three animals per group were euthanized on the same day.

The median survival in all treatment groups was significantly prolonged compared with that in the control group (Figure 18A). There was no significant difference in median survival between treatment groups except in the group treated with the 33A conjugate, where it was significantly shorter than in any other treatment group. Immunohistochemical analysis of tumors for HER3 expression showed homogenous expression of HER3 in control tumors and weaker expression in the periphery of lobules in tumors from treatment groups (Figure 19B).

Monitoring of animal weight, pathological examination of liver and kidneys, and analysis of blood serum did not show any difference between control and treated animals and no signs of toxic damage in the treatment groups.

NanoPET/CT imaging was performed to visualize HER3 expression when tumor volume had reached 700 mm<sup>3</sup> and one day after therapeutic injection. PET imaging using [<sup>68</sup>Ga]Ga-Z<sub>HER3</sub> ([<sup>68</sup>Ga]Ga-(HE)<sub>3</sub>-Z<sub>HER3</sub>-NODAGA, previously developed and evaluated in Papers II–IV) could visualize HER3 expression in xenografts of control animals, but not in animals treated with the afibody conjugates or seribantumab (Figure 19A). Uptake of [<sup>68</sup>Ga]Ga-(HE)<sub>3</sub>-Z<sub>HER3</sub>-NODAGA was also seen in the kidneys in all groups. Hepatic uptake was visualized in control animals, 3A- and seribantumab-treated groups, although uptake in the liver appeared lower in the 3A-treated group.

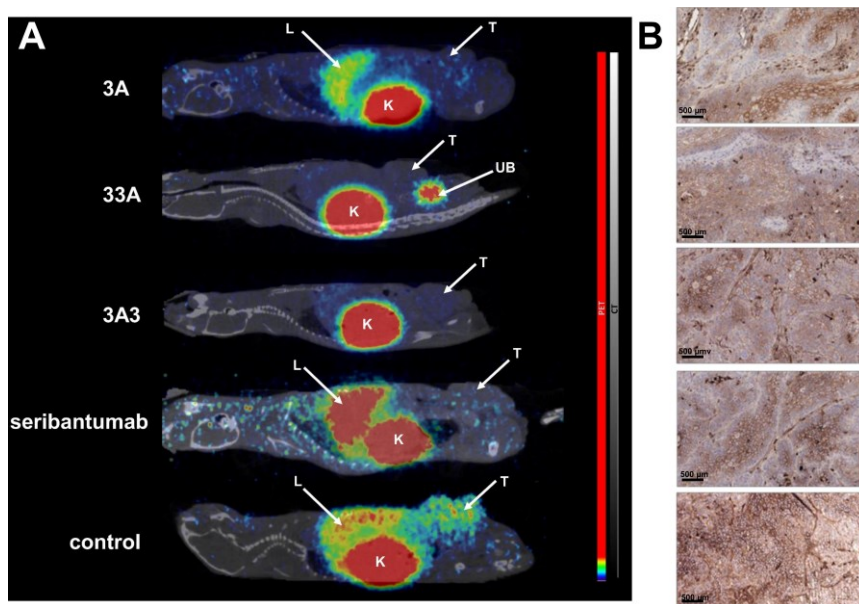


**Figure 19.** (A) nanoPET/CT images of BxPC-3 xenografted therapy animals. Images were acquired one day after therapeutic injection and 1 h pi of 2 μg [<sup>68</sup>Ga]Ga-Z<sub>HER3</sub>. Letters and arrows indicate tumors (T), liver (L), kidneys (K), and urinary bladder (UB). (B) Immunohistochemistry staining of HER3-expressing xenografts taken at endpoint.

## Discussion

The versatile framework of affibody molecules allows for straightforward modification and rearrangement of the molecular building blocks. Our group had previously shown that a HER3-targeting affibody conjugate (entitled TAM-HER3) consisting of two HER3-targeting affibody molecules linked by an ABD could delay the growth of HER3-expressing xenografts in mice (119). In this study, we aimed to investigate if and how the position of the molecular building blocks and the valency of the affibody construct could influence the therapeutic efficacy in a preclinical mouse model. The study included a structurally similar variant to TAM-HER3 entitled 3A3, the affibody conjugates 3A and 33A, which were selected based on their favorable biodistribution and tumor-targeting properties (148), in addition to the HER3-targeting antibody seribantumab.

Treatment with the affibody conjugates and seribantumab *in vivo* showed a clear therapeutic effect, significantly delaying tumor growth and prolonging median survival, as well as downregulation of HER3 expression in xenografts compared with the control treatment (PBS), without any signs of toxicity. Although we did not observe any differences in potency in inhibiting cell proliferation *in vitro*, *in vivo* data revealed an effect of the molecular design of the affibody constructs on the therapeutic efficacy. Treatment with 33A was significantly less effective in delaying tumor growth and prolonging survival than treatment with 3A, 3A3, or seribantumab. We speculated that the lower efficacy of 33A was related to the faster clearance of the construct from the body and resulting lower bioavailability (148).

Schardt et al. hypothesized that multivalent affibody constructs would be more effective in inhibiting tumor progression than monovalent molecules due to increased affinity through avidity and more efficient inhibition of HER3 phosphorylation and downstream signaling. They confirmed this hypothesis in a preclinical therapy study (120,149). In contrast to this, our study showed that the treatment with the monovalent 3A affibody conjugate was equally potent as treatment with bivalent 3A3 construct and seribantumab. Among our developed affibody conjugates, 3A cleared the slowest from blood. The resulting increased bioavailability of 3A and the better affinity of 3A compared with 3A3 and 33A could be a possible explanation for its potency. Better bioavailability due to prolonged circulation might also be the reason why seribantumab showed good effect, despite worse inhibition of HER3 phosphorylation in the Phospho-ELISA assay. The difference between the *in vivo* model and HER3-targeting affibody molecule used by Schardt et al. and the set-up used in this study could be another possible explanation for this contradiction. The lower HER3 receptor density in our model might hinder bivalent binding of the dimeric constructs and enable more efficient tumor penetration with a monomer.

In this study, we further demonstrated the ability of our  $^{68}\text{Ga}$ -labeled affibody [ $^{68}\text{Ga}$ ]Ga-Z<sub>HER3</sub> to image HER3 receptor occupancy in the treated xenografts. No uptake of [ $^{68}\text{Ga}$ ]Ga-Z<sub>HER3</sub> was observed in treated tumors one day after therapeutic injection, indicating the occupancy of HER3 receptors by the respective therapeutic agents. As expected, PET images of the non-treated control animals showed activity uptake in the xenografts. Differences in hepatic uptake between animals in the treated group could possibly be explained by differences in cellular processing between normal and tumor cells. In addition, biodistribution studies have shown higher concentration of 3A in blood and lower uptake in the liver compared with 33A and 3A3 (148). It has also been speculated that multivalent affibody molecules have higher hepatic accumulation than monovalent affibody molecules due to slower dissociation of multivalent molecules and HER3 sequestration (150). We could speculate that this is the reason for higher hepatic uptake of [ $^{68}\text{Ga}$ ]Ga-Z<sub>HER3</sub> in the 3A-treated group compared with that the 33A- and 3A3-treated groups.

## Conclusions

In Paper V, we evaluated the therapeutic efficacy of three monovalent and bivalent ABD-fused affibody constructs for HER3-targeted therapy in a pre-clinical model. Our results further strengthen the argument for affibody molecules as potential therapeutic agents for HER3-expressing malignancies. The most potent affibody conjugates demonstrated similar therapeutic efficacy to the HER3-targeting antibody seribantumab. We also showed that careful molecular design of affibody conjugates in terms of valency and arrangement of the molecular building blocks is important to ensure therapeutic efficacy.

While it was not the main objective of this study, we further demonstrated that the affibody molecule [ $^{68}\text{Ga}$ ]Ga-Z<sub>HER3</sub> could be a useful diagnostic companion, not only in affibody-based HER3-targeted therapy, but also in antibody-based HER3-targeted therapy.

## Concluding Remarks

HER3 is a challenging target for molecular imaging and targeted therapy in cancer. Affibody-based diagnostic and therapeutic agents could be a promising alternative to existing targeting strategies. Overall, the projects included in this thesis aimed to investigate how changes in the molecular design of HER3-binding affibody molecules could improve their diagnostic and therapeutic utility in HER3-expressing cancers.

Papers I–III investigated the influence of different molecular modifications on the biodistribution and imaging properties of  $^{111}\text{In}$ -,  $^{68}\text{Ga}$ -, and radiocobalt-labeled variants of the  $Z_{\text{HER3}}$  affibody molecule, with particular focus on reducing non-specific uptake. Moreover, Paper III compared early time point PET imaging using a  $^{68}\text{Ga}$ -labeled variant of  $Z_{\text{HER3}}$ , with later time point imaging using a less conventional radiocobalt label.

**Papers I and II** showed that replacing the local positive charge of the radiometal/chelator complex with a neutral or negatively charged complex reduced the off-target interaction of  $^{111}\text{In}$ - and  $^{68}\text{Ga}$ -labeled  $Z_{\text{HER3}}$ , particularly in the liver, and improved the overall HER3 image contrast.

**Paper II** showed that introduction of a hydrophilic  $(\text{HE})_3$ -tag to the N-terminus of  $Z_{\text{HER3}}$  improved clearance and in combination with a neutrally charged  $[^{68}\text{Ga}]\text{Ga-NODAGA}$  complex provided the most favorable PET image contrast.

**Paper III** further supported the findings from Papers I and II. However, the results of this study also revealed that there might be limitations to the beneficial effect of increased negative charge of the radiometal/chelator complex. In Paper III, it was also demonstrated that HER3 PET image contrast could be improved by next-day imaging using the radiocobalt-labeled  $Z_{\text{HER3}}$  affibody variant  $(\text{HE})_3\text{-}Z_{\text{HER3}}\text{-DOTA}$ .

Working under the hypothesis that tracers based on affibody molecules might be better suited for molecular imaging of HER3 expression, it was subsequently investigated how the optimized affibody-based tracer would compare to PET tracers based on therapeutic antibodies and antibody fragments.

**Paper IV** demonstrated that the optimized affibody-based tracer [ $^{68}\text{Ga}$ ]Ga- $Z_{\text{HER3}}$  could provide higher contrast PET images of HER3 expression than the full-length antibody [ $^{89}\text{Zr}$ ]Zr-seribantumab, and a seribantumab-derived [ $^{68}\text{Ga}$ ]Ga/[ $^{89}\text{Zr}$ ]Zr-labeled F(ab')<sub>2</sub> fragment at their respective favorable time points for imaging. The superior image contrast provided by [ $^{68}\text{Ga}$ ]Ga- $Z_{\text{HER3}}$  already shortly after injection could mainly be attributed to its appreciably faster clearance and lower off-target interaction.

HER3-targeting affibody molecules are known to have a cytostatic effect on HER3-expressing cancer cells. In Paper V, the therapeutic efficacies of three monovalent and bivalent affibody-ABD conjugates for HER3-targeted therapy were compared with each other and with that of the antibody seribantumab.

**Paper V** showed that the arrangement of the molecular building blocks of HER3-targeting affibody-based therapeutic agents influenced their therapeutic efficacy. The monovalent 3A and bivalent 3A3 conjugates exhibited similar therapeutic efficacy as the HER3-targeting antibody seribantumab. This paper further showed that [ $^{68}\text{Ga}$ ]Ga- $Z_{\text{HER3}}$  could be suited as a diagnostic companion for HER3-targeted therapy.

In summary, the results presented in this thesis show that HER3-targeting affibody molecules could be well-suited candidates for molecular imaging and treatment of HER3 expressing cancer. It was shown that careful optimization of the radiolabel, the local charge, and hydrophilicity can be important to improve affibody-based imaging of HER3 expression. Increased hydrophilicity and a radiometal/chelator complex with a negative charge was generally beneficial for HER3 image contrast. However, individual optimization to determine the favorable combination for each radiotracer may be required. The results in this thesis have also shown that the efficacy of ABD-fused  $Z_{\text{HER3}}$  affibody conjugates for HER3-targeted therapy is linked to their molecular design in terms of valency and the arrangement of the individual building blocks.

Most importantly, the results have shown the competitiveness of affibody-based agents with existing antibody-based approaches for imaging and therapy of HER3-expressing cancer.

## Future Directions

Developing imaging agents for low-expressing targets and targets with natural expression in healthy tissue adds an additional layer of challenges to the existing demands for high-contrast imaging agents. I hope that adding our findings to the “molecular imaging tool box” could aid the development of imaging agents – scaffold-based or not – for other low-expressing molecular targets in the future.

Keeping in mind that several antibody-based tracers for imaging of HER3 expression have been evaluated in clinical trials without major success, we hope to pursue the use of affibody-based tracers for HER3 imaging in translational studies in the future.

The HER3-targeting therapeutic affibody constructs have, thus far, only shown a growth-delaying cytostatic effect. Affibody molecules are also well-suited vehicles for targeted drug delivery. In the future, we plan to explore a two-in-one approach for affibody-based HER3-targeting therapy to improve therapeutic efficacy. We plan to use HER3-binding affibody constructs to induce the known cytostatic effect, while simultaneously using them for the delivery of a cytotoxic drug. In more detail, we plan to conjugate the 3A and 3A3 affibody constructs characterized in this thesis with a tubulin inhibitor and evaluate their therapeutic potential in an *in vivo* therapy study.

Since HER3 is commonly co-expressed with other cancer-associated markers and is a mediator for therapy resistance, we would also like to explore the development of co-targeted cancer therapy. Because of the nature of cancer-associated HER3 overexpression, combining HER3-targeted treatment with other therapeutic agents might increase the treatment effect. In particular, we want to investigate the use of our HER3-targeting affibody molecules in combination with other targeted therapeutic agents against, for example, EGFR, HER2, or the epidermal cell adhesion molecule (EpCAM).

# Popular Science Summary

Targeted cancer therapy refers to the use of drugs and treatment strategies that are directed towards cancer cell-specific markers in order to inhibit tumor growth and metastatic spread, and kill cancer cells. This approach enables the delivery of treatment specifically to cancer cells and has the potential to make patient care more efficient, as the treatment can be matched to the molecular characteristics of the patient's disease.

To increase the chances of therapy success, the patients whose cancer expresses the intended therapeutic target need to be identified. PET and SPECT are imaging techniques that can detect the presence of cell surface proteins in the body by using so called radiotracers. Therefore, they can be used to select patients who are eligible for a certain targeted therapy. The radiotracer consists of a radionuclide attached to a molecule that binds to the biomarker of interest, and should therefore accumulate in areas where the biomarker is present. The location of the molecule in the body (and thus the presence of the biomarker) can then be visualized by using a PET or SPECT camera that detects the radiation emitted from the radionuclide.

The human epidermal growth factor receptor type 3 (HER3) is a cell surface protein that can be overexpressed in many different cancers, for example breast, prostate, and gastric cancers. Its presence is often associated with a poor prognosis and resistance to therapy. Currently, no cancer treatment directed against HER3 and no radiotracers for imaging of HER3 expression have been approved for clinical use.

Affibody molecules are a type of protein that could be used as a foundation for the development of agents for targeted therapy and molecular imaging. They can be engineered to bind to different molecular markers, such as HER3. The affibody molecule  $Z_{\text{HER3}}$  is known to bind strongly to HER3.

The aim of this thesis was to develop and improve strategies for the diagnosis and treatment of HER3-expressing cancer using affibody molecules. **Papers I–III** looked at how small changes to the design of  $Z_{\text{HER3}}$ -based radiotracers would change their distribution in the body and their ability to visualize HER3 expression using PET and SPECT. **Paper IV** showed that we could achieve PET images with better contrast when using the  $Z_{\text{HER3}}$ -radiotracers we had optimized in preceding studies than when using more traditional types of radiotracer. **Paper V** described a preclinical therapy study investigating different  $Z_{\text{HER3}}$ -based molecules for treatment of HER3-expressing cancer. The

most effective  $Z_{\text{HER3}}$ -based therapeutic molecules showed a therapeutic effect equal to that of a therapy which has been evaluated in clinical studies.

Overall, the findings included in this thesis indicate that HER3-binding affibody molecules are well-suited for detection and targeted therapy of HER3-expressing cancer. In preclinical models, it has been shown that HER3-targeting affibody molecules can provide superior diagnostic images and similar therapeutic effect to more traditional approaches.

# Populärvetenskapligt Sammanfattning

Syftet med målinriktad cancerterapi är att minska tumörtillväxt och spridning av metastaser genom att använda behandlingsstrategier som är riktade mot cancerrelaterade biomarkörer. Denna strategi medför leverans av läkemedel till specifika biomarkörer som uttrycks på cancerceller och har därmed potential att effektivisera behandlingen genom att individanpassa terapivalet till de biomarkörer som uttrycks hos varje enskild patient.

För att öka chanserna till en lyckad behandling är det viktigt att identifiera de patienter vars cancerceller uttrycker det specifika behandlingsmålet. Detta kan göras med hjälp av avbildningstekniker som exempelvis PET och SPECT. Dessa tekniker kan, genom användning av radioaktivt märkta molekyler, så kallade radiotracer, detektera och avbilda biomarkörer som uttrycks på cellytan hos cancerceller och på så sätt användas för att selektera de patienter som kan dra nytta av målinriktad cancerterapi. En radiotracer består av en radionuklid som är ihopkopplad med en molekyl som kan binda till en specifik biomarkör. Det är viktigt att den radiotracer som används ackumuleras i de områden där den specifika biomarkören uttrycks samt har så lågt upptag som möjligt i övrig vävnad. På så sätt kan biomarkörerna och därmed cancercellerna lokaliseras i kroppen genom att PET eller SPECT kameror kan detektera radionuklidens sönderfall.

Human epidermal growth factor receptor type 3 (HER3) är ett protein som överuttrycks på ytan av vissa typer av cancerceller som exempelvis bröst-, prostata-, och magsäckscancerceller. Höga nivåer av HER3 är ofta associerat med en dålig sjukdomsprognos och terapiresistens. Fram tills idag har ingen cancerbehandling eller radiotracer riktad mot HER3 godkänts för användning i klinik.

Affibody molekyler är en typ av protein som kan användas för utveckling av målinriktad cancerterapi och molekylär avbildning av specifika biomarkörer.  $Z_{HER3}$  är en affibody molekyl som i olika experiment har visat stark förmåga att binda specifikt till HER3. Syftet med denna avhandling var att utveckla och förbättra de existerande tillvägagångssätten för diagnos och behandling av HER3-uttryckande cancertyper med hjälp av affibody molekyler.

**Artikel I-III** beskriver hur små förändringar i designen av radiotracer baserade på  $Z_{HER3}$  påverkar distributionen i kroppen och därmed förmågan att avbilda HER3 med hjälp av PET och SPECT. **Artikel IV** påvisar hur kontrasten för avbildning av HER3 kan förbättras genom användning av en optimerad  $Z_{HER3}$ -baserad radiotracer som utvecklats under de tidigare studierna jämfört

med användningen av en mer traditionell typ av radiotracer. **Artikel V** beskriver en preklinisk terapistudie som undersökte vilken effekt behandling med olika  $Z_{HER3}$ -baserade molekyler hade på HER3-uttryckande cancertyper. De mest effektiva  $Z_{HER3}$ -baserad molekylen uppvisade likvärdig terapeutisk effekt som en behandling som tidigare har utvärderats i kliniska studier.

Sammanfattningsvis visar de resultat som presenteras i denna avhandling att  $Z_{HER3}$ -baserade affibody molekyler är väl lämpade för avbildning och målriktad behandling av HER3-uttryckande cancertyper. I prekliniska modeller har  $Z_{HER3}$ -baserade affibody molekyler visats sig vara mer fördelaktiga att använda för avbildning av HER3 samt ha likvärdig terapeutisk effekt som traditionella behandlingsstrategier. Förhoppningsvis kan detta bidra till fortsatt utveckling och implementering av HER3-riktad cancerbehandling i kliniken.

# Populärwissenschaftliche Zusammenfassung

Die zentrale Idee der sogenannten zielgerichteten Krebstherapie ("targeted cancer therapy") ist es Krebspatienten mit Medikamenten zu behandeln, die auf spezifische molekulare Merkmale von Krebszellen abgestimmt sind. Idealerweise könnte dadurch der Therapiewirkstoff direkt an die Krebszellen geliefert werden, um diese zu zerstören, während gesundes Gewebe verschont bliebe. Allerdings hat diese Behandlungsstrategie nur dann Aussicht auf Erfolg, wenn bei einem Patienten das Zielmerkmal des Medikamentes auch vorhanden ist. Um die Chancen auf eine erfolgreiche Behandlung zu erhöhen, ist es daher wichtig vor Therapiebeginn herauszufinden, ob ein Patient Träger eines Zielmerkmals ist oder nicht.

Nuklearmedizinische Bildgebungsverfahren (PET oder SPECT) können, unter anderem, dazu genutzt werden die Präsenz von biologischen Merkmalen (auch Biomarkern) zu analysieren. Hierzu wird dem Patienten ein radioaktivmarkiertes Molekül, ein sogenannter Radiotracer, verabreicht, der einen bestimmten Biomarker bindet. SPECT und PET Kameras können dann die vom Radiotracer ausgesandte Strahlung detektieren und dadurch die Präsenz des Biomarker feststellen und abbilden.

Der humane epidermale Wachstumsfaktor Rezeptor Typ 3 (HER3) ist ein Rezeptor Protein, das auf der Zelloberfläche verschiedener Krebszellen gefunden werden kann. Im Normalfall ist HER3 in elementare Zellvorgänge, zum Beispiel Zellwachstum, involviert. In Krebszellen kann es zu einer erhöhten Präsenz und Deregulation dieses Rezeptors kommen, welche oft mit einer schlechten Prognose und Therapieresistenz verbunden ist. Derzeit sind keine HER3-gerichteten Medikamente oder Radiotracer für die klinische Anwendung zugelassen.

Affibody-Moleküle sind eine Art von Proteinen, die vielversprechende Eigenschaften für die Entwicklung von zielgerichteten Medikamenten und Radiotracer für die molekulare Bildgebung besitzen. Das Affibody-Molekül  $Z_{HER3}$  bindet den HER3 Rezeptor und hat in präklinischen Studien schon erste Eignung zur Behandlung und Diagnose von HER3-positiven Tumoren gezeigt.

Das Ziel der in dieser Arbeit präsentierten Forschung ist es auf Affibody-Molekülen basierende HER3-bindende Radiotracer für die diagnostische Bildgebung und HER3-gerichtete Medikamente zur Behandlung von HER3-positiven Krebserkrankungen zu entwickeln und zu verbessern. **Artikel I-III** untersuchen wie verschiedene molekulare Veränderungen die Fähigkeit von

$Z_{\text{HER3}}$ -Radiotracer beeinflussen HER3-positive Tumore zu detektieren. **Artikel IV** zeigt schließlich, dass mit dem in Artikel I-III optimierten  $Z_{\text{HER3}}$ -Radiotracer besserer Bildkontrast erreicht werden kann als mit traditionellen Arten von Radiotracer. **Artikel V** beschreibt eine präklinische Therapiestudie, die den Effekt von verschiedenen  $Z_{\text{HER3}}$ -basierenden Molekülen für die Behandlung von HER3-positiven Tumoren miteinander vergleicht. Hier wurde gezeigt, dass das wirkungsvollste Affibody-Konstrukt den gleichen therapeutischen Effekt erzielen kann wie ein HER3-bindender Antikörper, der derzeit in klinischen Studien getestet wird.

Diese Ergebnisse deuten darauf hin, dass HER3-bindenden Affibody-Moleküle nicht nur exzellente Kandidaten für die Diagnose und Behandlung von HER3-positiven Krebserkrankungen sind, sondern auch mit traditionellen Strategien der zielgerichteten Krebsbehandlung konkurrieren können.

# Acknowledgements

This thesis work was conducted at the Department of Medicinal Chemistry (Theranostics Group) at Uppsala University. I am thankful for everyone who has helped and encouraged me during my time as PhD student. I would especially like to thank a few people who have – in many different ways – contributed to this thesis and have supported me on this scientific, professional and personal journey:

My main supervisor, **Prof. Anna Orlova**, for, first of all, taking me on as a PhD student, and then guiding and supporting me throughout this journey. Thank you for always taking time out of your schedule when I needed help, advice, encouragement or anything else. You helped me grow as a researcher and a person and made my time as a PhD student a great experience overall.

My co-supervisors:

**Vladimir** – For gladly sharing your immense knowledge at any time. For your patience, support and guidance along the way, and sharing your endless drive and enthusiasm for science.

**Mohamed** – I cannot thank you enough for all your support and encouragement, both professionally and personally. Thank you for always taking the time to listen, discuss or help even when you were busy or all the way in Lund!

**Anzhelika** – For always having an open door and being there to give advice and discuss thoughts and ideas. For happily sharing your experiences and supporting me in the lab and always having kind words on encouragement!

Current and former Group members:

**Tianqi, Yongsheng, Maryam, Javad** – Thank you for being fantastic team players and always being there to help out! Thank you for all the interesting discussions and fun during fikas and on conference trips. I am lucky to have such an awesome team around me!

**Ayman and Bogdan** – You both had the luck (or burden?!) of sharing the office me for the better part of my PhD journey. Thank you for being fantastic office mates! I might not say it enough, but I really appreciate you and all the countless times you helped me in the lab (and outside the lab) and patiently

dealt with the 5 million different moods I go through in a day. Bogdan, thank you for being so cool about all the times I (accidentally) invaded your desk. Also, just for the record: I can beat you at Kubb at any time. Ayman, I cannot thank you enough for always going out of your way to help! Also, I am sorry for all the times I almost bored you to death with my gymnastics talk.

**Maria R. and Emmi P.** – This would not have been possible without – at any time – having you just a desk, a couple doors or a phone call away! I learned so much from both of you and know that I can always count on you for anything – advice on science, life, hands on help, venting, emotional support – or just a snack. Thank you for pulling me back to earth when I needed it. You are such intelligent, strong and kindhearted women and role models. I am so thankful I have had you by my side during this journey and hopefully will have you there for many more years to come! To the China Spinny Panda Ring Trinity!

**Fanny** – There is no person I would rather share my desk with! Thank you for always being there to listen, give advice and ball thoughts and ideas around. Somehow, we always end up talking for hours about life and research. You are incredibly smart, strong and driven, and still always there to help, encourage and motivate everyone around you!

Our collaborators at KTH, particularly **Charlie, Stefan and John** – Thank you for this fantastic collaboration. Without you, this work would not have been possible!

**PPP – Veronika, Sergio, Ram, Ola, Gry**

Thank you for making our corridor such a welcoming and fun place to be! The fun conversations on science and life during breakfast, lunch or fika definitely were something I looked forward to when coming to work every day! TheraTPPPI(?) (or TPIPPPBonostics?) would not be the same without you!

**Emmi E.** – Tack för alla gym mornings when we tried to lift away our problems och alla terapi måndagar. Tack för att du alltid lyssnar och ibland bara fattar.

**Maria T.** – who would have thought that when we entered that classroom many years ago that we would become friends for life. Even though our professional paths separated shortly after we met, I am incredibly thankful for your continuous support and friendship!

**Sophia** – When I was first looking for a flat mate, I was just hoping for the person not to be a serial killer. Honestly, I do not know how many stars had to align for it to work out the way it did! I did not just find a flat mate but also

a friend! We have been on this journey together – And soon both of us will be PhDs!

**My Family** – Danke, dass ihr immer an mich glaubt, und mich meinen Weg gehen lasst. Danke, dass ihr immer für mich da seid und die unendliche Liebe und Unterstützung bei diesem Abenteuer! Ich habe euch lieb!

# References

1. Rinne SS, Orlova A, Tolmachev V. PET and SPECT Imaging of the EGFR Family (RTK Class I) in Oncology. *International Journal of Molecular Sciences*. 2021 Jan;22(7):3663.
2. Rinne SS, Vorobyeva A. Radiometals—Chemistry and radiolabeling. In: Reference Module in Biomedical Sciences [Internet]. Elsevier; 2021. Available from: <https://www.sciencedirect.com/science/article/pii/B9780128229606000442>
3. International Agency in Research on Cancer. Latest global cancer data: Cancer burden rises to 19.3 million new cases and 10.0 million cancer deaths in 2020 – IARC [Internet]. [cited 2021 Oct 27]. Available from: <https://www.iarc.who.int/news-events/latest-global-cancer-data-cancer-burden-rises-to-19-3-million-new-cases-and-10-0-million-cancer-deaths-in-2020/>
4. Hanahan D, Weinberg RA. The hallmarks of cancer. *Cell*. 2000 Jan 7;100(1):57–70.
5. Hanahan D. Hallmarks of Cancer: New Dimensions. *Cancer Discov*. 2022 Jan 1;12(1):31–46.
6. Marusyk A, Almendro V, Polyak K. Intra-tumour heterogeneity: a looking glass for cancer? *Nat Rev Cancer*. 2012 May;12(5):323–34.
7. Shin SH, Bode AM, Dong Z. Precision medicine: the foundation of future cancer therapeutics. *NPJ Precis Oncol*. 2017;1(1):12.
8. Strebhardt K, Ullrich A. Paul Ehrlich's magic bullet concept: 100 years of progress. *Nat Rev Cancer*. 2008 Jun;8(6):473–80.
9. Seebacher NA, Stacy AE, Porter GM, Merlot AM. Clinical development of targeted and immune based anti-cancer therapies. *Journal of Experimental & Clinical Cancer Research*. 2019 Apr 11;38(1):156.
10. Appert-Collin A, Hubert P, Crémel G, Bennisroune A. Role of ErbB Receptors in Cancer Cell Migration and Invasion. *Front Pharmacol* [Internet]. 2015 Nov 24 [cited 2017 Jan 10];6. Available from: <http://www.ncbi.nlm.nih.gov/pmc/articles/PMC4657385/>
11. Hendler FJ, Ozanne BW. Human squamous cell lung cancers express increased epidermal growth factor receptors. *J Clin Invest*. 1984 Aug 1;74(2):647–51.
12. Schechter AL, Stern DF, Vaidyanathan L, Decker SJ, Drebin JA, Greene MI, et al. The neu oncogene: an erb-B-related gene encoding a 185,000-Mr tumour antigen. *Nature*. 1984 Dec 6;312(5994):513–6.
13. Roskoski R. The ErbB/HER family of protein-tyrosine kinases and cancer. *Pharmacol Res*. 2014 Jan;79:34–74.
14. Thomas R, Weihua Z. Rethink of EGFR in Cancer With Its Kinase Independent Function on Board. *Front Oncol* [Internet]. 2019 [cited 2020 Dec 11];9. Available from: <https://www.frontiersin.org/articles/10.3389/fonc.2019.00800/full>
15. Loibl S, Gianni L. HER2-positive breast cancer. *Lancet*. 2017 Jun 17;389(10087):2415–29.
16. Oh D-Y, Bang Y-J. HER2-targeted therapies — a role beyond breast cancer. *Nat Rev Clin Oncol*. 2020 Jan;17(1):33–48.

17. Segers VFM, Dugaucquier L, Feyen E, Shakeri H, De Keulenaer GW. The role of ErbB4 in cancer. *Cell Oncol (Dordr)*. 2020 Jun;43(3):335–52.
18. Kraus MH, Issing W, Miki T, Popescu NC, Aaronson SA. Isolation and characterization of ERBB3, a third member of the ERBB/epidermal growth factor receptor family: evidence for overexpression in a subset of human mammary tumors. *Proc Natl Acad Sci USA*. 1989 Dec;86(23):9193–7.
19. Haikala HM, Jänne PA. Thirty Years of HER3: From Basic Biology to Therapeutic Interventions. *Clin Cancer Res*. 2021 Feb 19;27(13):3528–39.
20. Jura N, Shan Y, Cao X, Shaw DE, Kuriyan J. Structural analysis of the catalytically inactive kinase domain of the human EGF receptor 3. *PNAS*. 2009 Dec 22;106(51):21608–13.
21. Shi F, Telesco SE, Liu Y, Radhakrishnan R, Lemmon MA. ErbB3/HER3 intracellular domain is competent to bind ATP and catalyze autophosphorylation. *PNAS*. 2010 Apr 27;107(17):7692–7.
22. Kraus MH, Fedi P, Starks V, Muraro R, Aaronson SA. Demonstration of ligand-dependent signaling by the erbB-3 tyrosine kinase and its constitutive activation in human breast tumor cells. *Proc Natl Acad Sci U S A*. 1993 Apr 1;90(7):2900–4.
23. Amin DN, Campbell MR, Moasser MM. The role of HER3, the unpretentious member of the HER family, in cancer biology and cancer therapeutics. *Semin Cell Dev Biol*. 2010 Dec;21(9):944–50.
24. Campbell MR, Amin D, Moasser MM. HER3 comes of age: new insights into its functions and role in signaling, tumor biology, and cancer therapy. *Clin Cancer Res*. 2010 Mar 1;16(5):1373–83.
25. Ocana A, Vera-Badillo F, Seruga B, Templeton A, Pandiella A, Amir E. HER3 overexpression and survival in solid tumors: a meta-analysis. *J Natl Cancer Inst*. 2013 Feb 20;105(4):266–73.
26. Lee Y, Ma J, Lyu H, Huang J, Kim A, Liu B. Role of erbB3 receptors in cancer therapeutic resistance. *Acta Biochim Biophys Sin (Shanghai)*. 2014 Mar;46(3):190–8.
27. Mishra R, Patel H, Alanazi S, Yuan L, Garrett JT. HER3 signaling and targeted therapy in cancer. *Oncol Rev*. 2018 Jan 30;12(1):355.
28. Frogne T, Benjaminsen RV, Sonne-Hansen K, Sorensen BS, Nexø E, Laenkholm A-V, et al. Activation of ErbB3, EGFR and Erk is essential for growth of human breast cancer cell lines with acquired resistance to fulvestrant. *Breast Cancer Res Treat*. 2009 Mar;114(2):263–75.
29. Yang L, Li Y, Shen E, Cao F, Li L, Li X, et al. NRG1-dependent activation of HER3 induces primary resistance to trastuzumab in HER2-overexpressing breast cancer cells. *Int J Oncol*. 2017 Nov;51(5):1553–62.
30. Jathal MK, Chen L, Mudryj M, Ghosh PM. Targeting ErbB3: the New RTK(id) on the Prostate Cancer Block. *Immunol Endocr Metab Agents Med Chem*. 2011 Jun;11(2):131–49.
31. Sergina NV, Rausch M, Wang D, Blair J, Hann B, Shokat KM, et al. Escape from HER-family tyrosine kinase inhibitor therapy by the kinase-inactive HER3. *Nature*. 2007 Jan 25;445(7126):437–41.
32. Ma J, Lyu H, Huang J, Liu B. Targeting of erbB3 receptor to overcome resistance in cancer treatment. *Mol Cancer*. 2014 May 8;13:105.
33. Kiavue N, Cabel L, Melaabi S, Bataillon G, Callens C, Lerebours F, et al. ERBB3 mutations in cancer: biological aspects, prevalence and therapeutics. *Oncogene*. 2020 Jan;39(3):487–502.
34. Jaiswal BS, Kljavin NM, Stawiski EW, Chan E, Parikh C, Durinck S, et al. Oncogenic ERBB3 mutations in human cancers. *Cancer Cell*. 2013 May 13;23(5):603–17.

35. Sergina NV, Moasser MM. The HER family and cancer: emerging molecular mechanisms and therapeutic targets. *Trends Mol Med.* 2007 Dec;13(12):527–34.
36. Yamaoka T, Kusumoto S, Ando K, Ohba M, Ohmori T. Receptor Tyrosine Kinase-Targeted Cancer Therapy. *Int J Mol Sci.* 2018 Nov 6;19(11):3491.
37. Drago JZ, Modi S, Chandarlapaty S. Unlocking the potential of antibody–drug conjugates for cancer therapy. *Nat Rev Clin Oncol.* 2021 Jun;18(6):327–44.
38. Huang L, Jiang S, Shi Y. Tyrosine kinase inhibitors for solid tumors in the past 20 years (2001–2020). *J Hematol Oncol.* 2020 Dec;13(1):1–23.
39. Li S, Schmitz KR, Jeffrey PD, Wiltzius JJW, Kussie P, Ferguson KM. Structural basis for inhibition of the epidermal growth factor receptor by cetuximab. *Cancer Cell.* 2005 Apr 1;7(4):301–11.
40. Dubois EA, Cohen AF. Panitumumab. *Br J Clin Pharmacol.* 2009 Oct;68(4):482–3.
41. Capelan M, Pugliano L, De Azambuja E, Bozovic I, Saini KS, Sotiriou C, et al. Pertuzumab: new hope for patients with HER2-positive breast cancer. *Annals of Oncology.* 2013 Feb 1;24(2):273–82.
42. Jacob W, James I, Hasmann M, Weisser M. Clinical development of HER3-targeting monoclonal antibodies: Perils and progress. *Cancer Treat Rev.* 2018 Jul;68:111–23.
43. Rahmim A, Zaidi H. PET versus SPECT: strengths, limitations and challenges. *Nucl Med Commun.* 2008 Mar;29(3):193–207.
44. Qaim SM. Nuclear data for production and medical application of radionuclides: Present status and future needs. *Nuclear Medicine and Biology.* 2017 Jan 1;44:31–49.
45. Hicks RJ, Hofman MS. Is there still a role for SPECT–CT in oncology in the PET–CT era? *Nat Rev Clin Oncol.* 2012 Dec;9(12):712–20.
46. Dhingra VK, Mahajan A, Basu S. Emerging clinical applications of PET based molecular imaging in oncology: the promising future potential for evolving personalized cancer care. *Indian J Radiol Imaging.* 2015;25(4):332–41.
47. Almuhaideb A, Papanthasiou N, Bomanji J. 18F-FDG PET/CT imaging in oncology. *Ann Saudi Med.* 2011 Feb;31(1):3–13.
48. Lau J, Rousseau E, Kwon D, Lin K-S, Bénard F, Chen X. Insight into the Development of PET Radiopharmaceuticals for Oncology. *Cancers.* 2020 May;12(5):1312.
49. Krasniqi A, D’Huyvetter M, Devoogdt N, Frejd FY, Sørensen J, Orlova A, et al. Same-Day Imaging Using Small Proteins: Clinical Experience and Translational Prospects in Oncology. *J Nucl Med.* 2018;59(6):885–91.
50. Tolmachev V, Tran TA, Rosik D, Sjöberg A, Abrahmsén L, Orlova A. Tumor targeting using affibody molecules: interplay of affinity, target expression level, and binding site composition. *J Nucl Med.* 2012 Jun;53(6):953–60.
51. Schenk S, Schoenhals GJ, de Souza G, Mann M. A high confidence, manually validated human blood plasma protein reference set. *BMC Med Genomics.* 2008 Sep 15;1:41.
52. Covell DG, Barbet J, Holton OD, Black CD, Parker RJ, Weinstein JN. Pharmacokinetics of monoclonal immunoglobulin G1, F(ab’)2, and Fab’ in mice. *Cancer Res.* 1986 Aug;46(8):3969–78.
53. Hosseinimehr SJ, Tolmachev V, Orlova A. Liver uptake of radiolabeled targeting proteins and peptides: considerations for targeting peptide conjugate design. *Drug Discov Today.* 2012 Nov;17(21–22):1224–32.
54. Fu R, Carroll L, Yahioğlu G, Aboagye EO, Miller PW. Antibody Fragment and Affibody ImmunoPET Imaging Agents: Radiolabelling Strategies and Applications. *ChemMedChem.* 2018 06;13(23):2466–78.

55. Pereira PMR, Abma L, Henry KE, Lewis JS. Imaging of human epidermal growth factor receptors for patient selection and response monitoring - From PET imaging and beyond. *Cancer Lett.* 2018 Apr 10;419:139–51.
56. Dammes N, Peer D. Monoclonal antibody-based molecular imaging strategies and theranostic opportunities. *Theranostics.* 2020 Jan 1;10(2):938–55.
57. Thomas GD. Effect of Dose, Molecular Size, and Binding Affinity on Uptake of Antibodies. In: Francis GE, Delgado C, editors. *Drug Targeting: Strategies, Principles, and Applications* [Internet]. Totowa, NJ: Humana Press; 2000 [cited 2021 Mar 2]. p. 115–32. (Methods in Molecular Medicine™). Available from: <https://doi.org/10.1385/1-59259-075-6:115>
58. Mackness BC, Jaworski JA, Boudanova E, Park A, Valente D, Mauriac C, et al. Antibody Fc engineering for enhanced neonatal Fc receptor binding and prolonged circulation half-life. *MAbs.* 2019 Jul 18;11(7):1276–88.
59. Wester H-J, Kessler H. Molecular Targeting with Peptides or Peptide-Polymer Conjugates: Just a Question of Size? *J Nucl Med.* 2005 Dec 1;46(12):1940–5.
60. Xenaki KT, Oliveira S, van Bergen en Henegouwen PMP. Antibody or Antibody Fragments: Implications for Molecular Imaging and Targeted Therapy of Solid Tumors. *Front Immunol.* 2017 Oct 12;8:1287.
61. Muyldermans S. A guide to: generation and design of nanobodies. *The FEBS Journal.* 2021;288(7):2084–102.
62. Miao Z, Levi J, Cheng Z. Protein scaffold-based molecular probes for cancer molecular imaging. *Amino Acids.* 2011 Nov;41(5):1037–47.
63. Gebauer M, Skerra A. Engineered Protein Scaffolds as Next-Generation Therapeutics. *Annu Rev Pharmacol Toxicol.* 2020 Jan 6;60:391–415.
64. Tolmachev V, Orlova A. Affibody Molecules as Targeting Vectors for PET Imaging. *Cancers.* 2020 Mar;12(3):651.
65. Stern LA, Case BA, Hackel BJ. Alternative Non-Antibody Protein Scaffolds for Molecular Imaging of Cancer. *Curr Opin Chem Eng.* 2013 Nov;2(4):10.1016/j.coche.2013.08.009.
66. Lee S, Xie J, Chen X. Peptide-Based Probes for Targeted Molecular Imaging. *Biochemistry.* 2010 Feb 23;49(7):1364–76.
67. Fani M, Maecke HR, Okarvi SM. Radiolabeled peptides: valuable tools for the detection and treatment of cancer. *Theranostics.* 2012;2(5):481–501.
68. Sugiura G, Kühn H, Sauter M, Haberkorn U, Mier W. Radiolabeling Strategies for Tumor-Targeting Proteinaceous Drugs. *Molecules.* 2014 Feb 18;19(2):2135–65.
69. Vermeer AW, Norde W. The thermal stability of immunoglobulin: unfolding and aggregation of a multi-domain protein. *Biophys J.* 2000 Jan;78(1):394–404.
70. Zheng S, Qiu D, Adams M, Li J, Mantri RV, Gandhi R. Investigating the Degradation Behaviors of a Therapeutic Monoclonal Antibody Associated with pH and Buffer Species. *AAPS PharmSciTech.* 2017 Jan 1;18(1):42–8.
71. Ekblad T, Orlova A, Feldwisch J, Wennborg A, Eriksson Karlström A, Tolmachev V. Positioning of <sup>99m</sup>Tc-chelators influences radiolabeling, stability and biodistribution of Affibody molecules. *Bioorg Med Chem Lett.* 2009 Jul 15;19(14):3912–4.
72. Honarvar H, Strand J, Perols A, Orlova A, Selvaraju RK, Eriksson Karlström A, et al. Position for site-specific attachment of a DOTA chelator to synthetic affibody molecules has a different influence on the targeting properties of <sup>68</sup>Ga-compared to <sup>111</sup>In-labeled conjugates. *Mol Imaging.* 2014;13.

73. Altai M, Strand J, Rosik D, Selvaraju RK, Eriksson Karlström A, Orlova A, et al. Influence of nuclides and chelators on imaging using affibody molecules: comparative evaluation of recombinant affibody molecules site-specifically labeled with <sup>68</sup>Ga and <sup>111</sup>In via maleimido derivatives of DOTA and NODAGA. *Bioconjug Chem.* 2013 Jun 19;24(6):1102–9.
74. de Jong M, Breeman WA, Bakker WH, Kooij PP, Bernard BF, Hofland LJ, et al. Comparison of (111)In-labeled somatostatin analogues for tumor scintigraphy and radionuclide therapy. *Cancer Res.* 1998 Feb 1;58(3):437–41.
75. Mitran B, Varasteh Z, Selvaraju RK, Lindeberg G, Sörensen J, Larhed M, et al. Selection of optimal chelator improves the contrast of GRPR imaging using bombesin analogue RM26. *Int J Oncol.* 2016 May;48(5):2124–34.
76. Hofström C, Orlova A, Altai M, Wangsell F, Graslund T, Tolmachev V. Use of a HEHEHE purification tag instead of a hexahistidine tag improves biodistribution of affibody molecules site-specifically labeled with (99m)Tc, (111)In, and (125)I. *J Med Chem.* 2011 Jun 9;54(11):3817–26.
77. Hofström C, Altai M, Honarvar H, Strand J, Malmberg J, Hosseinimehr SJ, et al. HAAAA, HEHEHE, HIIHHI, or HKHKHK: influence of position and composition of histidine containing tags on biodistribution of [(99m)Tc(CO)3](+)-labeled affibody molecules. *J Med Chem.* 2013 Jun 27;56(12):4966–74.
78. Price EW, Orvig C. Matching chelators to radiometals for radiopharmaceuticals. *Chem Soc Rev.* 2013 Dec 2;43(1):260–90.
79. Schwarzenbach G. Der Chelateffekt. *Helvetica Chimica Acta.* 1952;35(7):2344–59.
80. Hancock RD. Chelate ring size and metal ion selection. The basis of selectivity for metal ions in open-chain ligands and macrocycles. *J Chem Educ.* 1992 Aug 1;69(8):615.
81. Brechbiel MW. Bifunctional Chelates for Metal Nuclides. *Q J Nucl Med Mol Imaging.* 2008 Jun;52(2):166–73.
82. Robinson MK, Hodge KM, Horak E, Sundberg ÅL, Russeva M, Shaller CC, et al. Targeting ErbB2 and ErbB3 with a bispecific single-chain Fv enhances targeting selectivity and induces a therapeutic effect in vitro. *Br J Cancer.* 2008 Nov 4;99(9):1415–25.
83. Ross JS, Fletcher JA, Bloom KJ, Linette GP, Stec J, Symmans WF, et al. Targeted therapy in breast cancer: the HER-2/neu gene and protein. *Mol Cell Proteomics.* 2004 Apr;3(4):379–98.
84. Molavipordanjani S, Hosseinimehr SJ. The Radiolabeled HER3 Targeting Molecules for Tumor Imaging. *Iran J Pharm Res.* 2021;20(1):141–52.
85. Menke-van der Houven van Oordt CW, McGeoch A, Bergstrom M, McSherry I, Smith DA, Cleveland M, et al. Immuno-PET Imaging to Assess Target Engagement: Experience from <sup>89</sup>Zr-Anti-HER3 mAb (GSK2849330) in Patients with Solid Tumors. *J Nucl Med.* 2019 Jul;60(7):902–9.
86. Bensch F, Lamberts LE, Smeenk MM, Jorritsma-Smit A, Lub-de Hooge MN, Terwisscha van Scheltinga AGT, et al. (<sup>89</sup>Zr)-Lumretuzumab PET Imaging before and during HER3 Antibody Lumretuzumab Treatment in Patients with Solid Tumors. *Clin Cancer Res.* 2017 Oct 15;23(20):6128–37.
87. Lockhart AC, Liu Y, Dehdashti F, Laforest R, Picus J, Frye J, et al. Phase 1 Evaluation of [(<sup>64</sup>Cu)DOTA]-Patritumab to Assess Dosimetry, Apparent Receptor Occupancy, and Safety in Subjects with Advanced Solid Tumors. *Mol Imaging Biol.* 2016 Jun;18(3):446–53.
88. Yuan Q, Furukawa T, Tashiro T, Okita K, Jin Z-H, Aung W, et al. Immuno-PET Imaging of HER3 in a Model in which HER3 Signaling Plays a Critical Role. *PLoS ONE.* 2015;10(11):e0143076.

89. Pool M, Kol A, de Jong S, de Vries EGE, Lub-de Hooge MN, Terwisscha van Scheltinga AGT. (89)Zr-mAb3481 PET for HER3 tumor status assessment during lapatinib treatment. *MAbs*. 2017 Sep 5;9:1–9.
90. Warnders FJ, Terwisscha van Scheltinga AGT, Knuehl C, van Roy M, de Vries EFJ, Kosterink JGW, et al. Human Epidermal Growth Factor Receptor 3-Specific Tumor Uptake and Biodistribution of 89Zr-MSB0010853 Visualized by Real-Time and Noninvasive PET Imaging. *J Nucl Med*. 2017 Aug;58(8):1210–5.
91. Larimer BM, Phelan N, Wehrenberg-Klee E, Mahmood U. Phage Display Selection, In Vitro Characterization, and Correlative PET Imaging of a Novel HER3 Peptide. *Mol Imaging Biol*. 2017 Jul 21;
92. Orlova A, Malm M, Rosestedt M, Varasteh Z, Andersson K, Selvaraju RK, et al. Imaging of HER3-expressing xenografts in mice using a (99m)Tc(CO) 3-HEHEHE-Z HER3:08699 affibody molecule. *Eur J Nucl Med Mol Imaging*. 2014 Jul;41(7):1450–9.
93. Rosestedt M. Affibody Molecules for HER3-targeted Theranostics of Malignant Tumours [Doctoral Thesis]. Uppsala University; 2018.
94. Da Pieve C, Allott L, Martins CD, Vardon A, Ciobota DM, Kramer-Marek G, et al. Efficient [18F]AIF Radiolabeling of ZHER3:8698 Affibody Molecule for Imaging of HER3 Positive Tumors. *Bioconjugate Chem*. 2016 Aug 17;27(8):1839–49.
95. Martins CD, Da Pieve C, Burley TA, Smith R, Ciobota DM, Allott L, et al. HER3-Mediated Resistance to Hsp90 Inhibition Detected in Breast Cancer Xenografts by Affibody-Based PET Imaging. *Clin Cancer Res*. 2018 Apr 15;24(8):1853–65.
96. Rosestedt M, Andersson KG, Mitran B, Rinne SS, Tolmachev V, Löfblom J, et al. Evaluation of a radiocobalt-labelled affibody molecule for imaging of human epidermal growth factor receptor 3 expression. *Int J Oncol*. 2017 Dec;51(6):1765–74.
97. Andersson KG, Rosestedt M, Varasteh Z, Malm M, Sandström M, Tolmachev V, et al. Comparative evaluation of 111In-labeled NOTA-conjugated affibody molecules for visualization of HER3 expression in malignant tumors. *Oncol Rep*. 2015 Aug;34(2):1042–8.
98. Rinne SS, Xu T, Dahlsson Leitao C, Ståhl S, Löfblom J, Orlova A, et al. Influence of Residualizing Properties of the Radiolabel on Radionuclide Molecular Imaging of HER3 Using Affibody Molecules. *Int J Mol Sci*. 2020 Feb 15;21(4).
99. Wehrenberg-Klee E, Turker NS, Heidari P, Larimer B, Juric D, Baselga J, et al. Differential Receptor Tyrosine Kinase PET Imaging for Therapeutic Guidance. *J Nucl Med*. 2016;57(9):1413–9.
100. Alsaid H, Skedzielewski T, Rambo MV, Hunsinger K, Hoang B, Fieles W, et al. Non invasive imaging assessment of the biodistribution of GSK2849330, an ADCC and CDC optimized anti HER3 mAb, and its role in tumor macrophage recruitment in human tumor-bearing mice. *PLoS ONE*. 2017;12(4):e0176075.
101. Terwisscha van Scheltinga AG, Lub-de Hooge MN, Abiraj K, Schröder CP, Pot L, Bossenmaier B, et al. ImmunoPET and biodistribution with human epidermal growth factor receptor 3 targeting antibody 89Zr-RG7116. *MAbs*. 2014 Jul 1;6(4):1051–8.
102. Razumienko EJ, Scollard DA, Reilly RM. Small-animal SPECT/CT of HER2 and HER3 expression in tumor xenografts in athymic mice using trastuzumab Fab-hergulin bispecific radioimmunoconjugates. *J Nucl Med*. 2012 Dec;53(12):1943–50.
103. Wehrenberg-Klee E, Sinevici N, Nesti S, Kalomeris T, Austin E, Larimer B, et al. HER3 PET Imaging Identifies Dynamic Changes in HER3 in Response to HER2 Inhibition with Lapatinib. *Mol Imaging Biol*. 2021 Jun 8;

104. Rosestedt M, Andersson KG, Mitran B, Tolmachev V, Löfblom J, Orlova A, et al. Affibody-mediated PET imaging of HER3 expression in malignant tumours. *Sci Rep*. 2015 Oct 19;5:15226.
105. Nord K, Gunneriusson E, Ringdahl J, Ståhl S, Uhlén M, Nygren PA. Binding proteins selected from combinatorial libraries of an alpha-helical bacterial receptor domain. *Nat Biotechnol*. 1997 Aug;15(8):772–7.
106. Löfblom J, Feldwisch J, Tolmachev V, Carlsson J, Ståhl S, Frejd FY. Affibody molecules: Engineered proteins for therapeutic, diagnostic and biotechnological applications. *FEBS Letters*. 2010 Jun 18;584(12):2670–80.
107. Ståhl S, Gräslund T, Eriksson Karlström A, Frejd FY, Nygren P-Å, Löfblom J. Affibody Molecules in Biotechnological and Medical Applications. *Trends Biotechnol*. 2017;35(8):691–712.
108. Sörensen J, Sandberg D, Sandström M, Wennborg A, Feldwisch J, Tolmachev V, et al. First-in-human molecular imaging of HER2 expression in breast cancer metastases using the <sup>111</sup>In-ABY-025 affibody molecule. *J Nucl Med*. 2014 May;55(5):730–5.
109. Sörensen J, Velikyan I, Sandberg D, Wennborg A, Feldwisch J, Tolmachev V, et al. Measuring HER2-Receptor Expression In Metastatic Breast Cancer Using [<sup>68</sup>Ga]ABY-025 Affibody PET/CT. *Theranostics*. 2016;6(2):262–71.
110. Zielinski R, Lyakhov I, Hassan M, Kuban M, Shafer-Weaver K, Gandjbakhche A, et al. HER2-Affitoxin: A Potent Therapeutic Agent for the Treatment of HER2-Overexpressing Tumors. *Clin Cancer Res*. 2011 Aug 1;17(15):5071–81.
111. Tolmachev V, Orlova A, Pehrson R, Galli J, Bastrup B, Andersson K, et al. Radionuclide Therapy of HER2-Positive Microxenografts Using a <sup>177</sup>Lu-Labeled HER2-Specific Affibody Molecule. *Cancer Res*. 2007 Mar 15;67(6):2773–82.
112. Malm M. Generation and characterization of Affibody molecules targeting HER3 [Doctoral Thesis]. KTH Royal Institute of Technology; 2017.
113. Bass T. Affibody molecules targeting HER3 for cancer therapy [Doctoral Thesis]. KTH Royal Institute of Technology; 2017.
114. Kronqvist N, Malm M, Göstring L, Gunneriusson E, Nilsson M, Höiden Guthenberg I, et al. Combining phage and staphylococcal surface display for generation of ErbB3-specific Affibody molecules. *Protein Eng Des Sel*. 2011 Apr;24(4):385–96.
115. Malm M, Kronqvist N, Lindberg H, Gudmundsdotter L, Bass T, Frejd FY, et al. Inhibiting HER3-mediated tumor cell growth with affibody molecules engineered to low picomolar affinity by position-directed error-prone PCR-like diversification. *PLoS ONE*. 2013;8(5):e62791.
116. Göstring L, Malm M, Höiden-Guthenberg I, Frejd FY, Ståhl S, Löfblom J, et al. Cellular effects of HER3-specific affibody molecules. *PLoS ONE*. 2012;7(6):e40023.
117. Malm M, Bass T, Gudmundsdotter L, Lord M, Frejd FY, Ståhl S, et al. Engineering of a bispecific affibody molecule towards HER2 and HER3 by addition of an albumin-binding domain allows for affinity purification and in vivo half-life extension. *Biotechnol J*. 2014 Sep;9(9):1215–22.
118. Bass TZ, Rosestedt M, Mitran B, Frejd FY, Löfblom J, Tolmachev V, et al. In vivo evaluation of a novel format of a bivalent HER3-targeting and albumin-binding therapeutic affibody construct. *Sci Rep*. 2017 Feb 23;7:43118.
119. Orlova A, Bass TZ, Rinne SS, Leitao CD, Rosestedt M, Atterby C, et al. Evaluation of the Therapeutic Potential of a HER3-Binding Affibody Construct TAM-HER3 in Comparison with a Monoclonal Antibody, Seribantumab. *Mol Pharm*. 2018 Aug 6;15(8):3394–403.

120. Schardt JS, Oubaid JM, Williams SC, Howard JL, Aloimonos CM, Bookstaver ML, et al. Engineered Multivalency Enhances Affibody-Based HER3 Inhibition and Downregulation in Cancer Cells. *Mol Pharm*. 2017 03;14(4):1047–56.
121. Vosjan MJWD, Perk LR, Visser GWM, Budde M, Jurek P, Kiefer GE, et al. Conjugation and radiolabeling of monoclonal antibodies with zirconium-89 for PET imaging using the bifunctional chelate p -isothiocyanatobenzyl-desferrioxamine. *Nature Protocols*. 2010 Apr;5(4):739–43.
122. Rinne SS, Dahlsson Leitao C, Saleh-Nihad Z, Mitran B, Tolmachev V, Ståhl S, et al. Benefit of Later-Time-Point PET Imaging of HER3 Expression Using Optimized Radiocobalt-Labeled Affibody Molecules. *Int J Mol Sci*. 2020 Mar 13;21(6).
123. Wällberg H, Orlova A. Slow internalization of anti-HER2 synthetic affibody monomer <sup>111</sup>In-DOTA-ZHER2:342-pep2: implications for development of labeled tracers. *Cancer Biother Radiopharm*. 2008 Aug;23(4):435–42.
124. Koyo N, Chiaki T, Sachi N, Yoshinobu T, Mitsuru H, Hitoshi S. Effect of electric charge on the hepatic uptake of macromolecules in the rat liver. *International Journal of Pharmaceutics*. 1990 Nov 28;65(1):7–17.
125. Rosestedt M, Andersson KG, Mitran B, Rinne SS, Tolmachev V, Löfblom J, et al. Evaluation of a radiocobalt-labelled affibody molecule for imaging of human epidermal growth factor receptor 3 expression. accepted manuscript.
126. Westerlund K, Honarvar H, Norrström E, Strand J, Mitran B, Orlova A, et al. Increasing the Net Negative Charge by Replacement of DOTA Chelator with DOTAGA Improves the Biodistribution of Radiolabeled Second-Generation Synthetic Affibody Molecules. *Mol Pharm*. 2016 May 2;13(5):1668–78.
127. Rinne SS, Leitao CD, Mitran B, Bass TZ, Andersson KG, Tolmachev V, et al. Optimization of HER3 expression imaging using affibody molecules: Influence of chelator for labeling with indium-111. *Sci Rep*. 2019 24;9(1):655.
128. Tolmachev V, Hofström C, Malmberg J, Ahlgren S, Hosseinimehr SJ, Sandström M, et al. HEHEHE-tagged affibody molecule may be purified by IMAC, is conveniently labeled with [<sup>99m</sup>Tc(CO)<sub>3</sub>](+), and shows improved biodistribution with reduced hepatic radioactivity accumulation. *Bioconjug Chem*. 2010 Nov 17;21(11):2013–22.
129. Akizawa H, Arano Y, Mifune M, Iwado A, Saito Y, Mukai T, et al. Effect of molecular charges on renal uptake of <sup>111</sup>In-DTPA-conjugated peptides. *Nucl Med Biol*. 2001 Oct;28(7):761–8.
130. Hoffman TJ, Gali H, Smith CJ, Sieckman GL, Hayes DL, Owen NK, et al. Novel series of <sup>111</sup>In-labeled bombesin analogs as potential radiopharmaceuticals for specific targeting of gastrin-releasing peptide receptors expressed on human prostate cancer cells. *J Nucl Med*. 2003 May;44(5):823–31.
131. Wadas TJ, Wong EH, Weisman GR, Anderson CJ. Coordinating Radiometals of Copper, Gallium, Indium, Yttrium and Zirconium for PET and SPECT Imaging of Disease. *Chem Rev*. 2010 May 12;110(5):2858–902.
132. Kubiček V, Havlíčková J, Kotek J, Tircsó G, Hermann P, Tóth É, et al. Gallium(III) Complexes of DOTA and DOTA–Monoamide: Kinetic and Thermodynamic Studies. *Inorg Chem*. 2010 Dec 6;49(23):10960–9.
133. Garousi J, Andersson KG, Mitran B, Pichl M-L, Ståhl S, Orlova A, et al. PET imaging of epidermal growth factor receptor expression in tumours using <sup>89</sup>Zr-labelled ZEGFR:2377 affibody molecules. *Int J Oncol*. 2016 Apr;48(4):1325–32.
134. Heppeler A, André JP, Buschmann I, Wang X, Reubi J-C, Hennig M, et al. Metal-Ion-Dependent Biological Properties of a Chelator-Derived Somatostatin Analogue for Tumour Targeting. *Chemistry – A European Journal*. 2008;14(10):3026–34.

135. Mitran B, Thisgaard H, Rosenström U, Dam JH, Larhed M, Tolmachev V, et al. High Contrast PET Imaging of GRPR Expression in Prostate Cancer Using Cobalt-Labeled Bombesin Antagonist RM26. *vosja*. 2017;2017:6873684.
136. Dahlsson Leitao C, Rinne SS, Mitran B, Vorobyeva A, Andersson KG, Tolmachev V, et al. Molecular Design of HER3-Targeting Affibody Molecules: Influence of Chelator and Presence of HEHEHE-Tag on Biodistribution of <sup>68</sup>Ga-Labeled Tracers. *Int J Mol Sci*. 2019 Mar 2;20(5).
137. Rinne SS, Dahlsson Leitao C, Mitran B, Bass TZ, Andersson KG, Tolmachev V, et al. Optimization of HER3 expression imaging using affibody molecules: Influence of chelator for labeling with indium-111. *Sci Rep*. 2018;In Press.
138. Mitran B, Andersson KG, Lindström E, Garousi J, Rosestedt M, Tolmachev V, et al. Affibody-mediated imaging of EGFR expression in prostate cancer using radiocobalt-labeled DOTA-ZEGFR:2377. *Oncol Rep*. 2019 Jan;41(1):534–42.
139. Okamoto S, Eltis LD. The biological occurrence and trafficking of cobalt. *Metalomics*. 2011 Oct 4;3(10):963–70.
140. Rinne SS, Dahlsson Leitao C, Gentry J, Mitran B, Abouzayed A, Tolmachev V, et al. Increase in negative charge of <sup>68</sup>Ga/chelator complex reduces unspecific hepatic uptake but does not improve imaging properties of HER3-targeting affibody molecules. *Sci Rep*. 2019 Nov 27;9(1):17710.
141. Beylervig V, Morris PG, Smith-Jones PM, Modi S, Solit D, Hudis CA, et al. Pilot study of <sup>68</sup>Ga-DOTA-F(ab')<sub>2</sub>-trastuzumab in patients with breast cancer. *Nucl Med Commun*. 2013 Dec;34(12):1157–65.
142. Brandt M, Cowell J, Aulsebrook ML, Gasser G, Mindt TL. Radiolabelling of the octadentate chelators DFO\* and oxoDFO\* with zirconium-89 and gallium-68. *J Biol Inorg Chem*. 2020 Aug 1;25(5):789–96.
143. Tsiou MI, Knapp CE, Foley CA, Munteanu CR, Cakebread A, Imberti C, et al. Comparison of macrocyclic and acyclic chelators for gallium-68 radiolabelling †Electronic supplementary information (ESI) available. CCDC 1564603. For ESI and crystallographic data in CIF or other electronic format see DOI: 10.1039/c7ra09076e. *RSC Adv*. 2017 Oct 24;7(78):49586–99.
144. Altai M, Varasteh Z, Andersson K, Eek A, Boerman O, Orlova A. In vivo and in vitro studies on renal uptake of radiolabeled affibody molecules for imaging of HER2 expression in tumors. *Cancer Biother Radiopharm*. 2013 Apr;28(3):187–95.
145. Abou DS, Ku T, Smith-Jones PM. IN VIVO BIODISTRIBUTION AND ACCUMULATION OF <sup>89</sup>Zr IN MICE. *Nucl Med Biol*. 2011 Jul;38(5):675–81.
146. Raavé R, Sandker G, Adumeau P, Jacobsen CB, Mangin F, Meyer M, et al. Direct comparison of the in vitro and in vivo stability of DFO, DFO\* and DFOcyclo\* for <sup>89</sup>Zr-immunoPET. *Eur J Nucl Med Mol Imaging*. 2019 Aug;46(9):1966–77.
147. Sandström M, Lindskog K, Velikyan I, Wennborg A, Feldwisch J, Sandberg D, et al. Biodistribution and Radiation Dosimetry of the Anti-HER2 Affibody Molecule <sup>68</sup>Ga-ABY-025 in Breast Cancer Patients. *J Nucl Med*. 2016 Jun;57(6):867–71.
148. Altai M, Leitao CD, Rinne SS, Vorobyeva A, Atterby C, Ståhl S, et al. Influence of Molecular Design on the Targeting Properties of ABD-Fused Mono- and Bi-Valent Anti-HER3 Affibody Therapeutic Constructs. *Cells* [Internet]. 2018 Oct 11 [cited 2020 Jan 23];7(10). Available from: <https://www.ncbi.nlm.nih.gov/pmc/articles/PMC6210767/>
149. Schardt JS, Noonan-Shueh M, Oubaid JM, Pottash AE, Williams SC, Hussain A, et al. HER3-Targeted Affibodies with Optimized Formats Reduce Ovarian Cancer Progression in a Mouse Xenograft Model. *AAPS J*. 2019 04;21(3):48.

150. Rosestedt M, Andersson KG, Rinne SS, Leitao CD, Mitran B, Vorobyeva A, et al. Improved contrast of affibody-mediated imaging of HER3 expression in mouse xenograft model through co-injection of a trivalent affibody for in vivo blocking of hepatic uptake. *Sci Rep.* 2019 May 1;9(1):6779.



# Acta Universitatis Upsaliensis

*Digital Comprehensive Summaries of Uppsala Dissertations  
from the Faculty of Pharmacy 307*

Editor: The Dean of the Faculty of Pharmacy

A doctoral dissertation from the Faculty of Pharmacy, Uppsala University, is usually a summary of a number of papers. A few copies of the complete dissertation are kept at major Swedish research libraries, while the summary alone is distributed internationally through the series Digital Comprehensive Summaries of Uppsala Dissertations from the Faculty of Pharmacy. (Prior to January, 2005, the series was published under the title “Comprehensive Summaries of Uppsala Dissertations from the Faculty of Pharmacy”.)

Distribution: [publications.uu.se](http://publications.uu.se)  
urn:nbn:se:uu:diva-467281



ACTA  
UNIVERSITATIS  
UPSALIENSIS  
UPPSALA  
2022